NASA Technical Memorandum 103925

Thermal Response of Rigid and Flexible Insulations and Reflective Coating in an Aeroconvective Heating Environment

D. A. Kourtides, S. A. Chiu, D. J. Iverson, and D. M. Lowe, Ames Research Center,
Moffett Field, California

March 1992

National Aeronautics and
Space Administration

Ames Research Center
Moffett Field, California 94035-1000

PREFACE

This report describes the thermal performance of rigid and flexible thermal protection systems considered for potential use in future Aeroassist Space Transfer Vehicles. The thermal response of these materials subjected to aeroconvective heating from a plasma arc is described. Properties that were measured included the thermal conductivity of both rigid and flexible insulations at various temperatures and pressures and the emissivity of the fabrics used in the flexible insulations. The results are included from computerized thermal analysis models describing thermal response of these materials subjected to flight conditions.

The thermal performance of these thermal protection systems in the plasma arc is described in three sections: flexible insulations, rigid insulations, and reflective coating. The thermal conductivity measurements are described in two sections: flexible and rigid insulations. The thermal analysis section includes analyses for both the flexible and rigid insulations.

TABLE OF CONTENTS

LIST OF TABLES

Page

LIST OF FIGURES

Page

APPENDIX—LIST OF FIGURES

Page

EXECUTIVE SUMMARY

The thermal performance of rigid and flexible insulations and a reflective coating is described. The aeroconvective heating conditions for the test were simulated in the NASA Ames 20 MW Plasma Arc Facility. The test conditions simulated were the approximate peak heating conditions to be encountered on the aerobrake of the Aeroassist Flight Experiment (AFE) following a "Baseline VA" trajectory. The pressure conditions of the AFE "Baseline VA Nominal" trajectory were also simulated in the arc jet. Materials tested include

(a) Two types of rigid insulations: Alumina Sol-Modified Insulation (ASMI) and Alumina Enhanced Thermal Barrier (AETB). Each was tested in two densities: AETB-12 and AETB-8,

(b) A reflective coating on a rigid insulation: Fibrous Refractory Composite Insulation (FRCI-12)/Reaction Cured Glass (RCG),

(c) Two types of flexible insulations: Tailorable Advanced Blanket Insulation (TABI) and Composite Flexible Blanket Insulation (CFBI), with two variations of each type of insulations, and

(d) Similar flexible insulations coated with a Protective Ceramic Coating (PCC) or a RCG coating.

Surface and in-depth temperatures and surface recession were measured in the rigid insulations. Surface temperatures were measured on the FRCI-12/RCG coated with the reflective coating and surface and backface temperatures were measured in uncoated and coated flexible insulations. All the rigid insulations exhibited excellent performance up to heating rates of 47 Btu/ft^2•s and the AETB-12 up to 58 Btu/ft^2•s. The uncoated flexible insulations exhibited good thermal performance up to 31 Btu/ft^2•s. The use of a PCC to protect these insulations at higher heating rates is described. Thermal and optical properties were determined including thermal conductivity for the rigid and flexible insulations and emissivity for the insulation fabrics. These properties were utilized to calculate the thermal performance of the rigid and flexible insulations at the maximum heating rate.

INTRODUCTION

One of the experiments in the Aeroassist Flight Experiment (AFE) (ref. 1) was the Alternate Thermal Protection Materials (ATPM) experiment. As part of this experiment, two different types of rigid insulations (one in two different densities), two different types of flexible insulations, and one reflective coating on a rigid insulation were to be flown. The objective of the experiment was to determine thermal response of these materials under the AFE trajectory environment and to determine their ability to provide thermal protection for an aerobrake vehicle. According to previously established guidelines (ref. 1), "the thermal design requirement of the aerobrake is to protect the vehicle structure from aerodynamic heating such that the structure will not exceed 350°F during all phases of the design mission." Therefore, one of the key objectives of this study was to determine the backface temperature of the insulations when exposed to a simulated AFE heating environment.

The procedure used to accomplish the objective was to (a) attempt to simulate as closely as possible the radiation equilibrium temperature condition resulting from the nominal and peak heating rate trajectories reported in reference 2, (b) determine the thermal response of the rigid and flexible insulations in this environment, (c) determine any post-test physical damage to the insulations and coatings, (d) determine the effectiveness of the reflective coating to reflect the radiative portion of the heating environment, (e) determine the effect of special instrumentation on the physical integrity of one of the rigid insulations, (f) determine some of the thermal and optical properties of these materials, and (g) utilize these properties in an analytical model to predict the response of these materials in a maximum heating rate trajectory.

During the evolution of the AFE program, three different sets of entry trajectories were considered as described in references 2-4. The final set, reference 4, includes two heating rate profiles: "Nominal Adjusted" and "Nominal Adjusted Plus Methodology Uncertainty." The arc-jet test described here closely simulated these case described in reference 4. The test was designed to the heating rate and pressure conditions described in reference 3, but coincidentally, the test conditions obtained were very close to the heating rate conditions described in reference 4. The heat flux to the AFE surface depends on the location. The locations of the various rigid and flexible insulations and reflective coating to be flown on the AFE aerobrake are shown in figure 1. The three rigid insulations are located immediately below Stagnation to Length (S/L) ratio of 0.00, or (S/L) = 0.00, where S is the distance from the stagnation point and L is the diameter of the aerobrake vehicle. These are Alumina Enhanced Thermal Barrier (AETB-12 and AETB-8) and Alumina Sol Modified Insulation (ASMI).

The Tailorable Advanced Blanket Insulation (TABI) and the Composite Flexible Blanket Insulation (CFBI) are located between S/L = 0.47 and S/L = 0.55. The heating rate environment at S/L = 0.55 was chosen due to the possibility of fabric failure at higher heating rates. The center of the Fibrous Refractory Composite Insulation (FRCI)-12, Reaction Cured Glass (RCG), reflective coating is located approximately at S/L = 0.52. A similar heating rate was chosen for this tile since the difference between S/L = 0.52 and S/L = 0.55 was insignificant.

The AETB-8, AETB-12 and ASMI rigid insulations were tested at the S/L = 0.00 heating conditions. The TABI and CFBI flexible insulations and FRCI-12-RCG/reflective coating were tested at the S/L = 0.55 heating conditions which represents the coolest edge of these insulations. These conditions are very close to the "Baseline VA" conditions reported in reference 4.

The author wishes to acknowledge W. L. Love, H. K. Tran, D. J. Iverson, D. M. Lowe, and C. Y. Simonian for conducting the plasma arc tests and S. A. Chiu for performing the analytical studies.

PLASMA ARC TESTS

Test Conditions

The heating and temperature profiles are shown in figure 2 for the AFE trajectory for the two aerobrake locations of interest. These conditions were simulated in the NASA Ames 20 MW Plasma

Arc Jet Facility. The exact temperature profile cannot be duplicated in this facility. Instead, the arc was run at a constant condition that produced the surface temperature predicted for the AFE. The run time was selected to expose the model to about the same total heat load as the flight vehicle.

A comparison of the plasma arc radiation equilibrium temperatures measured during the calibration tests and the recently enacted "Baseline VA" trajectory reported in reference 4 is shown in table 1. The measured temperatures were extremely close to the predicted flight trajectory temperatures for the flexible insulation and reflective coating locations at S/L = 0.456. The measured temperatures on the flexible calibration model was 50°F lower than the AFE maximum radiative equilibrium temperature. The balance of the measured temperatures are very close to or higher than the trajectory temperatures. The stagnation pressure on the aerobrake at S/L = 0.0 varies from 0.02 psi at atmospheric entry to a maximum of 0.45 psi at peak heating. The stagnation pressures for the arc-jet tests are shown in table 1, along with the calculated heat flux rates.

The plasma arc test conditions are shown in table 2. All of the models were inserted instantaneously into the plasma arc stream held for 120 sec then removed instantaneously. This differs from the actual AFE heating rate profiles shown in figure 2 which gradually rise to a peak, then fall. After withdrawal, the arc was quenched but the pressure was maintained in the chamber for approximately 400 sec after exposure for the rigid insulations and for 600 sec for the flexible insulations or until the backface temperature approached equilibrium.

Calibration Model Description

Three calibration models were utilized to establish the test conditions for the three classes of materials tested: rigid insulations, flexible insulations, and reflective coating. The model geometry for the rigid insulations and reflective coating were similar. A larger model was used for the flexible insulations. A rigid insulation called Lockheed Insulation (LI-2200) (ref. 5) coated with RCG was used as the calibration model for the rigid insulations and reflective coating. It was instrumented on the surface with three type "R" thermocouples. The rigid models were approximately 2.75 in. in diameter × 0.95 in. in height and were inserted in a 4 in. diameter graphite holder. The calibration model for the flexible insulations consisted of a 6.5 in. round FRCI-12 holder with a 3.5 in. square × 1.03 in. thick FRCI-12 insert instrumented with three type "R" thermocouples. For the actual test, the flexible insulations were the same size as the calibration model inserts. All models used a gap filler between the model and the holder.

These calibration models were used to establish the power and pressure conditions and the resulting surface temperatures shown in table 2. The matrix of test conditions used to test the insulation materials is shown in table 3. The target temperatures and the measured maximum temperatures are also shown for each run. The calibration model temperatures were also measured with a pyrometer. These measurements were not corrected for emissivity or for reflective index of the window of the arc-jet chamber. The pyrometer readings were consistently 10% lower than the thermocouple readings. Both pyrometer and thermocouple readings were taken on all models for redundancy, but the thermocouple readings were considered more accurate. Thermocouple and pyrometer readings are compared in figure 3. The comparison was performed by testing an FRCI-12/RCG rigid insulation at various temperatures and measuring the surface temperatures with both the thermocouples and

pyrometer. The calibration temperature profiles obtained for the flexible insulations, the reflective coating, and the rigid insulations are shown in figures 4, 5, and 6 respectively.

FLEXIBLE INSULATIONS

Description of Materials

Two types of flexible insulations were tested: TABI and CFBI. Two variations of TABI insulations were tested: one with an angle interlock top fabric and another with a layer-to-layer top fabric. Two variations of CFBI were tested: one with a 5 harness satin weave top fabric and one with an interlock top fabric. The detail composition of these insulations is described in table 3. The two top fabric configurations for the CFBI blankets tested are shown in figure 7. The angle interlock fabric utilized in the TABI was essentially similar to the interlock fabric shown in figure 7, except it contains only two layers of fabrics. The layer-to-layer fabric is similar to the angle interlock, except it does not include the cross yarns. Two different coatings were evaluated for protecting these insulations at high heating rates: the RCG coating described previously (ref. 6) and a PCC also described previously (ref. 7). The purpose of the coatings is to increase the emittance of the surface when the system is subjected to a high-temperature environment and to protect the underlying silicon carbide fabric from oxidation and degradation. The uncoated silicon carbide fabric has an emittance of 0.6 at 2200°F, which results in excessive surface temperatures when the fabric is subjected to a high-heating environment, resulting in failure of the fabric. One major requirement of the coatings is that they provide thermal protection to the fabric instantaneously as the material is exposed to the high-heating environment. A second requirement is that the coating should adhere well to the fabric and should remain flexible prior to installation on the vehicle. The third requirement is that the coatings must not contain any organic binder that will produce volatiles, thus contaminating adjacent surfaces in a space vehicle.

Some of the coated flexible insulations were also subjected to a simulated installation procedure on a vehicle to determine the effect of physical pressure on the insulation and coating integrity. Prior to testing, these coated insulations were subjected to 5 cycles of vacuum bagging at 4 psi for 8 hr per cycle.

Plasma Arc Test Results

The geometry of flexible insulation test models was similar to the calibration test models described previously. The square rigid insulation insert (3.5 in. × 3.5 in. × 1.03 in. thick) was removed and replaced with the flexible insulation to be tested. The flexible insulation was instrumented with one type "R" surface thermocouple and one type "K" thermocouple embedded in RTV between the backface and 0.032 in. thick aluminum plate. The model was normal to the plasma arc stream.

Figures 8 through 11 show the thermal profiles for the uncoated TABI. Higher surface temperatures were obtained with these insulations compared to FRCI-12/RCG at similar test conditions. This

is attributed to the lower emissivity of the top fabric relative to RCG, and other factors such as fabric design and texture. Fabric design and texture effect surface temperature due to the catalycity and emissivity of the fabric. For example, an open weave configuration has a layer surface area exposed to the heating environment and therefore a higher catalytic efficiency than a tight weave configuration. Fabric failure was observed only at the higher heating rate for the TABI layer-to-layer while the TABI angle interlock failed at both test conditions. The backface temperature of the TABI angle interlock was significantly higher at both test conditions than the TABI layer-to-layer as shown in figures 10, 11, 8, and 9 respectively. This high backface temperature of the TABI angle interlock could be attributed due to the failure of the top silicon carbide fabric during the thermal exposure. This insulation reached 1003°F at the aluminum when tested at the high heating condition compared to 388°F for the TABI Layer-to-Layer. Of the two insulations, the TABI layer-to-layer provided better thermal response characteristics than the TABI angle interlock.

The thermal profiles for the uncoated CFBI insulations are shown in figures 12 through 15. The only difference in the composition of the two CFBI insulations was the surface fabric. The CFBI with the 5 harness satin weave fabric failed at both test conditions, resulting in holes in the fabric. There were no holes observed in the CFBI interlock for either test condition and the insulation seemed intact except for some discoloration of the fabric attributed to oxidation. The maximum backface for this insulation reached 409°F at the high heating conditions. Based on the above results, the best CFBI configuration was the CFBI interlock. Due to the failure of the TABI at the high heating condition and possibility of the CFBI interlock failing at higher heating conditions, the use of a high-emittance coating on the fabric was investigated.

The PCC coating was utilized to coat the CFBI and TABI blankets. Additional CFBI blankets were coated with RCG coating. Most of the coatings were brushed onto the surface of the top fabric and dried using a heat gun, but some models were sprayed with the coatings. The RCG was light gray and the PCC was slightly darker. Both coatings seemed to adhere to the fabric after drying and did not crack. When models coated with the PCC were handled, it was found that the fabric was still fairly flexible and the coatings cracked only slightly when pressed hard. Only a small amount of PCC was dusted off from the corners of the various models when they were installed in their holders. The fabric of the models coated with the RCG was found to be more rigid than that of the PCC coated models and the coating cracked severely when pressed hard. A substantial amount of RCG cracked and peeled off from the models with this coating when they were installed in their holders. The thickness of the two coatings were identical. Later models coated with a much thicker layer of PCC showed signs of cracking and peeling during installation. From other tests (ref. 7), it was determined that the thicker PCC coating ($\geq$ 1.33 oz/ft^2 or 0.006 in. thick) was not required.

All of the coated blankets were tested at the 34 Btu/ft^2•s test condition and no failures were observed with PCC coated blankets, except for one model showing a small fabric hole in the corner. The RCG coated blankets failed at this test condition. Figures 16 through 19 show the thermal profiles for the RCG and PCC coated CFBI insulations. Lower surface temperature was achieved with the PCC coated TABI (fig. 19) and coated CFBI (fig. 17) compared to the uncoated TABI (fig. 9) and uncoated CFBI (fig. 15) at the high-heating condition. Both uncoated and coated TABI insulations were identical in construction as were both uncoated and coated CFBI insulations. This reduction in surface temperature is attributed to the relatively high emissivity of the coating. Surface emissivity will be discussed later.

Additional plasma arc tests with RCG and PCC coated insulations were conducted to determine the effect of pressure and vacuum bagging on thermal performance. The thermal profiles are shown in figures 20 through 23. The samples were tested at the high-heating condition. The only fabric failure observed was with the RCG coated CFBI. These and previous samples were brush coated with RCG or PCC coatings. A small hole was observed in one corner and this could be attributed to insufficient coating due to the brush-on method. Additional models were sprayed with RCG and PCC. The dry-coating thickness (determined by weight) was identical. The thermal profiles for these are shown in figures 22 and 23. The RCG coated samples shown in figure 22 reached slightly higher temperature than the PCC coated sample shown in figure 23. The top fabric of the RCG coated sample failed, but the PCC sample was intact.

The test results can be summarized as follows:

- The maximum heating rate used for test was approximately 2 Btu/ft^2•s less than that predicted for the AFE trajectory.
- Of all the uncoated insulations tested, the only one that survived with no fabric damage at 34 Btu/ft^2•s was the CFBI interlock.
- The TABI layer-to-layer and CFBI interlock provided better thermal performance than the other two types of insulations. This is attributed to the OML silicon carbide fabric which exhibited minimum damage in the layer to layer and no damage to the Interlock.
- The use of a high emittance coating is necessary to protect these insulations at heating rates $\geq$ 34 Btu/ft^2•s appears to be suitable.
- Additional testing will be required of PCC coated TABI and CFBI insulations at a heating rate of 36 Btu/ft^2•s.
- There was no effect on the thermal performance of the insulations as a result of pre-test applied pressure or vacuum bagging.

RIGID INSULATIONS

Description of Materials

Materials tested in the plasma arc are described in table 4. All rigid insulations were coated with a RCG coating. These insulations and coating have been described previously in detail (refs. 5 and 6); therefore, it is not necessary to redescribe them here.

Plasma Arc Test Results

The geometry of rigid insulation test models was similar to the calibration test models described previously. The insulations were instrumented with type "R" thermocouples, three at the surface, embedded in RCG, one embedded in the insulation at 0.1 in. from the surface, and one at 0.35 in. from the surface. The model was normal to the plasma arc stream.

The thermal profiles for the rigid insulations are shown in figures 24 through 29. At the low-heating condition, lower in-depth temperatures were observed with ASMI insulation than the AETB-8 or AETB-12, even though the surface temperatures were similar among the three insulations. This could be attributed to the lower thermal conductivity of ASMI at 0.1 atm. The pressure during the test was 0.05 atm and 0.07 atm at the two test conditions. The AETB-12 insulation was instrumented with a non-functional experimental Resistance Temperature Detector (RTD) to determine the effect of this instrumentation on the surface of the insulation. None of the three insulations indicated any defect on the surface after testing at this condition.

The insulations were also tested at a heating rate of 58.7 Btu/ft^2•s. Again, the ASMI insulation exhibited the lowest temperature at 0.35 in. depth at peak temperature. The surface thermocouples failed after approximately 60–90 sec in the plasma arc stream, but the models were held in the stream for 120 sec. There was no surface penetration in the AETB-12 insulation indicating that the experimental RTD did not have any adverse effect on the surface of the insulation. Surface penetration is defined when the RCG melts and the underlying insulation appears on the surface. The RCG surface showed some partial melting, but there was no penetration. The AETB-8 and ASMI insulations showed some surface penetrations especially at the area where the thermocouples enter the insulation from the surface. The failures were not considered as damaging or propagating to the underlying structure in an actual aerobrake application, because the penetrations were not too deep. This is verified by the in-depth temperature profiles of the AETB-8 and ASMI insulations, which were not significantly different from the AETB-12 temperature profile. It should also be noted that the plasma-arc test condition exceeded the maximum heating rate of the AFE trajectory noted in figure 2 and table 1.

The surface recession (shrinkage) of the rigid insulations was also determined to be: ASMI: 0.011 in.; AETB-12: 0.019 in.; and AETB-8: 0.024 in. This shrinkage is considered insignificant. The test results can be summarized as follows:

- Although the aeroconvective environment chosen in the plasma arc does not replicate the AFE environment, it exceeded the heating environment discussed in reference 2 by 2–4 Btu/ft^2•s.

- The AETB-8, AETB-12, and ASMI exhibited excellent performance up to a heating rate of 47 Btu/ft^2•s.

- At heating rates of 58 Btu/ft^2•s, the AETB-12 exhibited some melting of the RCG, but there was no penetration of the surface. The surfaces of the AETB-8 and ASMI were penetrated, but this damage is considered non-propagating to an underlying aluminum structure.

- The RTD instrumentation had no detrimental effect on the surface of the AETB-12 insulation.

- The measured ASMI in-depth temperatures were lower than the AETB-8 or AETB-12 temperatures.

- Surface recession or shrinkage was insignificant in all the rigid insulations.

REFLECTIVE COATING

Description of Materials

The reflective coating is applied on the rigid FRCI-12 insulation as follows: the RCG coating is applied on the insulation to a dry thickness of approximately 0.012 in. It is air dried and a second coating of silica particles (Spectrosil®[1]) is applied to half the specimen to a dry thickness of approximately 2.3 μm. The RCG half surface serves as the reference surface. The combined coatings are fired at 2225°F for 90 min in air. Subsequently, an alumina (Ceralox®[2]) coating is applied to the combined coating at a thickness of 2.2 -7.1 μm and fired at 2225°F for 30 min. The coated models are detailed in table 5.

Plasma Arc Test Results

The geometry of reflective coating test models was similar to the calibration test models described previously. The reflective coatings were instrumented with one type "R" thermocouple at each coating and one differential thermocouple embedded between two adjacent coatings.

Figures 30 and 31 show the surface temperature profiles of the reference and reflective coatings at three different thicknesses: 7.1 μm, 2.5 μm and 2.2 μm. The models were instrumented with both surface and differential thermocouples.

As stated earlier, the purpose of the reflective coating is to reflect the radiative portion of the heating environment. Some of the incoming radiation should be "reflected" by the coating after a series of refraction and light scattering events within the coating which is applied on top of the RCG coating. Energy radiated from the RCG surface is either transmitted through the thin overcoat or emitted by it. The thickness of the coating is therefore critical, since it must be thin enough to permit the substrate to radiate through it, yet thick enough for scattering to reflect some of the incoming radiation. Also, the coating will need to be thick enough to retain its optical properties and not be absorbed into the RCG coating during exposure to high heat flux rates. The reflectance of the RCG and reflective coatings prior and after testing is shown in figures 32 through 35. As expected, the thicker coatings have a higher effective reflectance. In order to be effective in reducing the surface temperature of the tile, the overcoat in combination with the RCG coating must have the following properties: it does not degrade its emissivity properties; solar absorptivity to emissivity ratio is less than or equal to 0.4 after exposure to the aeroconvective environment (this ratio is dictated by a

[1] Registered trademark of Thermal Fused Quartz Inc.
[2] Registered trademark of Ceralox Corp.

typical absorbance of ≤ 0.3 of the overlay coating and an emittance of 0.8 of the underlying coating); and the combined total emittance of the RCG/reflective coating at higher temperatures should be equal to or higher than 0.85. In the present case, the reflectance at 300 nanometers of the combined RCG/reflective coating after thermal exposure in the arc-jet was approximately 60% for the 2.2 μm, 93% for the 2.5 μm and 94% for the 7.1 μm thick coating.

There was no degradation of any of the coatings after the test exposure and the optimum thickness of the coating was 2.5 μm since there was no increase in reflectance as a result of a thicker coating. Two of the coatings are compared in figure 30. A slightly hotter (43°F at 100 sec) surface temperature was observed with the thicker coating. The RCG is compared with the 2.2 μm coating is shown in figure 31. A slightly hotter (52°F at 100 sec) surface is observed with the reflective coating. This is attributed to the absence, or small amount of radiation from the plasma arc. The effect of the reflective coating should be more apparent in a higher radiation environment. This is shown in table 6 where the calculated surface temperatures of the RCG and RCG/reflective coating is presented as a function of various radiative heating rates at the coating location on the aerobrake. The total heating rate shown is reported in reference 3 which is lower than that reported in reference 4. Calculations were performed prior to the availability of reference 4. A reduction of the RCG/reflective coating temperature is observed as the radiative heating rate increases. As shown in table 6, no significant reduction in surface temperature is observed until the radiative heating rate is 25%–30% of the total. With a small (5–10%) radiative component such as that in the arc-jet, a slightly hotter surface was expected for the reflective coated surface due to the lower effective emissivity of the combined coatings, verified by the arc-jet measurements. Approximately 50°F hotter surface was observed with the reflective coating. The radiative heating rate on the AFE is expected to be approximately 15% of the total heating rate which may result in approximately 30°F hotter surface temperature of the reflective coating than the RCG. However, should this radiative heating rate be higher, the reflective coating should be extremely effective in reducing the surface temperature of the rigid insulation. The differences in surface temperatures were also measured and are shown in figures 36 and 37. The temperature difference measured between the absolute and differential thermocouples were close. The temperature shown in figure 36 is the difference between the two 2.5 μm and 7.1 μm coatings. The large temperature spikes shown during the first 10-30 sec, occur during the insertion of the test models in the arc stream and immediately thereafter. They could be attributed to the differential heating of the coatings during insertion since the coatings were separated in a vertical position in the model.

The test results can be summarized as follows:

- The optimum reflective coating thickness is 2.2–2.5 μm.
- The coating optical properties do not degrade after exposure to this heating environment of 34.8 $Btu/ft^2 \cdot s$.
- At the heating rate of 33.4 $Btu/ft^2 \cdot s$ in the arc-jet, the coating was 52°F hotter than the RCG coating.
- The coating can be effective in reducing the surface temperature provided a large (>15%) fraction of the heating environment is radiative.

- The differential thermocouples provide an accurate method of verifying the thermocouple measurements.

THERMAL CONDUCTIVITY TESTS

To provide input data for thermal analysis of the test results and relate them to the AFE environment, it is necessary to know the thermal and optical properties of the rigid and flexible insulations. This section describes the thermal conductivity measurements of the flexible and rigid insulations.

Flexible Insulations

The thermal conductivity of the flexible insulations was determined using a procedure described previously (ref. 8). Figures 38 and 39 show the apparent thermal conductivity of the two uncoated CFBI and TABI insulations. Samples were evaluated at pressures of 1, 0.1, and 0.01 atmosphere at each test temperature. The samples were tested in ascending temperature order, with all three pressure conditions evaluated prior to the test apparatus being brought up to the next higher temperature. Nitrogen gas was used as the cover gas, in an attempt to protect the specimens and the test equipment from oxidation. The apparent average thermal conductivity of the uncoated CFBI interlock is lower than the uncoated TABI layer-to-layer. This is attributed to effectiveness of the multilayer reflective foils as described previously (ref. 9).

Rigid Insulations

The thermal conductivity of the rigid insulations was measured using a procedure described previously (ref. 10). Figures 40 through 42 show the thermal conductivity of AETB-12, AETB-8 and ASMI at 1, 0.1, and 0.01 atmospheres as a function of temperature. The thermal conductivity of ASMI is approximately similar to AETB-8 and AETB-12 at 0.01 Atm at 2250°F, but significantly lower at 0.1 atmosphere. The above thermal conductivity values were utilized to calculate the thermal profiles of the rigid and flexible insulations discussed in the Thermal Analysis Section.

EMISSIVITY TESTS

To calculate the surface temperatures of the fabric in the flexible insulation, it is necessary to know its optical properties at elevated temperatures. The test methodology used to determine the emittance of the uncoated fabrics and the coated fabrics is described below. The emissivities of two different types of uncoated silicon carbide fabrics, 5 harness satin weave and interlock, were determined at 2000°F, 2100°F, and 2200°F.

The first test system consisted of a concentric cylinder system. The fabric was applied to the outer surface of the inner cylinder and instrumented with surface thermocouples. A high-temperature electric heater was located inside the inner cylinder, supplying the heat being transferred in the test system. The inner cylinder was surrounded by a second cylinder whose surface temperatures were also measured with attached thermocouples. A third, still larger diameter cylinder, surrounded the second cylinder completing the concentric system. This was then positioned under a stainless steel bell jar, where a vacuum could be created. The heat emitted by the central electric heater was monitored by laboratory volt and ammeters. A pressure gage indicated the vacuum level in the test system during the run. The fundamental equation relating the transfer of radiant energy to the emissivity is given:

$$\left(\frac{q}{A}\right)_{rad} = \frac{\sigma}{\frac{1}{\varepsilon_1} + \frac{A_1}{A_2}\left(\frac{1}{\varepsilon_2} - 1\right)}\left[T_1^4 - T_1^4\right]$$

Where:

σ, Stefan Boltzmann constant, 0.1714×10^{-8} Btu/hr•ft^2•°R^4

ε_1, gray body emissivity of inner cylinder surface (test fabric)

ε_2, gray body emissivity of surrounding cylinder surface

T_1, absolute surface temperature of inner cylinder surface (test fabric), °R

T_2, absolute surface temperature of surrounding cylinder surface, °R

A_1, radiating area of inner cylinder, ft^2

A_2, radiating area of surrounding cylinder, ft^2

The radiation flux, (q/A) rad, was determined from the heat output of the electric heater and corrected with a vacuum gas conduction term, which is negligible.

The second emissivity test system consisted of a ceramic cup whose bottom could be fitted with samples of test fabrics. The fabric surface temperatures were measured by fine gage thermocouples threaded into the fibers. This 2-in. diameter cup was oriented in a horizontal position so that the flames from an oxyacetylene torch could play into the open end of the cup. At a fixed distance of 13 in. from the surface of the cup, a vertical heat flux transducer was positioned so that the radiant flux from the 2-in. diameter disk of the test fabric could be measured. The heat flux transducer was very thin and had previously been accurately calibrated. By measuring the diameter of the hot fabric disk and its distance from the heat meter (which were normally aligned), the radiation factor is determined. The equation used to relate the emissivity to the measured radiant energy is given:

$$G = \varepsilon\sigma\left(\frac{a^2}{a^2 + b^2}\right)T_f^4$$

Where:

G, radiant flux falling on radiometer, Btu/hr•ft^2

ε, gray body emissivity of the fabric surface

σ, Stefan-Boltzmann constant, 0.1714×10^{-8} Btu/hr•ft^2•°R^4

a, radius of fabric disk, ft

b, distance between radiating surface of fabric disk and the heat meter (radiometer), ft

T_f, temperature of the fabric disk, °R

$(a^2/a^2 + b^2)$, angle factor for the radiation system

The two methods yielded results that were in good agreement. The systems were also checked on standard emissivity surfaces (Reynolds®[3] aluminum foil and high-emissivity surfaces). The emittance of the uncoated silicon carbide fabrics is shown as a function of temperature in figure 43. The CFBI interlock, which performed better in the plasma arc tests, showed slightly higher emittance than the 5 harness satin weave fabric. The interlock fabric emittance values were used for the thermal analysis of both the TABI and CFBI insulations. It was assumed that the optical properties of the TABI layer-to-layer fabrics were similar to the CFBI interlock fabrics.

The apparatuses used for the two methods described above are shown in figure 44.

THERMAL ANALYSIS

One-dimensional System Improved Numerical Differencing Analyzer (SINDA) (ref. 11) models were used to analyze the thermal responses of both rigid and flexible insulations. The rigid insulations analyzed include AETB-8, AETB-12 -12, and ASMI. The flexible insulations analyzed include uncoated and PCC coated CFBI interlock, as well TABI layer-to-layer.

Both in-depth and backface temperatures of the insulations were calculated under arc-jet test conditions to compare them with those measured by the thermocouples. The heat fluxes for the arc-jet tests were taken to be 58.7 and 34.3 Btu/ft^2•s for the rigid and flexible insulations, respectively, while the pressure was assumed to be at 0.01 Atm. The in-flight temperature responses were also predicted. The predicted AFE maximum-flux trajectory heat fluxes are shown in figure 2 "above

[3] Registered trademark of Reynolds Aluminum Corp.

right." The heat flux at S/L = 0.00 was used for the rigid insulation and S/L = 0.55 was used for the flexible insulation.

Figure 45 shows the components of the two thermal models used for both arc jet and AFE predictions. The rigid insulations, are bonded to a Nomex® Strain Isolation Pad (SIP) with Room Temperature Vulcanizing (RTV) silicone adhesive. The flexible insulations consist of silicon carbide fabrics and alumina battings. Both insulations are bonded to an aluminum plate. The bonding agent used is RTV560®.[4] The backface of the aluminum was assumed adiabatic.

Thermal conductivities of the insulations and the emittance of the interlock silicon carbide used in the models are shown in figures 38 through 43. A constant emittance of 0.85 was used for the RCG coating. The SINDA models linearly interpolate or extrapolate the thermal properties as functions of both temperature and pressure, as required. It should be noted that because the calculated insulation temperatures exceed the temperatures of which the thermal properties were measured, uncertainties due to extrapolation to high temperatures may be significant.

Figures 46-49 show the results of analyses performed for four different flexible insulations: uncoated CFBI interlock, PCC coated CFBI interlock, uncoated TABI layer-to-layer, and PCC coated TABI layer-to-layer.

Figures 46 through 49 "above" are the calculated thermal profiles of the insulations when the plasma arc test conditions are imposed on the models. These figures represent the uncoated CFBI interlock, PCC coated CFBI interlock, uncoated TABI layer-to-layer and PCC coated layer-to-layer. These thermal profiles are comparable to the measured temperature profiles shown for similar materials shown in figures 15, 21, 9, and 19, respectively. The measured and calculated thermal profiles are comparable only for the maximum surface temperatures. The heat-up and cool-down profiles are different possibly due to the ceramic holder that surrounded the plasma arc test specimen. The ceramic holder provided for slower heat-up and cool-down periods for the flexible insulation test specimen, while the calculated values do not take into account the rigid insulation holder. The measured and calculated aluminum temperatures correspond well.

Figures 46 through 49 "below" are the thermal profiles of the same uncoated and coated flexible insulations when the AFE maximum heating rate profile at S/L = 0.55, shown in figure 2 "above right," is imposed.

The uncoated CFBI interlock reaches 495°F at the aluminum (fig. 46 "below") while the PCC coated CFBI interlock reaches 434°F at the aluminum (fig. 47 "below"). Both of these insulations survived the maximum heating rate plasma arc tests. The uncoated TABI layer-to-layer reaches 595°F at the aluminum (fig. 48 "below") while the PCC coated TABI layer-to-layer reaches 533°F at the aluminum (fig. 49 "below").

The PCC coated CFBI and TABI insulations show a significantly lower surface temperature than the uncoated insulations. The uncoated TABI layer-to-layer did not survive the plasma arc tests and the fabric was damaged. Again, it should be emphasized that the aluminum temperatures shown are

[4] Registered Trademark of General Electric Co.

for a thin 0.032-in. adiabatic aluminum skin and lower temperatures will be encountered for an aluminum skin with aluminum stringers attached.

Figures 50 through 52 show the results of the thermal analysis of RCG coated AETB-8, AETB-12 and ASMI rigid insulations.

Figures 50 through 52 "upper" are the thermal profiles of the insulations when the plasma arc test conditions are imposed on the models. The calculated thermal response of the insulations correlates well with the measured surface and 0.1 in. depth temperatures shown in figures 25, 27, and 30. A discrepancy of 200-250°F was observed at 0.35 in. depth.

Figures 50 through 52 "below" are the thermal profiles of the insulations when the AFE maximum heating rate at S/L = 0.00 shown in figure 2 "above right" is imposed on the insulations. The primary purpose of these calculations was to estimate the aluminum temperature on the backface of the insulations.

The model utilized a rather thin aluminum skin. In an actual application, this aluminum skin is welded directly to massive aluminum stringers, thus resulting in much lower temperatures of the aluminum skin. More complex calculations will have to be performed to allow for this heat transfer from the aluminum skin to the stringers, thus establishing more realistic backface temperatures.

The AETB-8 reached a maximum backface temperature of 548°F at 20 min, the AETB-12, 494°F at 23 min and the ASMI, 469°F at 23 min.

The results of the analysis can be summarized as follows:

In regards to the flexible insulations:

- At the arc jet condition of 34 Btu/ft^2•s, the maximum measured backface aluminum temperatures for the uncoated CFBI and TABI were 409°F and 388°F, respectively. The calculated temperature from the model under similar conditions were 289°F and 307°F, respectively.

- A good correlation between the measured (117°F) and calculated (82°F) values was obtained in regard to the temperature difference between the backface of the PCC coated CFBI and PCC coated TABI insulations. The measured values were 380°F and 460°F, respectively, for the CFBI and TABI and the calculated values were 246°F and 363°F. The higher measured values could be attributed to the test model holder which surrounded the flexible insulation on the sides and back. The higher values (both measured and calculated) shown for the TABI are attributed to the higher thermal conductivity of this insulation.

- At the maximum AFE heating rate condition of 36 Btu/ft^2•s, the calculated aluminum temperatures for the model for the PCC coated CFBI and TABI were 434°F and 533°F, respectively.

- Lower aluminum temperatures are expected for both the rigid and flexible insulations as a result of additional aluminum mass (stringers). Additional calculations will have to be performed to define these temperatures.

In regards to the rigid insulations:

- At the maximum AFE heating rate condition, the backface aluminum temperature was $\geq 468°F$ for all insulations.

CONCLUSIONS

The thermal responses of rigid and flexible insulations and surface temperatures of a reflective coating subjected to aeroconvective heating from a plasma arc were determined. In addition, the thermal conductivities of both the rigid and flexible insulations were determined. The emissivity of the fabrics used in the flexible insulations were also measured. Based on these measurements and the thermal analysis discussed, the following conclusions may be made:

All the rigid insulations exhibited excellent survivability performance up to heating rates of 47 $Btu/ft^2 \cdot s$ and the AETB-12 up to 58 $Btu/ft^2 \cdot s$. These rigid insulations exhibited no physical damage when exposed to these heating rates at the test times indicated previously. However, a 0.032-in. aluminum skin under these insulations without stringers would exceed the design limit of 350°F.

The uncoated flexible insulations exhibited good thermal performance up to 31 $Btu/ft^2 \cdot s$, but some fabric failures occurred at heating rates of 34 $Btu/ft^2 \cdot s$. There was no damage to either fabric or insulation when these flexible insulations were coated with a PCC coating at these heating rates. As in the case of the rigid insulations, a thin aluminum skin would exceed the design limit of 350°F at the maximum heating rate condition of an aerobrake such as the AFE.

The optical properties of the reflective coating do not degrade up to a heating rate of 35 $Btu/ft^2 \cdot s$. The calculations indicate that this high reflective coating would be effective in reducing surface temperatures on RCG coated rigid insulations, if the radiative heating is in excess of 15% of the total heating rate on the aerobrake surface.

REFERENCES

1. Aeroassist Flight Experiment (AFE) Integrated Experiment Interface Requirements Document. NASA-MSFC-RQMT-1713 (December 1989).

2. Aerobrake Aeroheating Analysis for 4500 lb AFE for Nominal Peak Heat Load and Peak Heating Rate Trajectories. LESC Report ADP794 (February 1990).

3. Data Book Documentation, AFE Aerobrake Aerothermodynamic Data Book for Baseline V Trajectory Vol III: Baseline VA Heating Environment Along Plane. NASA-JSC No.23623 (October 1990).

4. Data Book Documentation Third Edition, AFE Aerobrake Aerothermodynamic Data Book for Baseline VA Trajectory, Part 1 Methodology and Results. NASA-JSC-25230 (September 1991).

5. Goldstein, H. E.: Fibrous Ceramic Insulations. NASA CP-2251 (November 1982).

6. Stewart, D. A.; Goldstein, H. E.; and Leiser, D. B.: High Temperature Glass Thermal Control Structure and Coating. U. S. Patent 4,381,333 (April 1983).

7. Kourtides, D. A.; Churchward, R. A.; and Lowe, D. M.: Protective Ceramic Coating for Ceramic Fabrics. U. S. Patent Application, NASA Case No. ARC 11969-1CU (July 1991).

8. ASTM C-177-85, Steady State Heat Flux Measurements and Thermal Transmission Properties by Means of the Guarded Hot Plate Apparatus. American Society of Testing Materials, Philadelphia, PA. (1985).

9. Kourtides, D. A.; Tran, H. K.; and Chiu, S. A.: Composite Flexible Insulation for Thermal Protection of Space Vehicles. NASA TM-103836 (February 1991).

10. Hong, A. E.: Thermal Characterization Test of Alternate Thermal Protection Materials (ATPM). Memorandum NASA-JSC ES 3-91-049 (March 1991).

11. Cullimore, B.; Goble, M.; Jenson, C.; and Ring, S.: SINDA '85/FLUINT, Systems Improved Numerical Differencing Analyzer and Fluid Integrator. Martin Marietta Corp., Denver, CO. (August 1986).

12. Alternate Thermal Protection Materials Experiment (ATPM) Fabrication of Composite Flexible Blanket Insulation (CFBI). NASA-ARC Document 9SP-9001-XR17.

Table 1. Comparison of AFE heating rates, radiation equilibrium temperatures and pressures with those obtained in plasma arc tests

	Baseline VA Nominal Adjusted					
Rigid or flexible insulation location and time	AFE maximum heating rate, Btu/ft^2•s	Plasma arc calculated heating rate, Btu/ft^2•s	AFE maximum radiative equilibrium temperature, °F	Plasma arc maximum calibrated temperature measured, °F	AFE stagnation pressure, psi	Plasma arc calculated stagnation pressure, psi
S/L 0.000 @ 117 s	45.0	47.0[a]	2789	2823[a]	0.45	0.69
S/L 0.456 @ 117 s	30.5	30.7[b] & 33.4[c]	2487	2491[b] & 2553[c]	0.36	0.35 – .38
	Baseline VA Nominal Adjusted Plus Methodology Uncertainty					
Rigid or flexible insulation location and time	AFE maximum heating rate, Btu/ft^2•s	Plasma arc calculated heating rate, Btu/ft^2•s	AFE maximum radiative equilibrium temperature, °F	Plasma arc maximum calibrated temperature measured, °F	AFE stagnation pressure, psi	Plasma arc calculated stagnation pressure, psi
S/L 0.000 @ 117 s	54.0	58.7[a]	2939	3010[a]	N/A	1.12
S/L 0.456 @ 117 s	36.6	34.3[b] & 34.8[c]	2624	2574[b] & 2586[c]	N/A	0.40 – 0.41

a = tiles; b = blanket; c = reflective coating

Table 2. Plasma arc test conditions for flexible insulations (*) reflective coating (**) and rigid insulations (***)

Target RCG surface temperature, °F	Current, amps	Arc-jet pressure, psia	Calculated stagnation pressure, psi	Calibration temperature measured, °F	Model distance from exit, in.	Calculated heat flux rates, Btu/ft^2•s
2499 *	1200	25	0.35	2491	14.00	30.7
2577 *	1350	25	0.40	2574	14.00	34.3
2499 **	1100	15	0.38	2553	13.75	33.4
2577 **	1300	15	0.41	2586	13.75	34.8
2830 ***	2150	45	0.69	2823	13.75	47.0
2929 ***	2000	40	1.12	3010	10.00	58.7

Table 3. Description of flexible insulation materials

Designation	Description of materials
Uncoated TABI layer-to-layer	Tailorable advanced blanket insulation (TABI) top fabric silicon carbide (Nicalon®[a] NLM 202), 600 denier layer to layer, alumina (Saffil®[b]) insulation and bottom fabric same as top fabric, blankets density 9.9 lb/ft^3
Uncoated TABI angle interlock	Tailorable advanced blanket insulation (TABI) top fabric silicon carbide (Nicalon® NLM 202) 600 denier angle interlock weave, alumina (Saffil®) insulation and bottom fabric same as top fabric, complete insulation density 9.5 lb/ft^3
RCG coated TABI layer-to-layer	Same as uncoated TABI layer-to-layer except brush coated with 1.0 oz /ft^2 RCG coating
PCC coated TABI layer-to-layer	Same as uncoated TABI layer-to-layer except brush coated with 1.0 oz /ft^2 protective ceramic coating
Uncoated CFBI 5HSW	Composite flexible blanket insulation (CFBI) top fabric silicon carbide (Nicalon® NLM 202), 5 harness satin weave, (5HSW) 600 denier, fabric weight 8 lb/ft^2; alumina (Saffil®) insulation, 10 alternating layer of polymide (Kapton®[c]) film, 0.003 in. thick coated on one side with 1000 angstroms vacuum deposited aluminum and aluminoborosilicate (Nextel 312®[d]) lino weave scrim cloth 0.013 lb/ft^2 bottom fabric aluminoborosilicate (Nextel 312®) fabric, 0.11 lb/ft^2, complete insulation density 9.9 lb/ft^3
Uncoated CFBI interlock	Composite flexible blanket insulation (CFBI) top fabric silicon carbide (Nicalon® NLM 202) 600 denier, interlock, balance of insulation similar to uncoated CFBI 5HSW , complete insulation density 13.0 lb/ft^3 (ref. 12)
RCG coated CFBI interlock	Same as uncoated CFBI interlock except brush coated with 1.0 oz/ft^2 RCG coating
PCC coated CFBI interlock	Same as uncoated CFBI interlock except brush coated with 1.0 oz/ft^2 PCC coating

[a]Registered Trademark of Dow Corning Corp.

[b]Registered Trademark of ICI Corp.

[c]Registered Trademark of Dupont de Nemours Corp.

[d]Registered Trademark of 3M Corp.

Table 4. Description of rigid insulation materials

Designation	Description of materials
AETB-12/RCG	Alumina enhanced thermal barrier (AETB-12, 12 lb/ft^3) with RCG coating
AETB-8/RCG	Alumina enhanced thermal barrier (AETB-8, 8 lb/ft^3) with RCG coating
ASMI/RCG	Alumina sol modified insulation (ASMI, 12 lb/ft^3) with RCG coating

Table 5. Description of reflective coating materials

Designation	Description of materials
FRCI-12/RCG/2.2 μm	Fibrous refractory composite insulation (FRCI-12, 12 lb/ft^3) half coated with reaction cured glass (RCG) and half coated with RCG, silica (Spectrosil®) and 2.2 μm thick alumina (Ceralox®) coating
FRCI-12/RCG/2.5 μm, 7.1 μm	Fibrous refractory composite insulation (FRCI-12 ,12 lb/ft^3) half coated with RCG, silica (Spectrosil®), 2.5 μm thick alumina (Ceralox®) coating and half with RCG, silica (Spectrosil®), and 7.1 μm alumina (Ceralox®) coating

Table 6. Calculated surface temperatures of RCG and RCG/reflective coating as function of various radiative heating rates at S/L = 0.55, baseline VA trajectory

Radiative heating rate, Btu/ft^2•s	Convective heating rate, Btu/ft^2•s	Total heating rate, Btu/ft^2•s	Time, sec	Surface temperature FRCI-12/RCG, °F	Surface temperature FRCI-12/RCG/ alumina overlay, °F	Δ°F
0	27.3	27.3	115	2354	2469	+115
4.0	23.5	27.5	118	2353	2381	+28
8.2	19.1	27.3	115	2334	2249	–85
12.3	15.0	27.3	115	2324	2093	–231

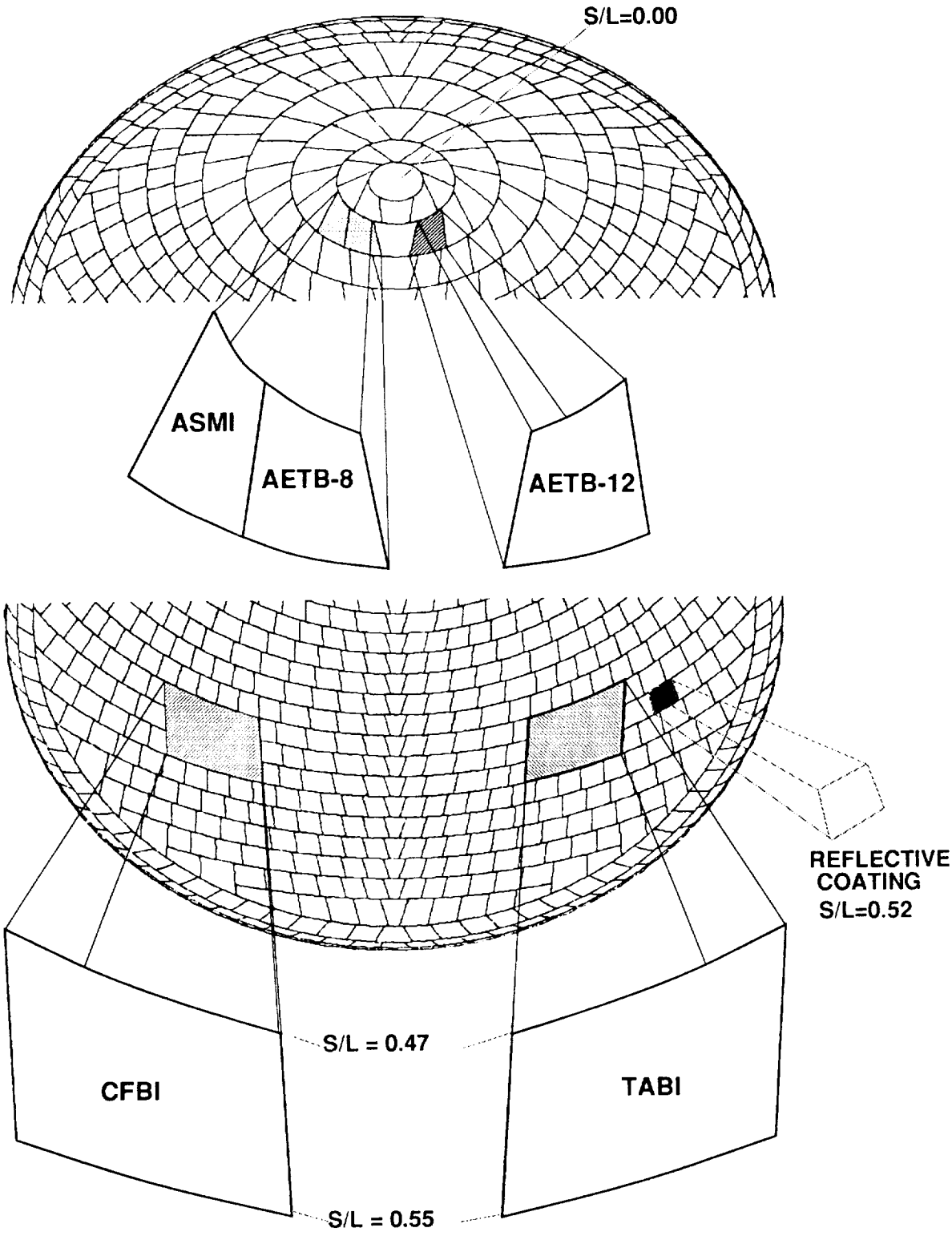

Figure 1. Location of rigid tiles, flexible insulations, and reflective coating on the AFE aerobrake.

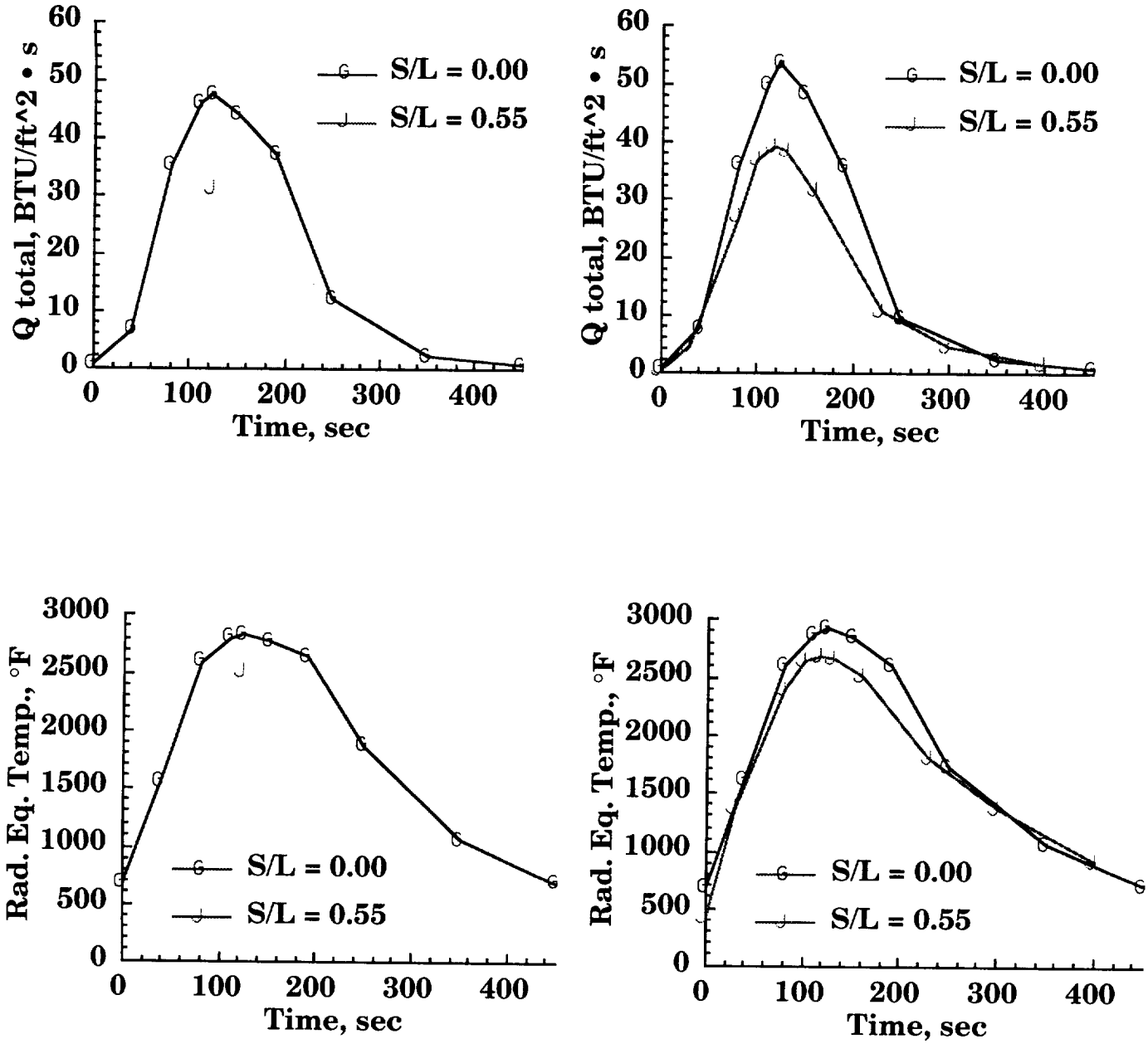

Figure 2. Baseline VA nominal adjusted trajectory: nominal heating rate (above left), nominal heating rate plus methodology uncertainty (above right), nominal RCG radiation equilibrium temperatures (bottom left), nominal RCG radiation equilibrium temperatures plus methodology uncertainty (bottom right).

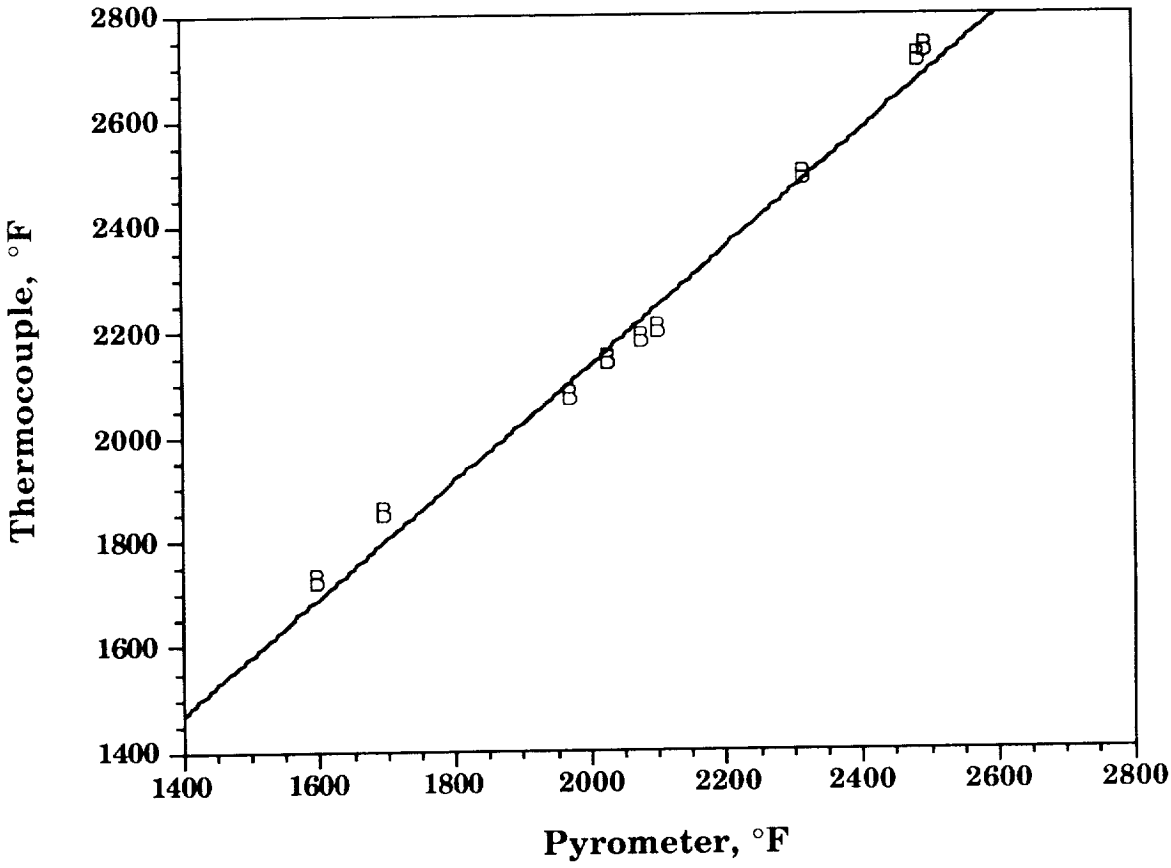

Figure 3. Correlation of thermocouple and pyrometer readings for FRCI-12/RCG.

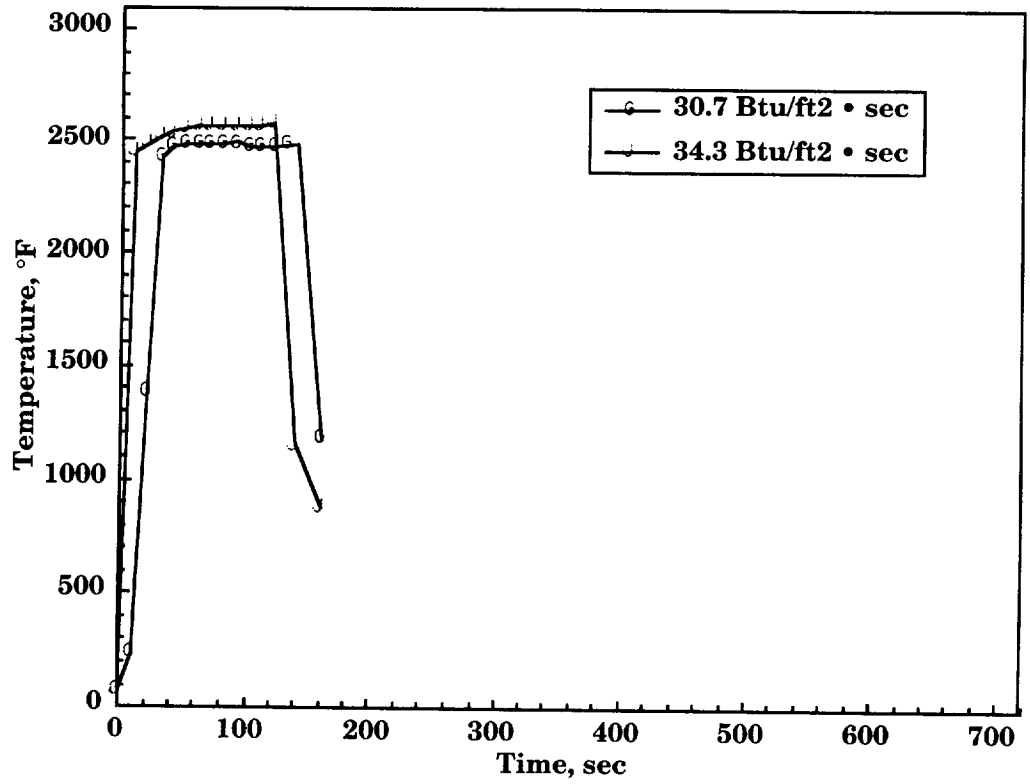

Figure 4. FRCI calibration for flexible insulation at 30.7 Btu/ft^2•s and 34.3 Btu/ft^2•s.

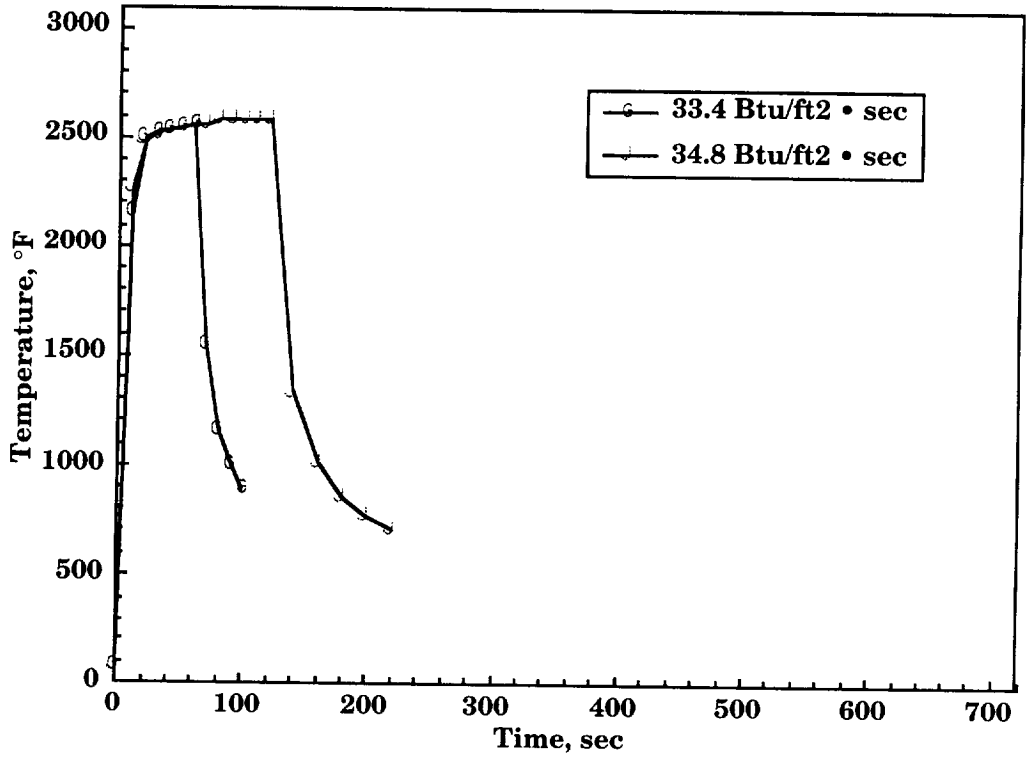

Figure 5. LI-2200 calibration for reflective coating at 33.4 Btu/ft^2•s and 34.8 Btu/ft^2•s.

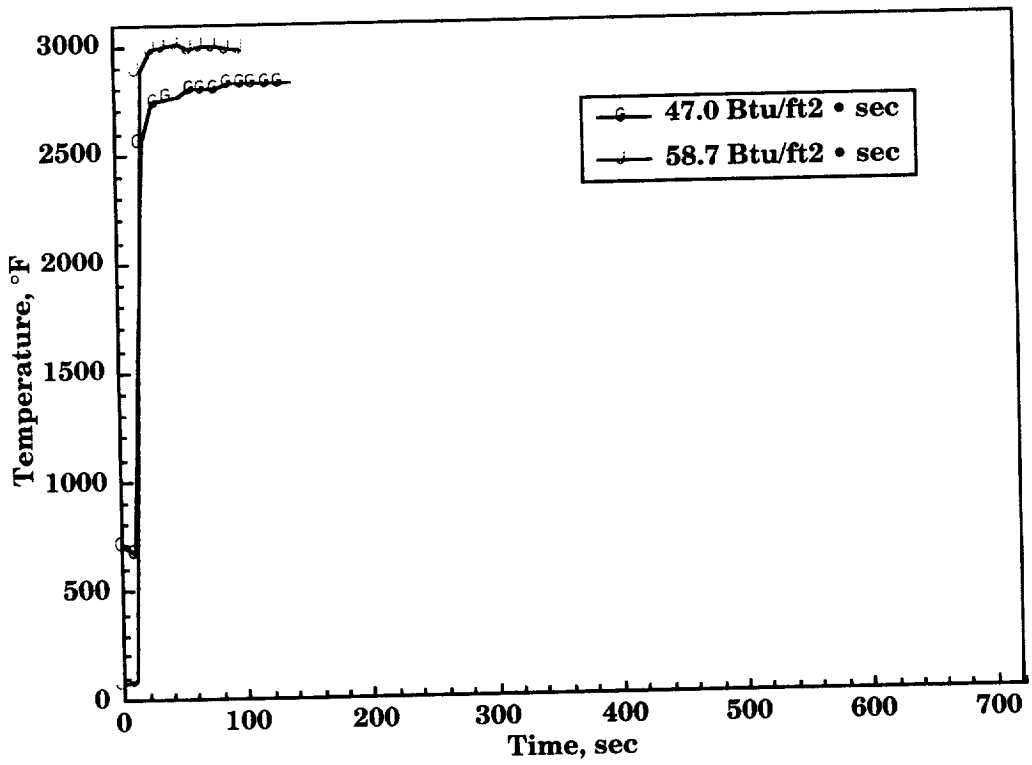

Figure 6. LI-2200 calibration for rigid tiles at 47.0 Btu/ft^2•s and 58.7 Btu/ft^2•s.

FIVE HARNESS SATIN WEAVE

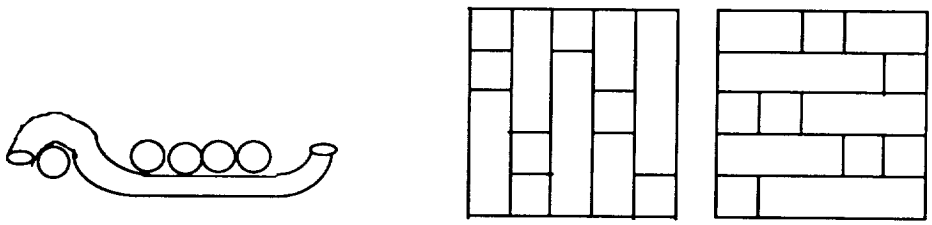

INTERLOCK FABRIC

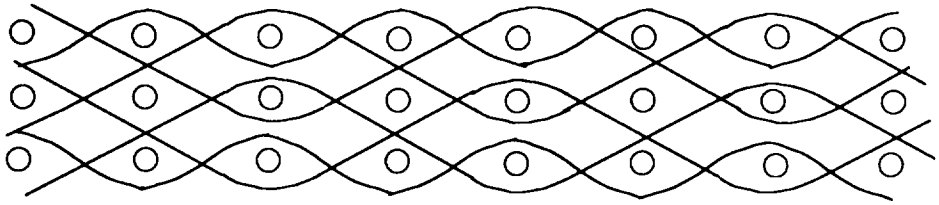

○ = Picks or fill

~ = Warp and binder yarn

Yarn : Nicalon R type 202 size P, 600 denier, 200 filaments/tow

Fabric Yarn Count: 93/inch (warp) x 87 inch (fill) ± 5%

Fabric Width: 30.5 inch minimum

Fabric Weight: 15.7 ±5% oz/yd^2

Fabric Thickness: 0.025 inch ±10%

Weave Type: Interlock 3 ply as shown above

Figure 7. Fabric architecture of CFBI blankets.

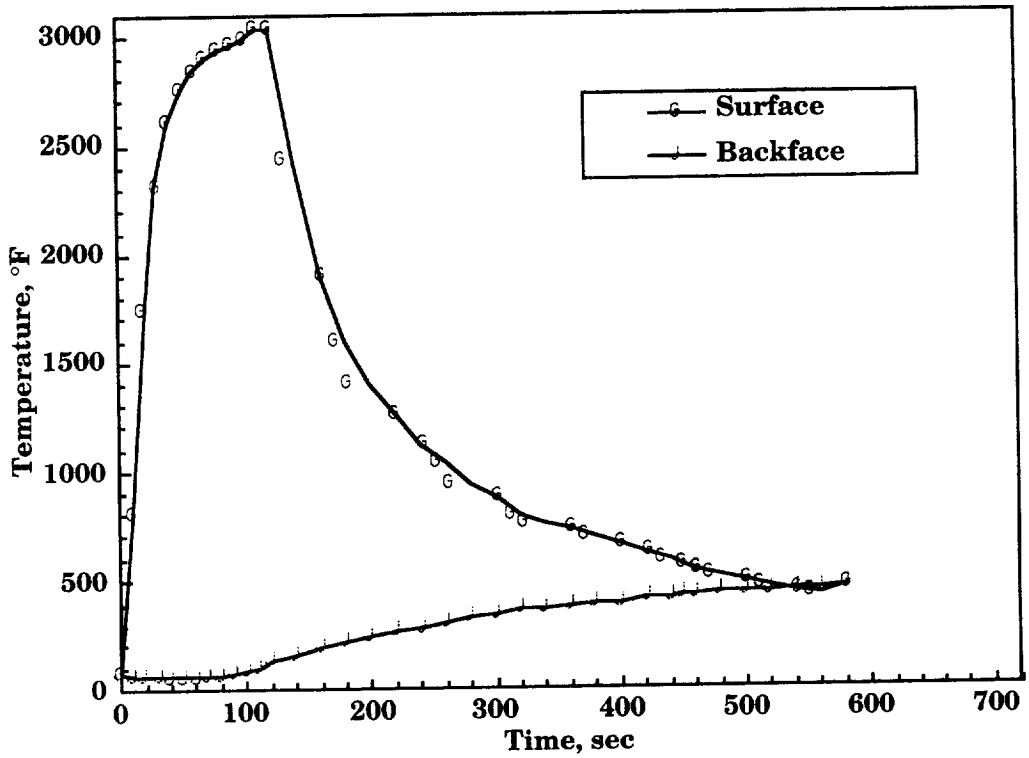

Figure 8. Thermal response of uncoated TABI layer to layer at 30.7 Btu/ft^2•s.

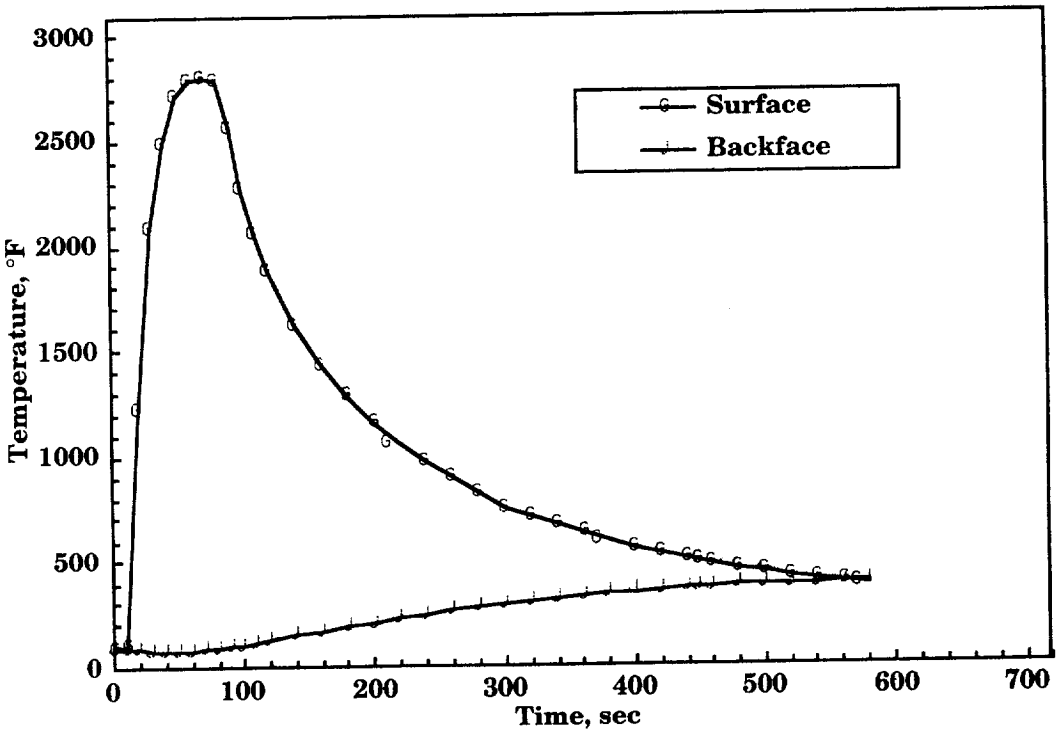

Figure 9. Thermal response of uncoated TABI layer to layer at 34.3 Btu/ft^2•s.

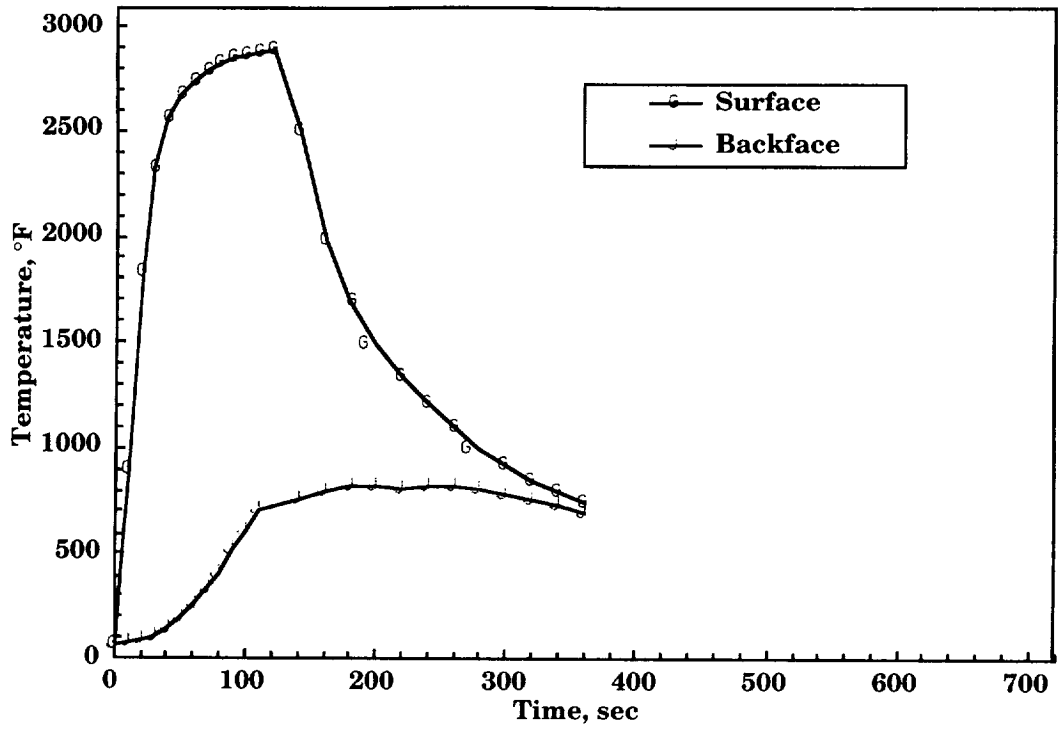

Figure 10. Thermal response of uncoated TABI angle interlock at 30.7 Btu/ft^2•s.

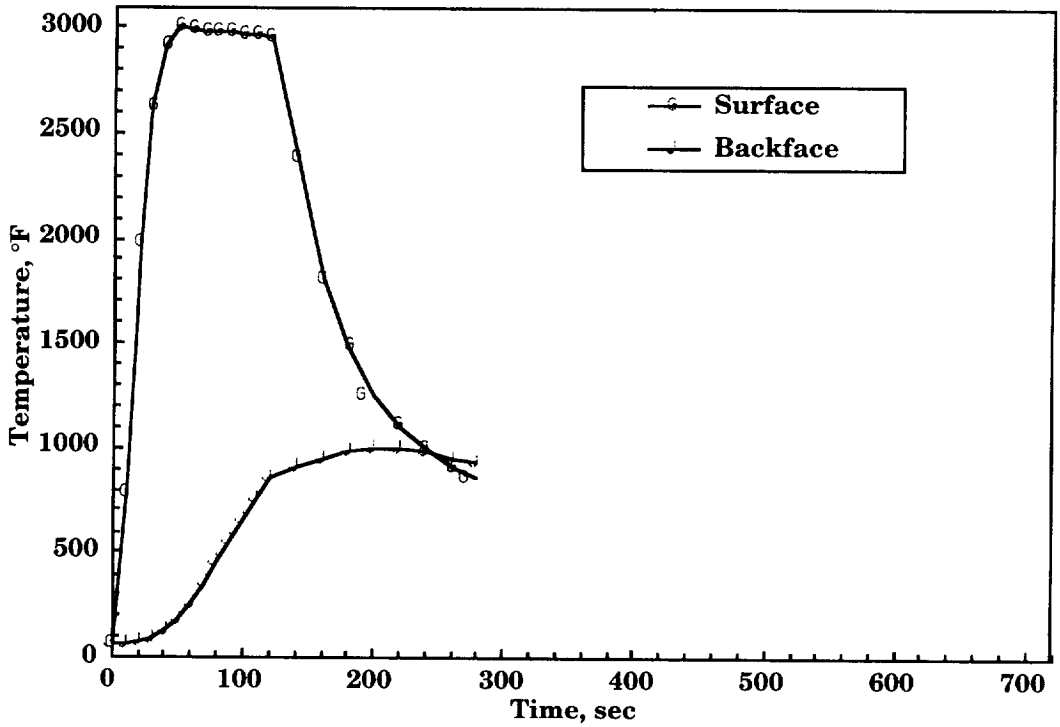

Figure 11. Thermal response of uncoated TABI angle interlock at 34.3 Btu/ft^2•s.

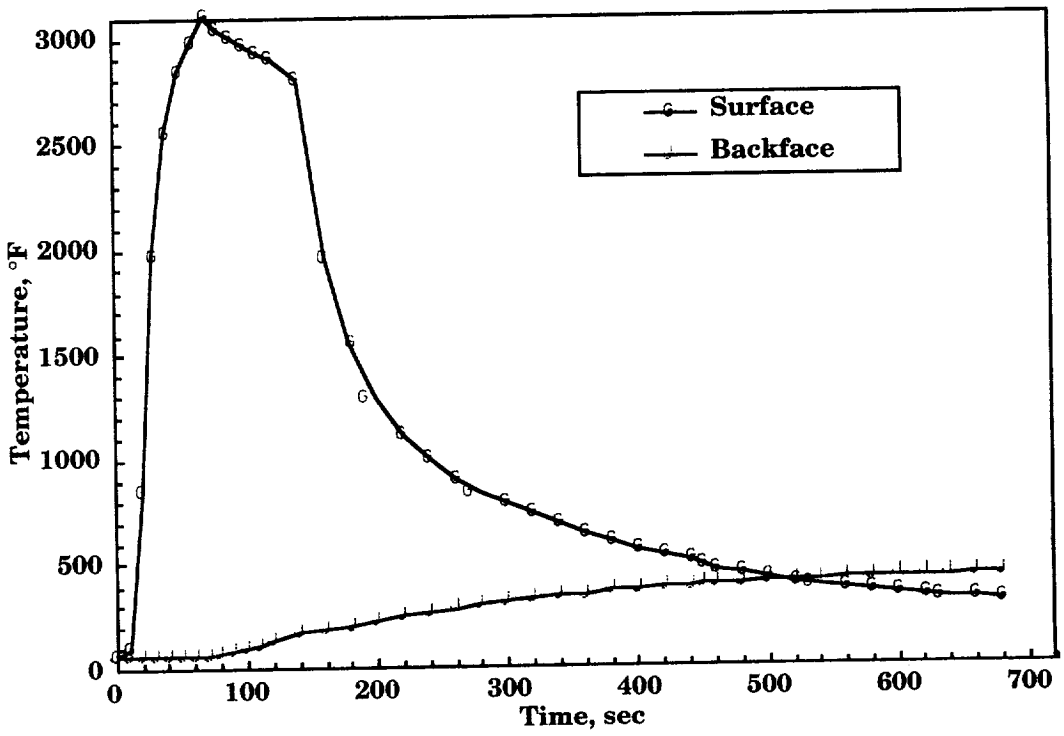

Figure 12. Thermal response of uncoated CFBI 5HSW at 30.7 Btu/ft^2•s.

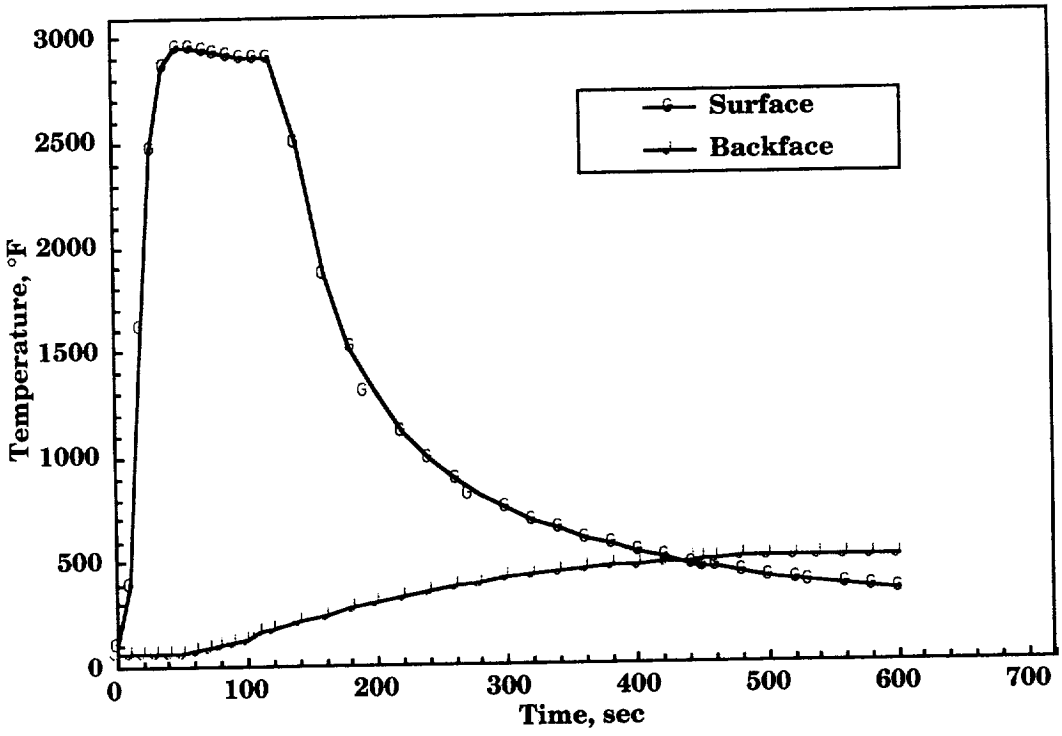

Figure 13. Thermal response of uncoated CFBI 5HSW at 34.3 Btu/ft^2•s.

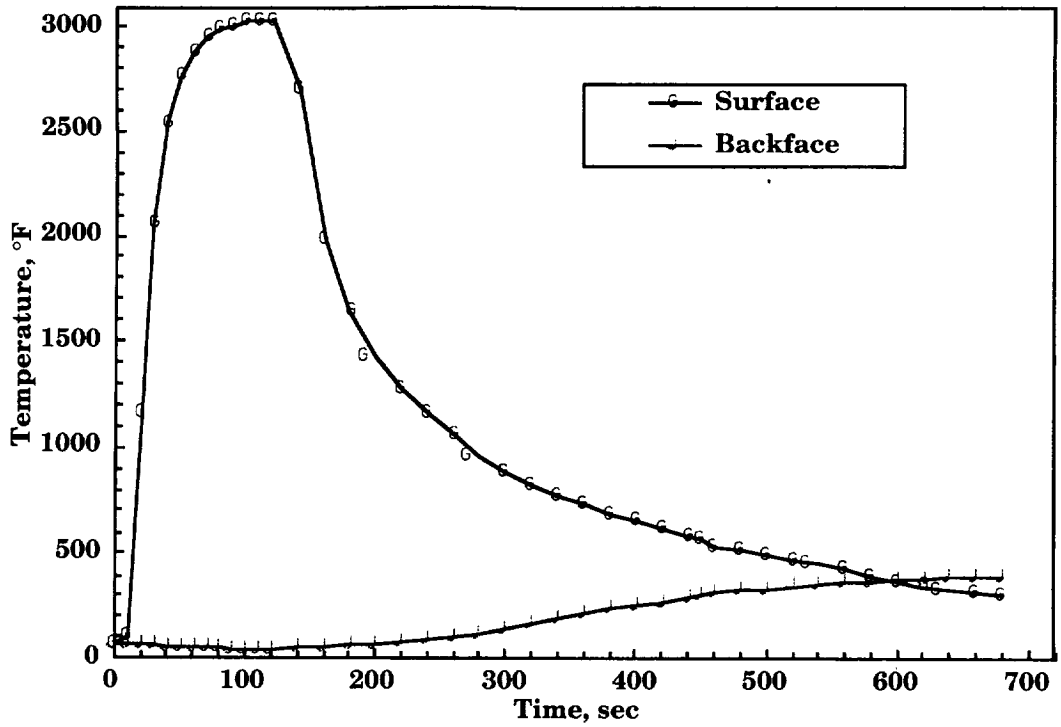

Figure 14. Thermal response of uncoated CFBI interlock at 30.7 Btu/ft^2•s.

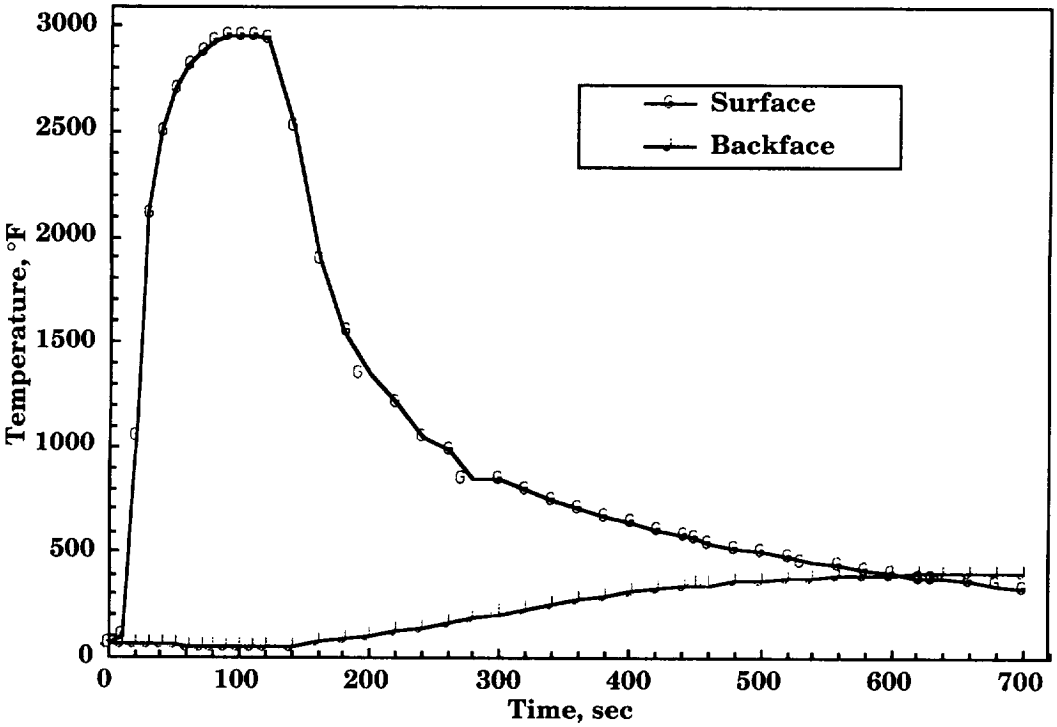

Figure 15. Thermal response of uncoated CFBI interlock at 34.3 Btu/ft^2•s.

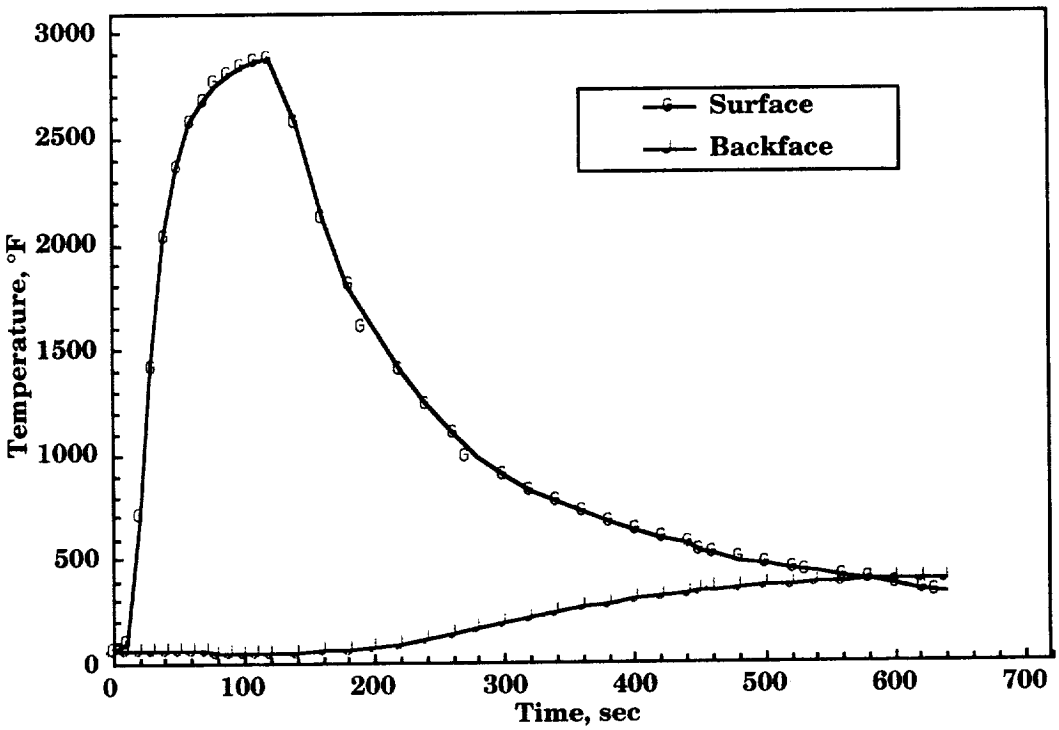

Figure 16. Thermal response of RCG coated CFBI interlock at 34.3 Btu/ft^2•s.

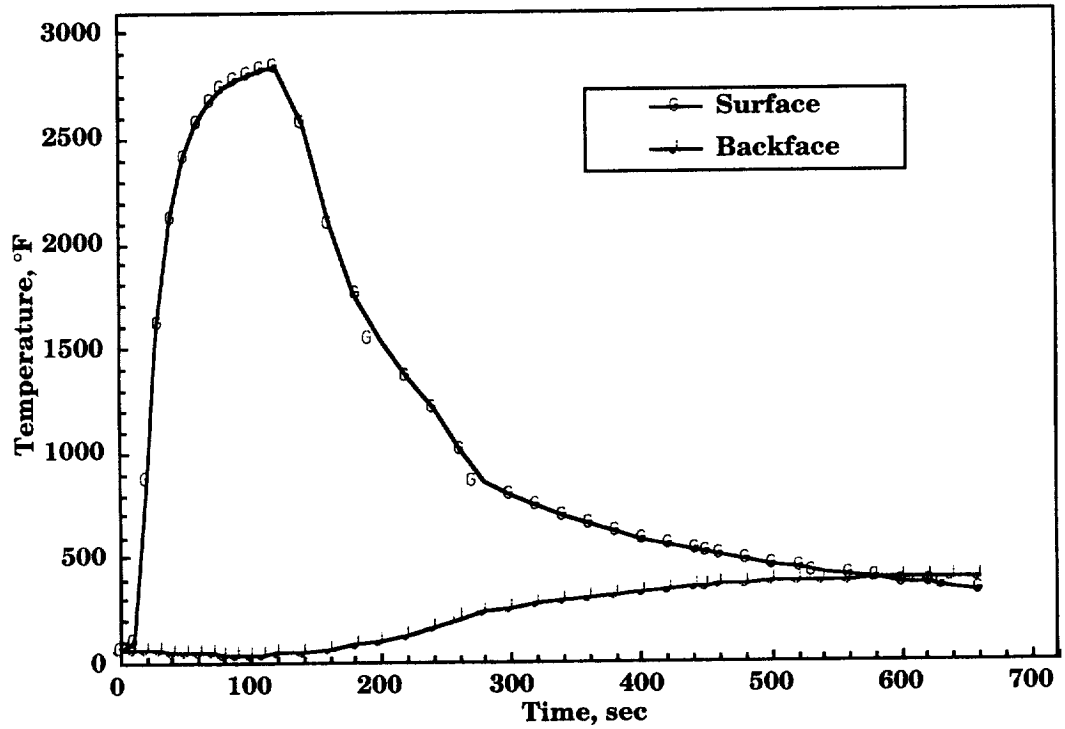

Figure 17. Thermal response of PCC coated CFBI interlock at 34.3 Btu/ft^2•s.

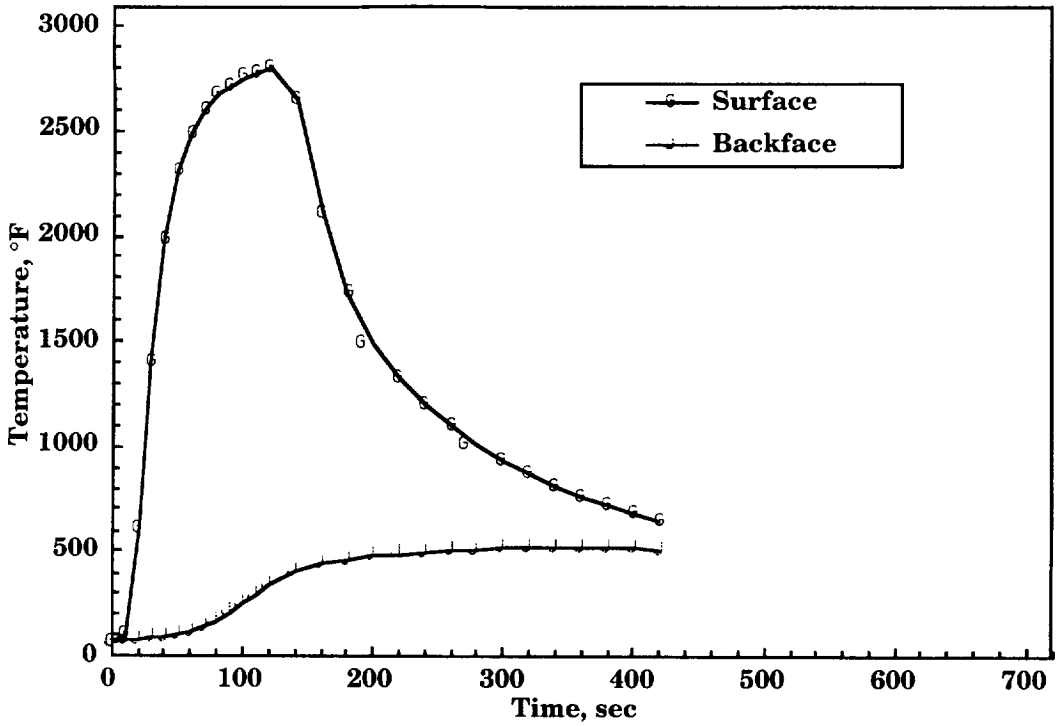

Figure 18. Thermal response of RCG coated TABI layer to layer at 34.3 Btu/ft^2•s .

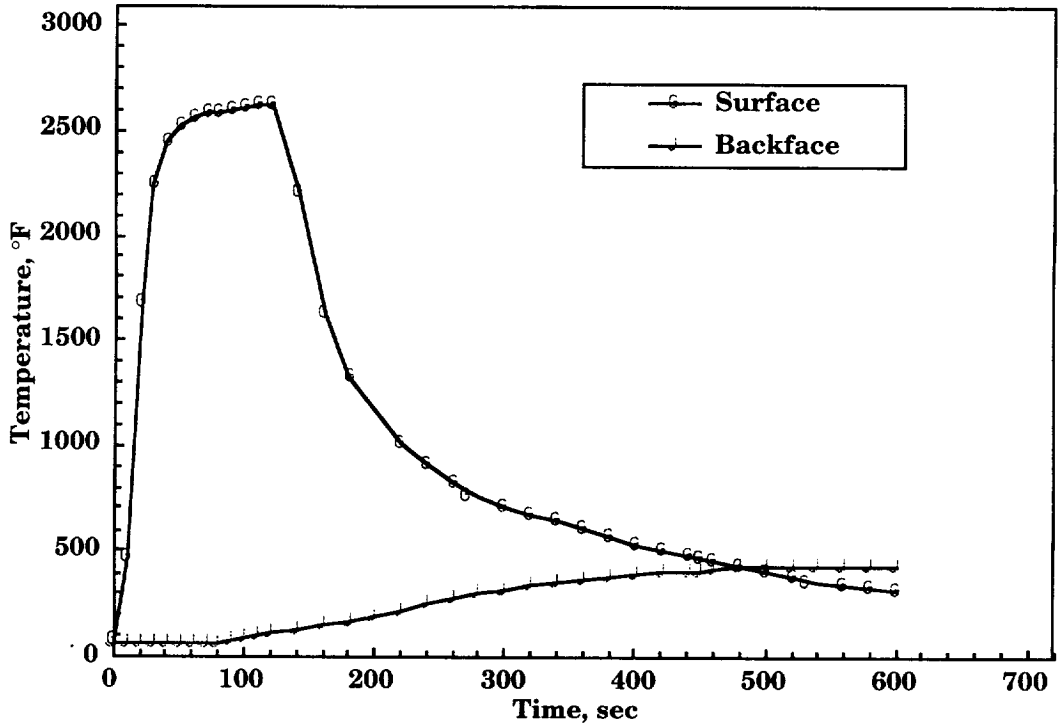

Figure 19. Thermal response of PCC coated TABI layer to layer at 34.3 Btu/ft^2•s.

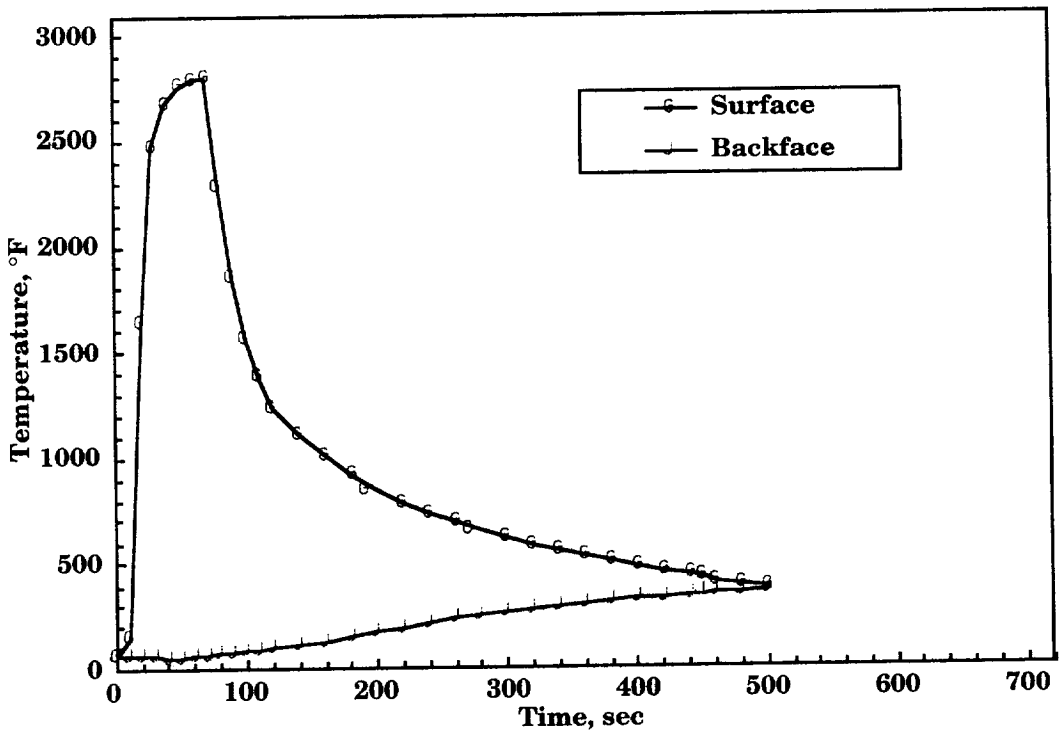

Figure 20. Thermal response of compressed RCG coated CFBI interlock at 34.3 Btu/ft^2•s.

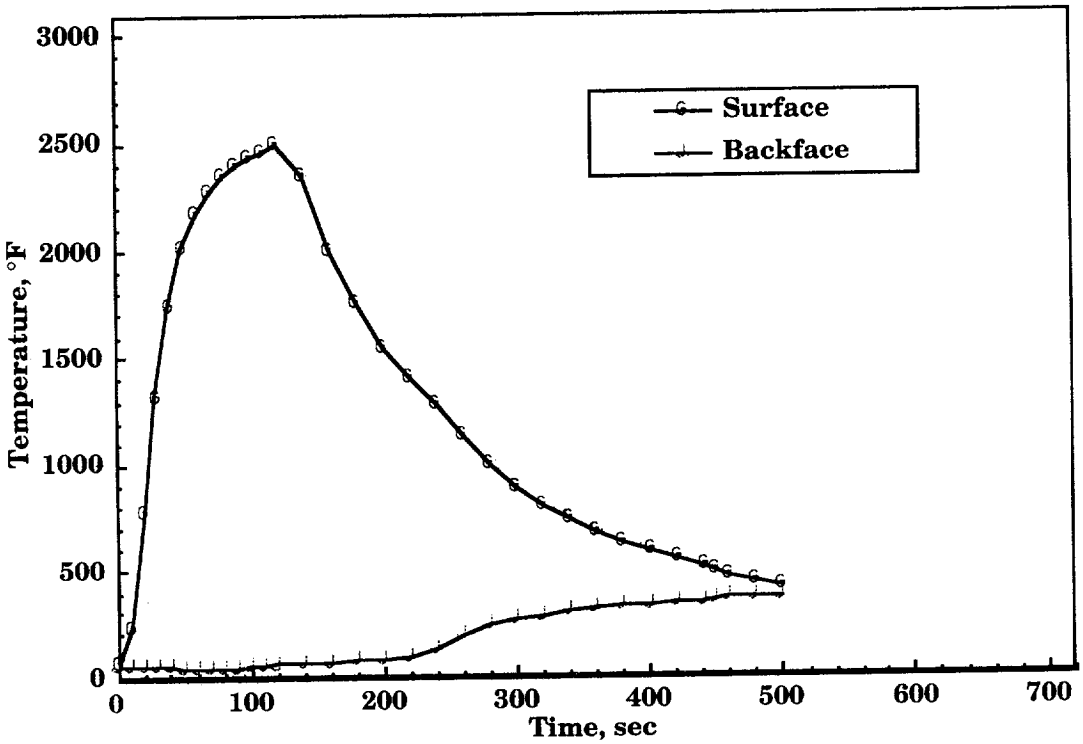

Figure 21. Thermal response of compressed PCC coated CFBI interlock at 34.3 Btu/ft^2•s.

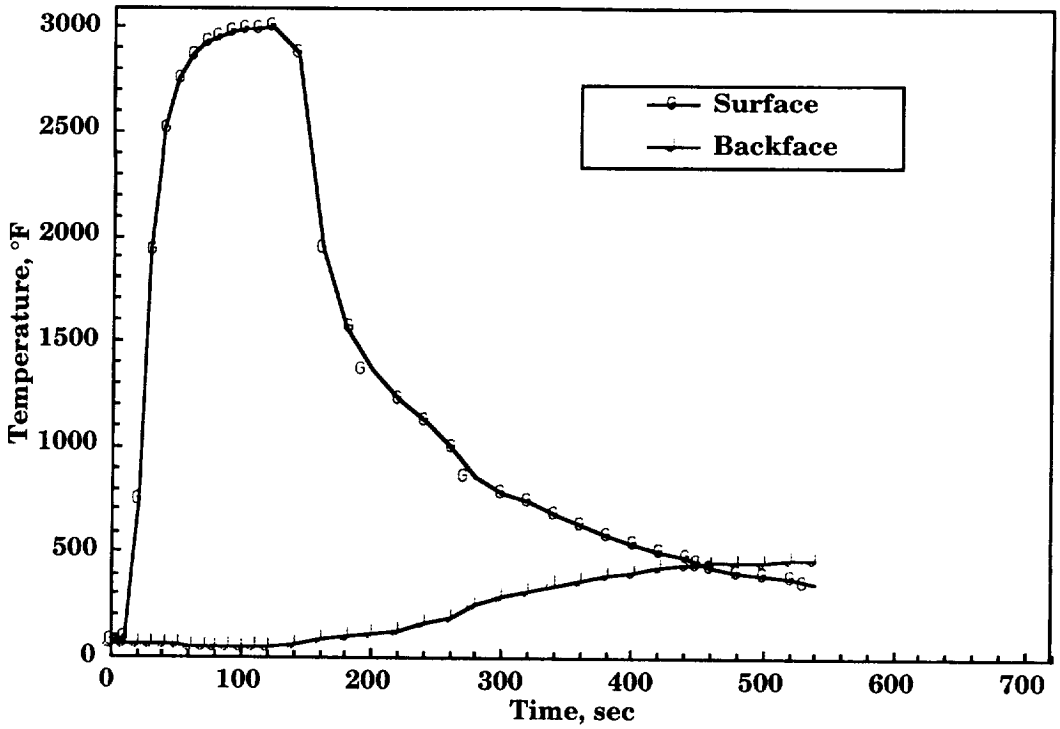

Figure 22. Thermal response of sprayed RCG coated CFBI interlock at 34.3 Btu/ft^2•s.

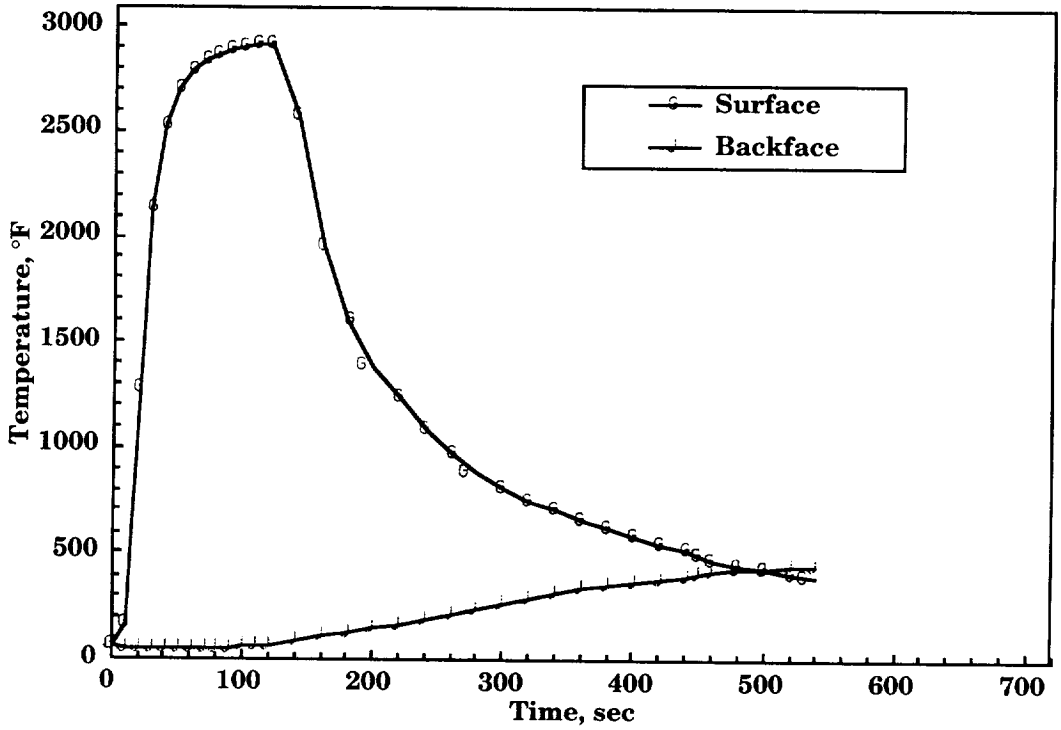

Figure 23. Thermal response of sprayed PCC coated CFBI interlock at 34.3 Btu/ft^2•s.

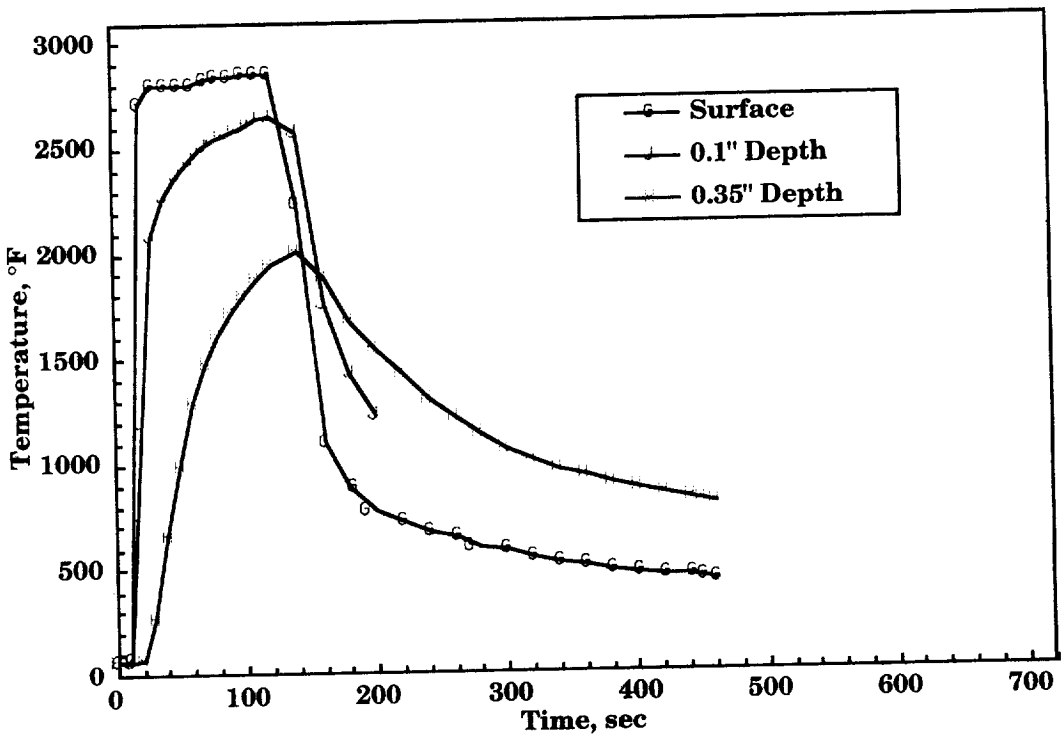

Figure 24. Thermal response of AETB-12 at 47.0 Btu/ft^2•s.

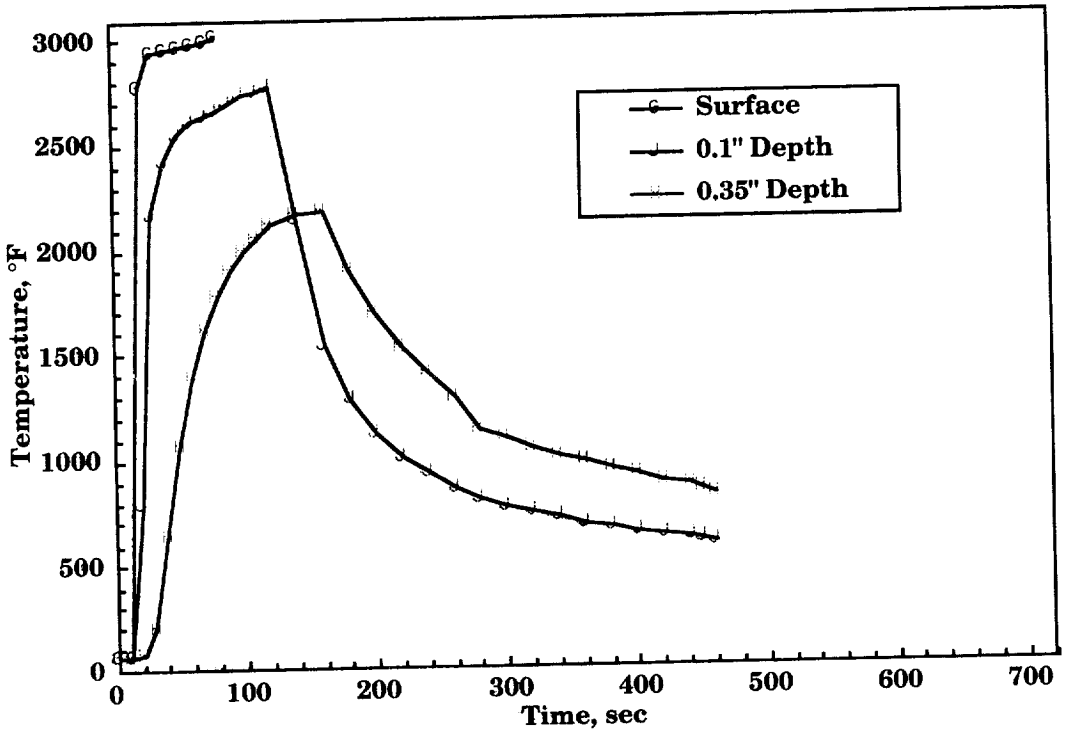

Figure 25. Thermal response of AETB-12 at 58.7 Btu/ft^2•s.

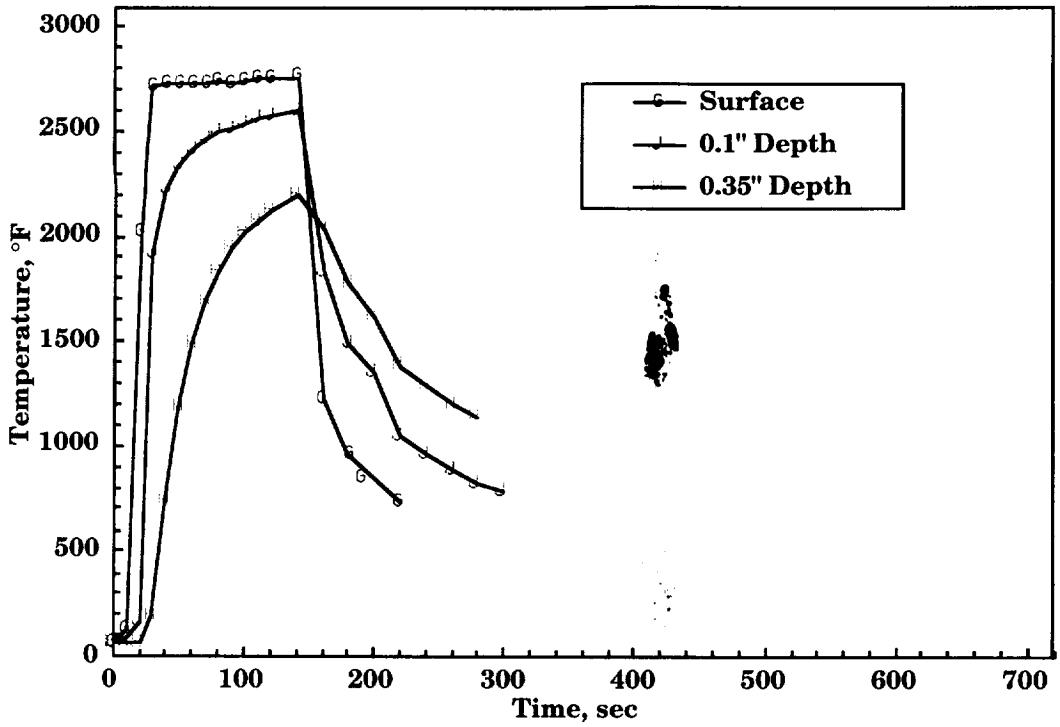

Figure 26. Thermal response of AETB-8 at 47.0 Btu/ft^2•s.

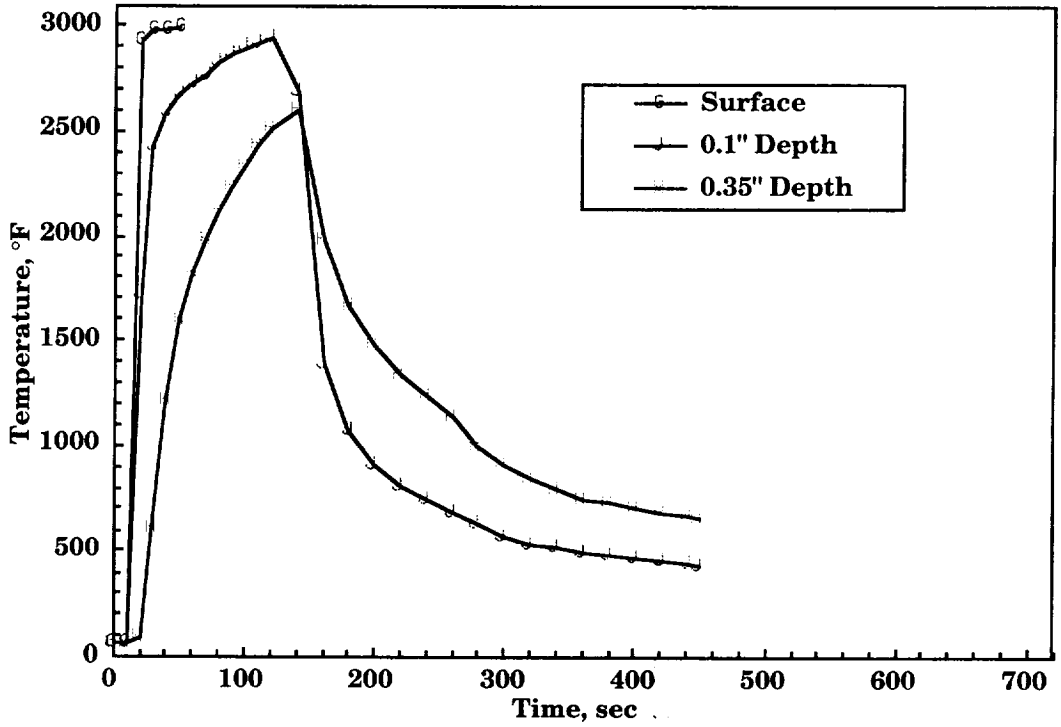

Figure 27. Thermal response of AETB-8 at 58.7 Btu/ft^2•s.

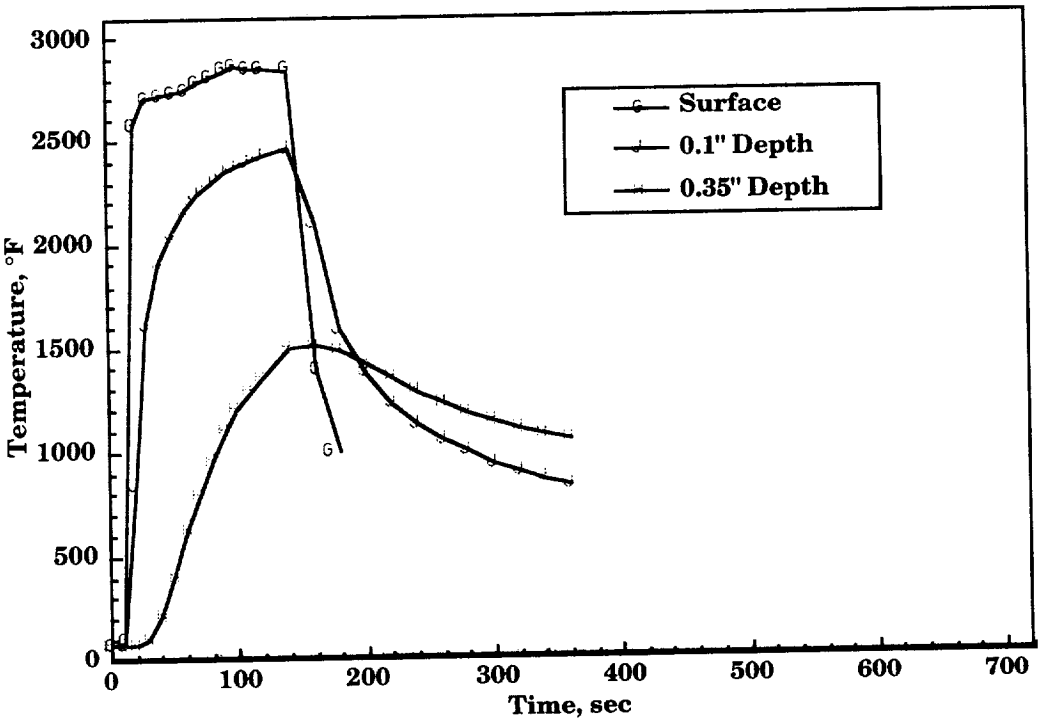

Figure 28. Thermal response of ASMI at 47.0 Btu/ft^2•s.

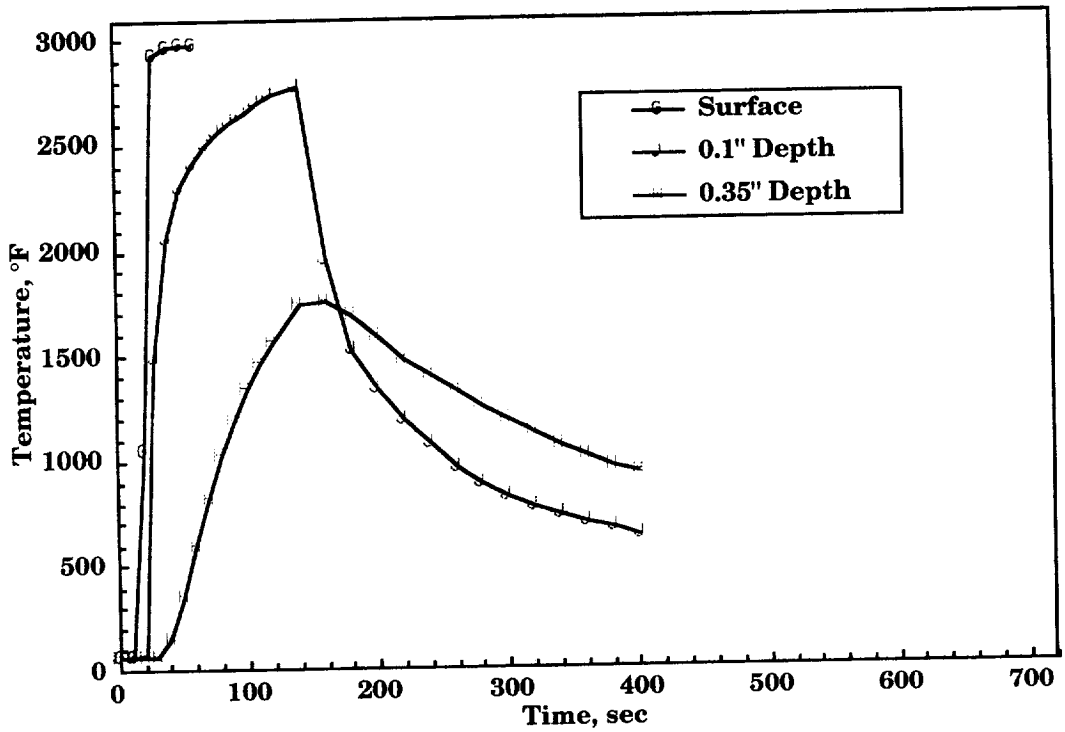

Figure 29. Thermal response of ASMI at 58.7 Btu/ft^2•s.

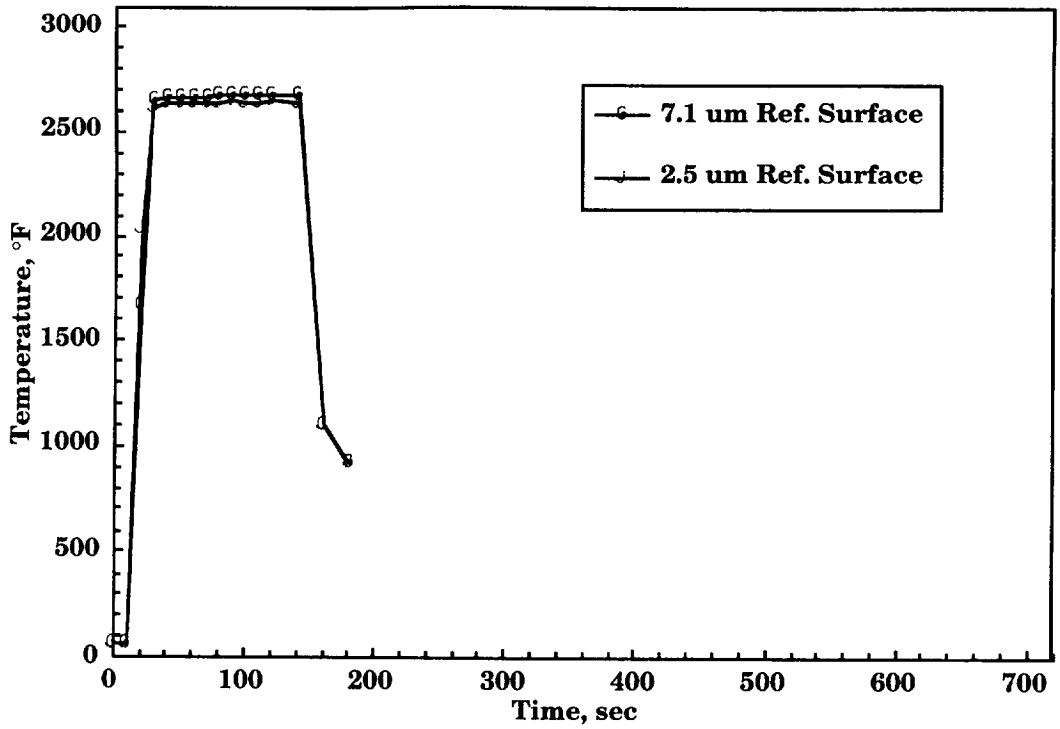

Figure 30. Surface temperature of FRCI-12/RCG with 2.5 μm and 7.1 μm reflective coating at 33.4 Btu/ft^2•s.

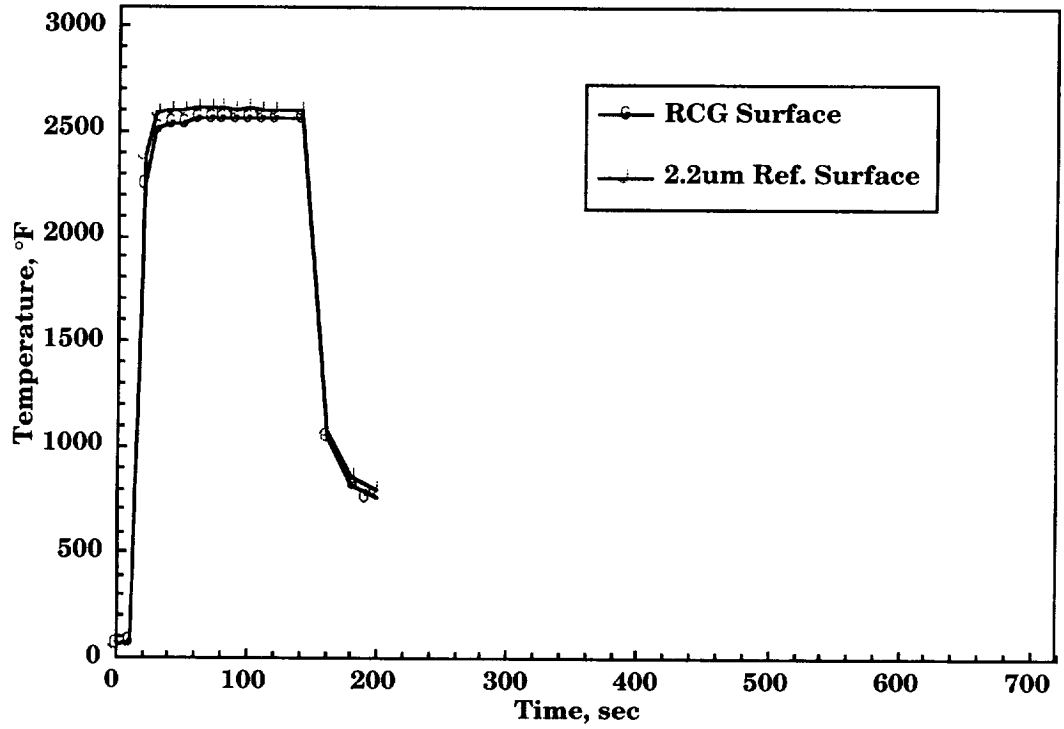

Figure 31. Surface temperature of FRCI-12/RCG with 2.2 μm reflective coating at 34.8 Btu/ft^2 •s.

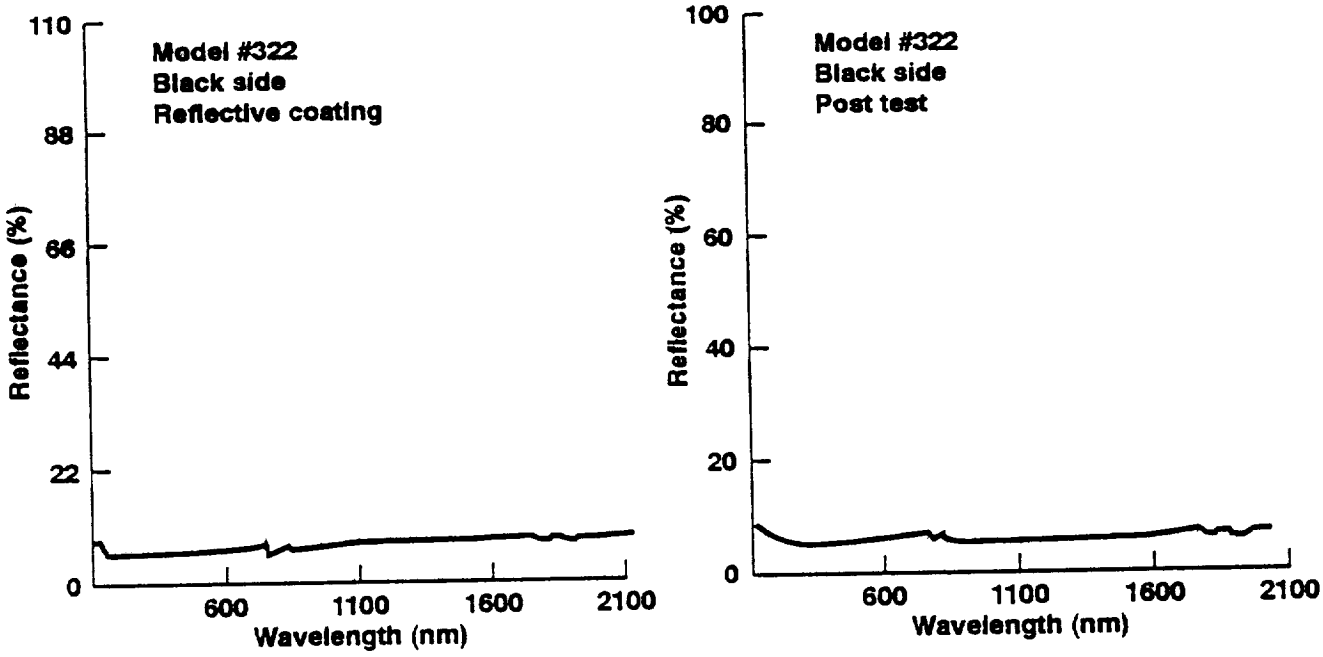

Figure 32. Reflectance of RCG prior (left) and after (right) heating at 34.8 Btu/ft^2•s for 2 min.

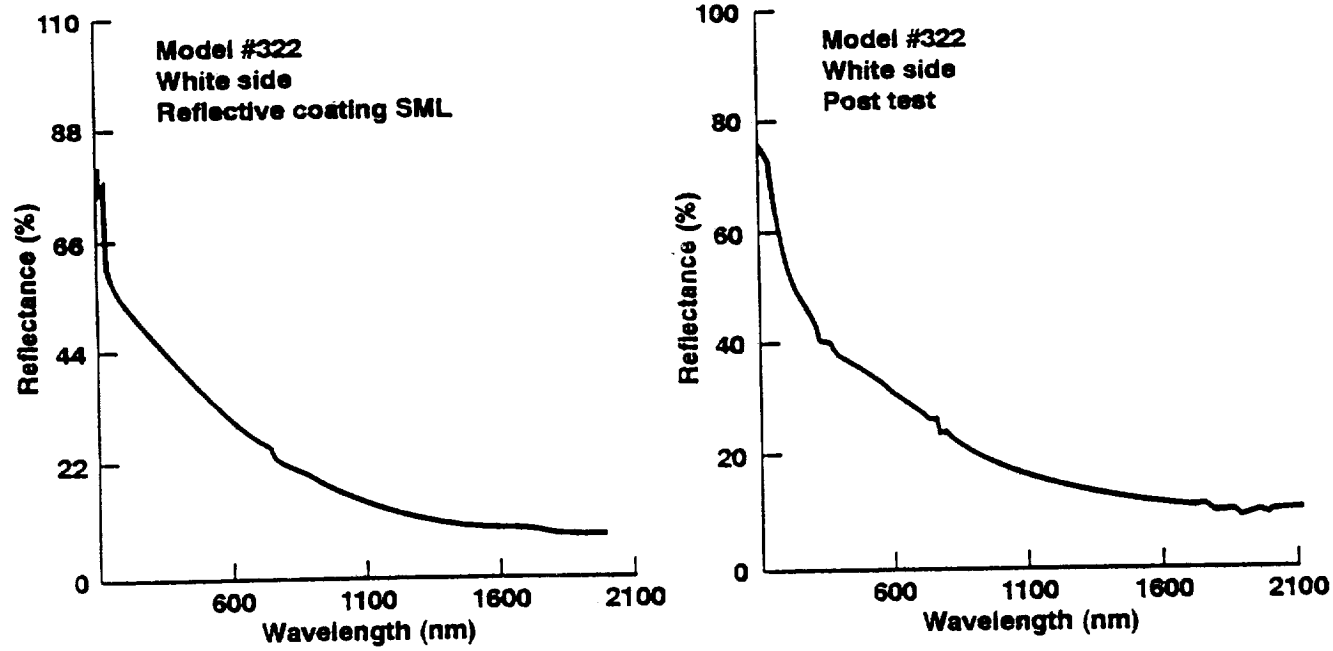

Figure 33. Reflectance of RCG/2.2 μm Al_2O_3 prior (left) and after (right) heating at 34.8 Btu/ft^2•s for 2 min.

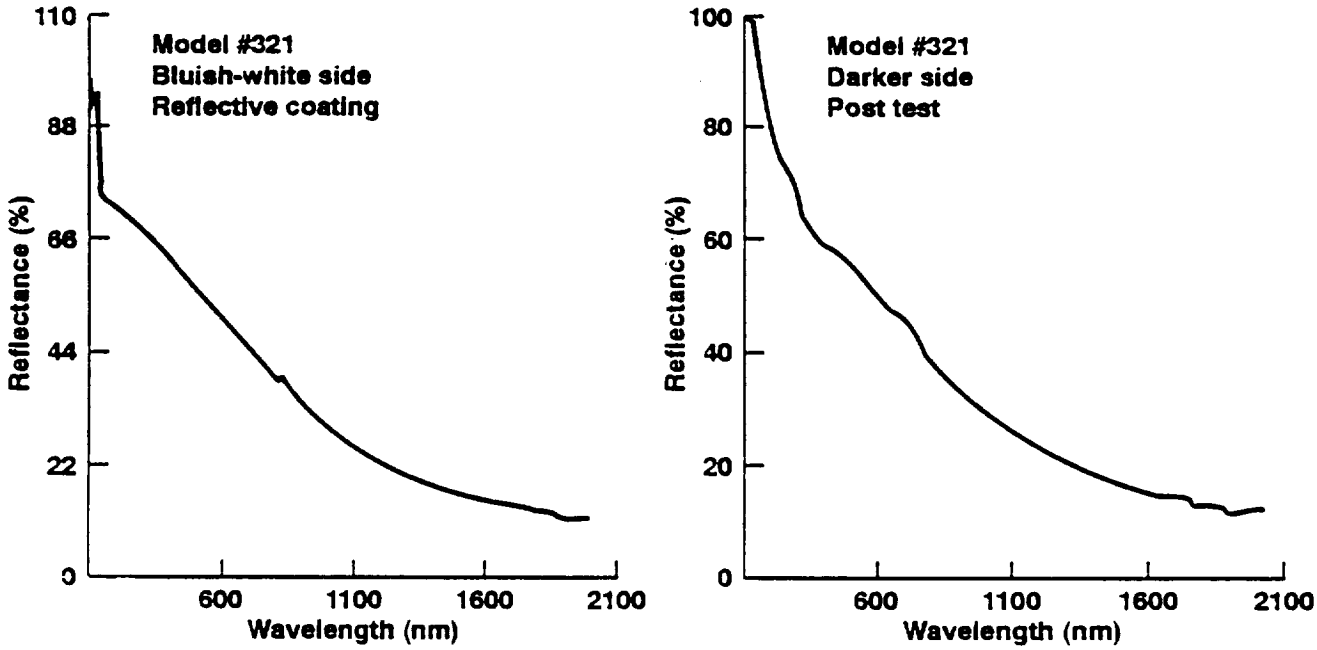

Figure 34. Reflectance of RCG/7.1 μm Al_2O_3 prior (left) and after (right) heating at 33.4 Btu/ft^2•s for 2 min.

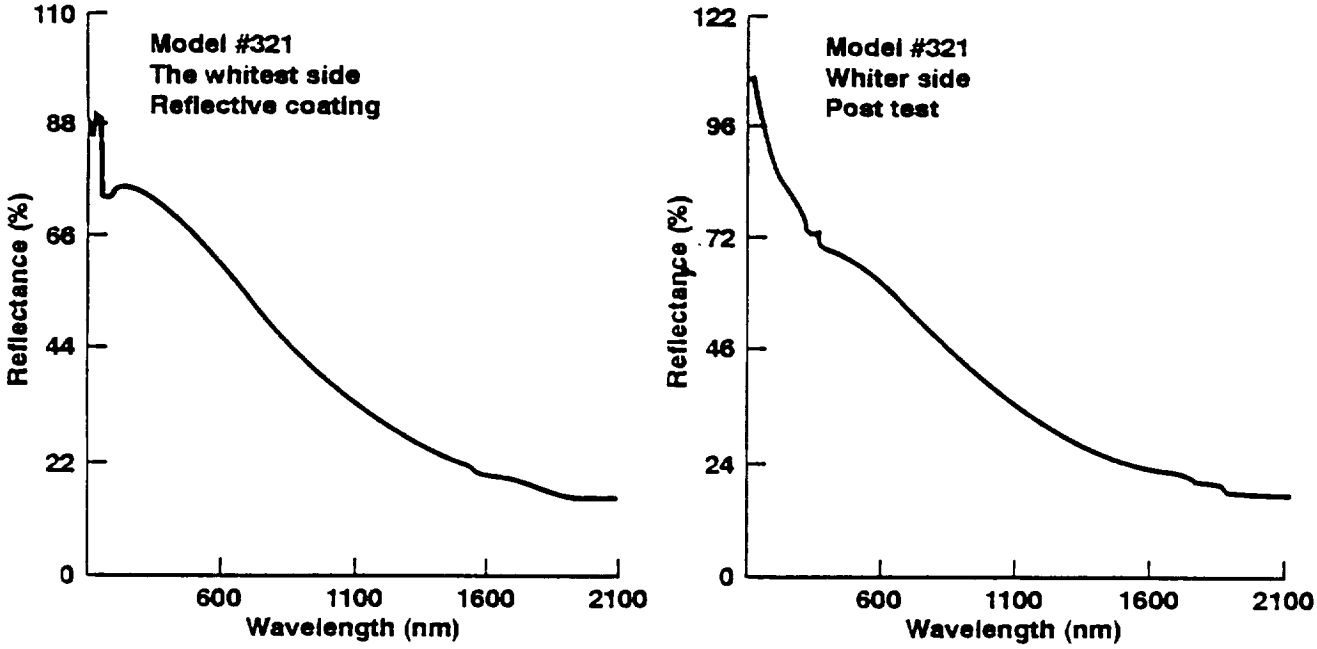

Figure 35. Reflectance of RCG/2.5 μm Al_2O_3 prior (left) and after (right) heating at 33.4 Btu/ft^2•s for 2 min.

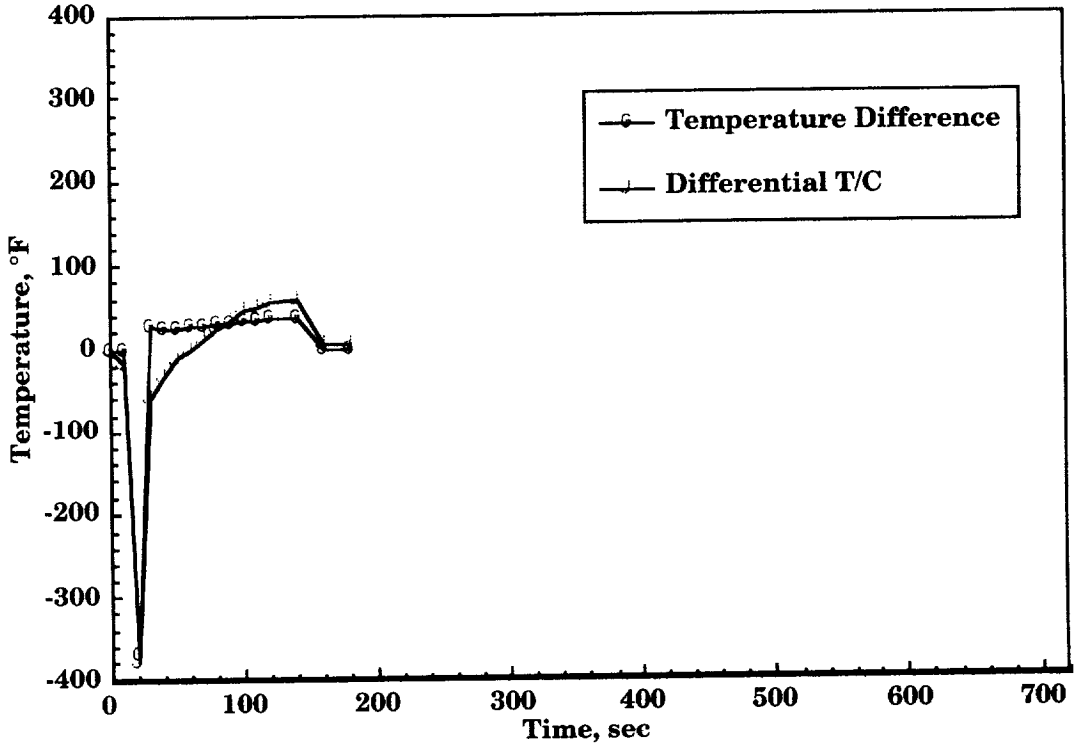

Figure 36. Differential temperature of FRCI-12/RCG with 2.5 µm and 7.1 µm reflective coating at 33.4 Btu/ft^2•s.

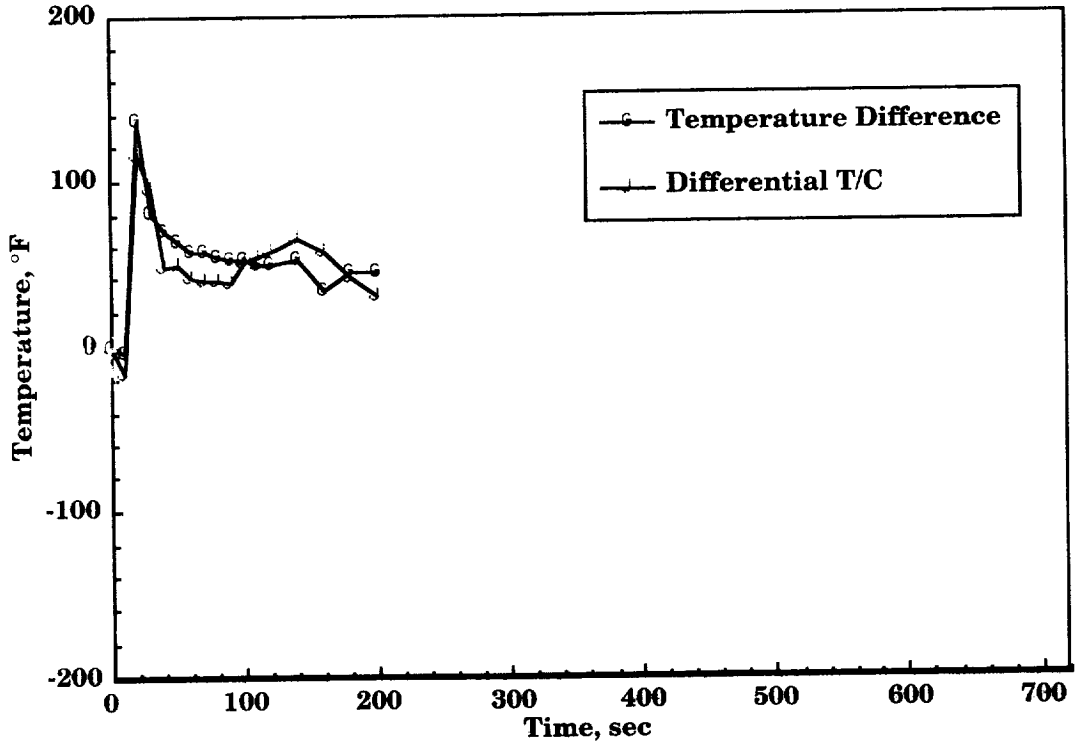

Figure 37. Differential temperature of FRCI-12/RCG with 2.2 µm reflective coating at 34.8 Btu/ft^2•s.

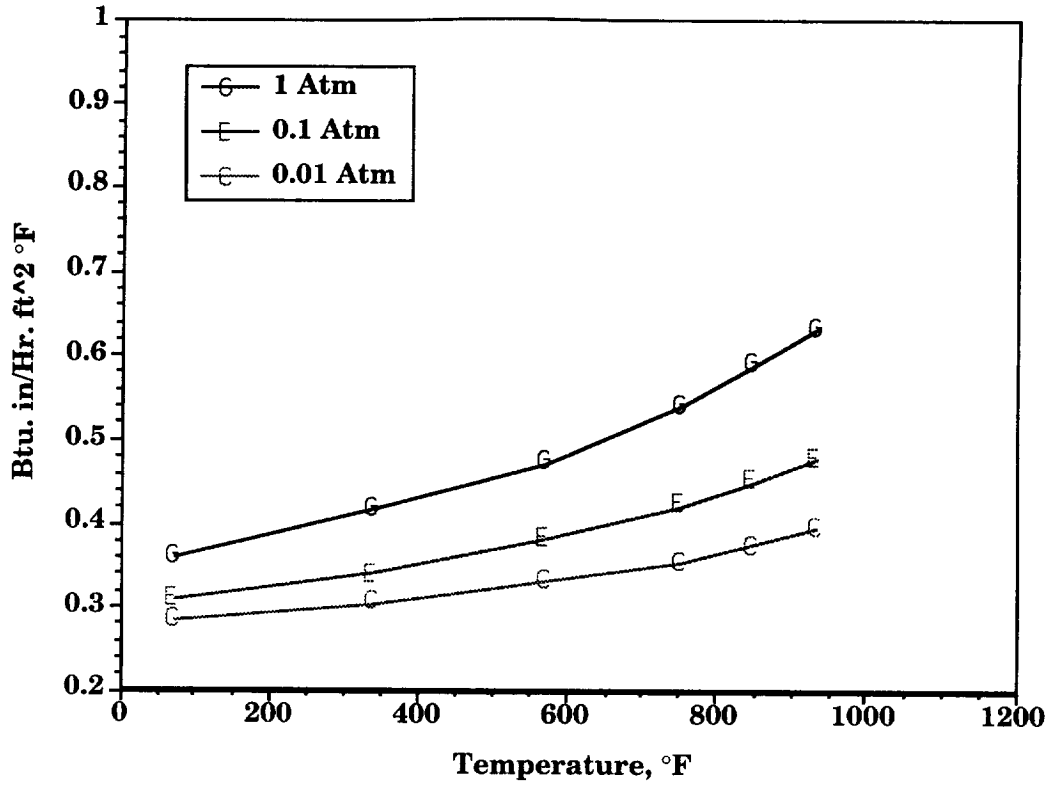

Figure 38. Thermal conductivity of uncoated CFBI interlock.

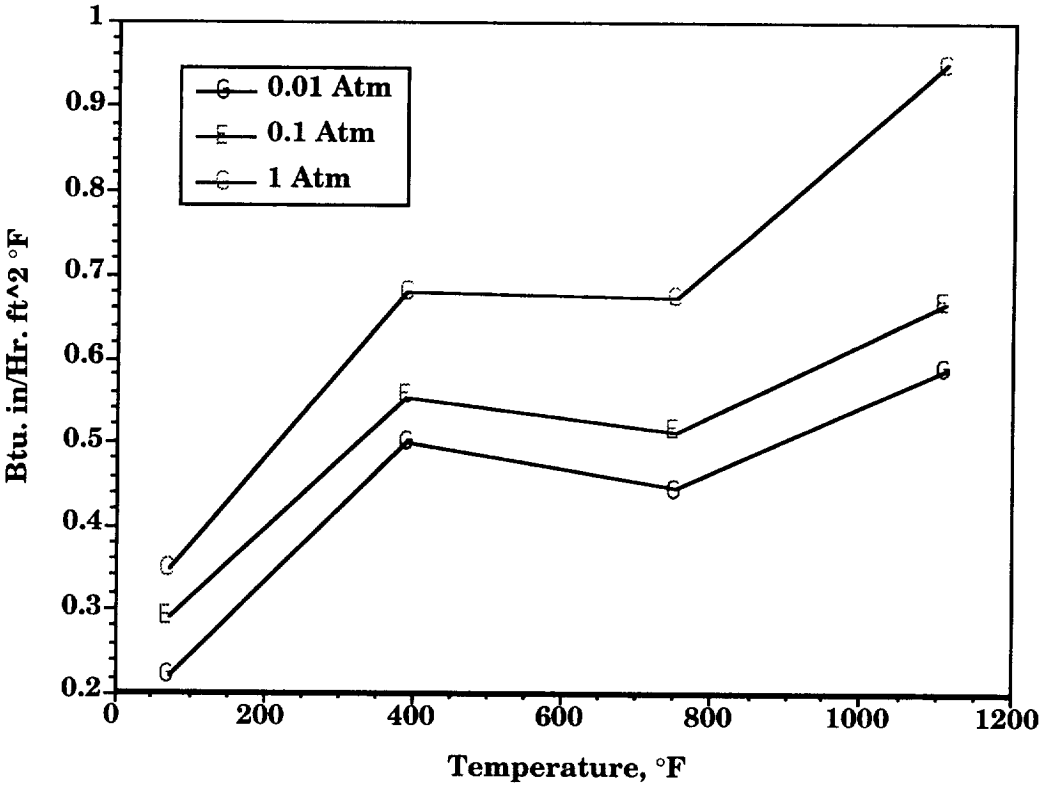

Figure 39. Thermal conductivity of uncoated TABI layer/layer.

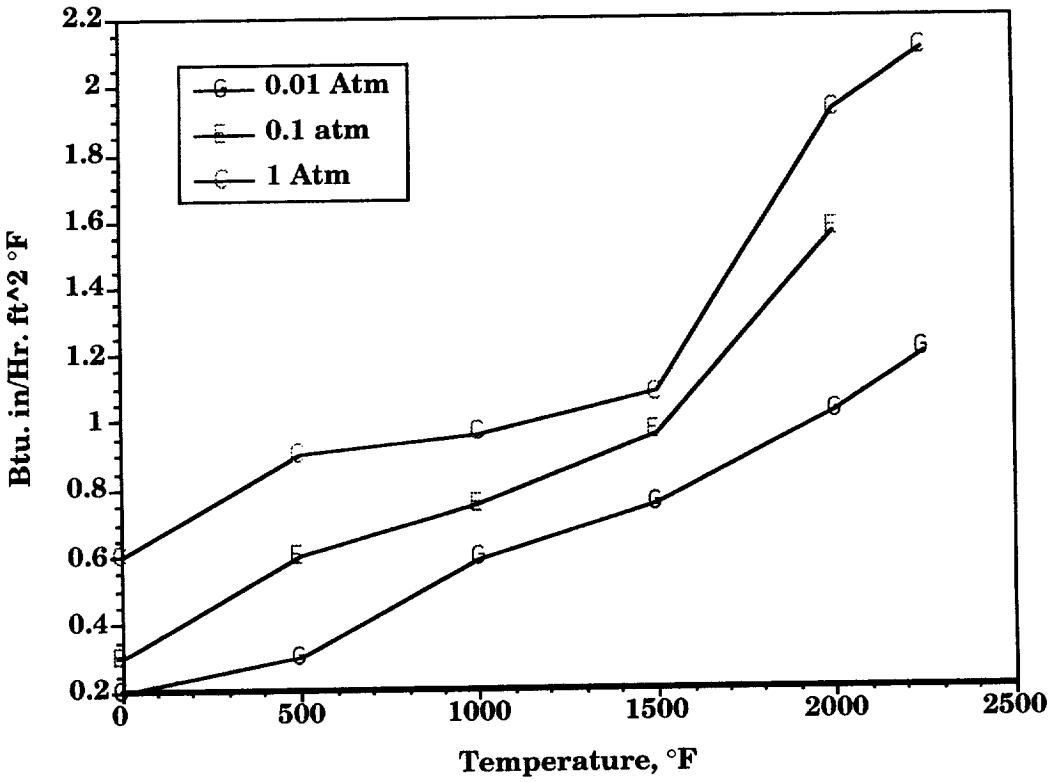

Figure 40. Thermal conductivity of AETB-12.

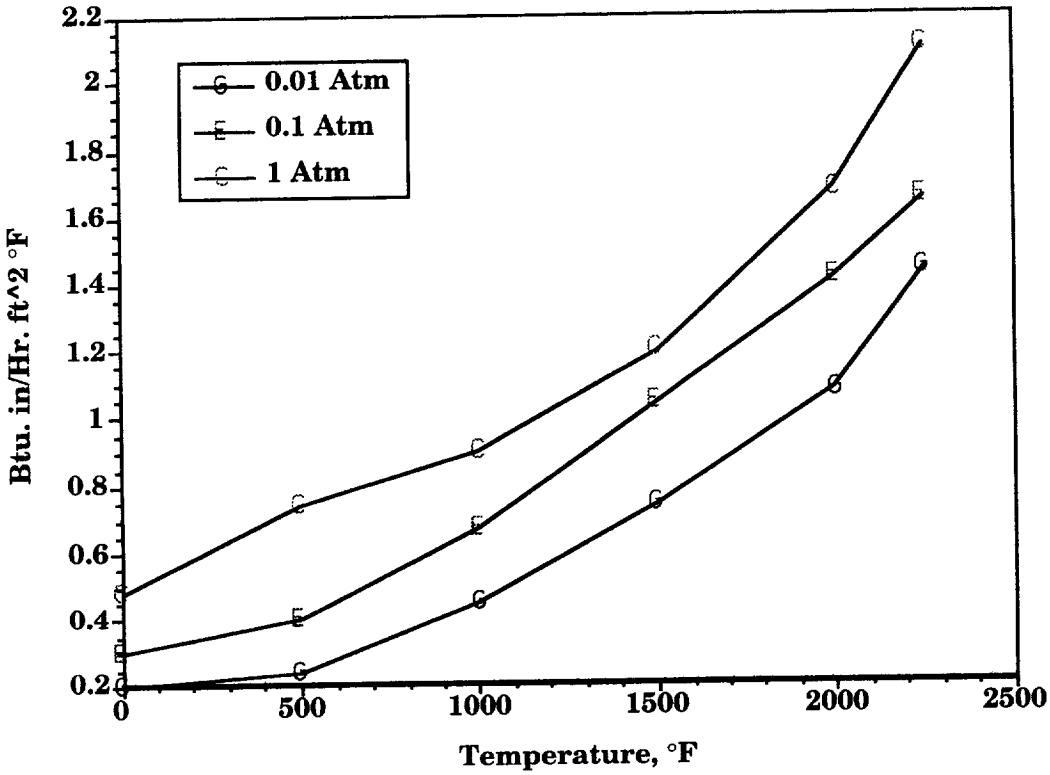

Figure 41. Thermal conductivity of AETB-8.

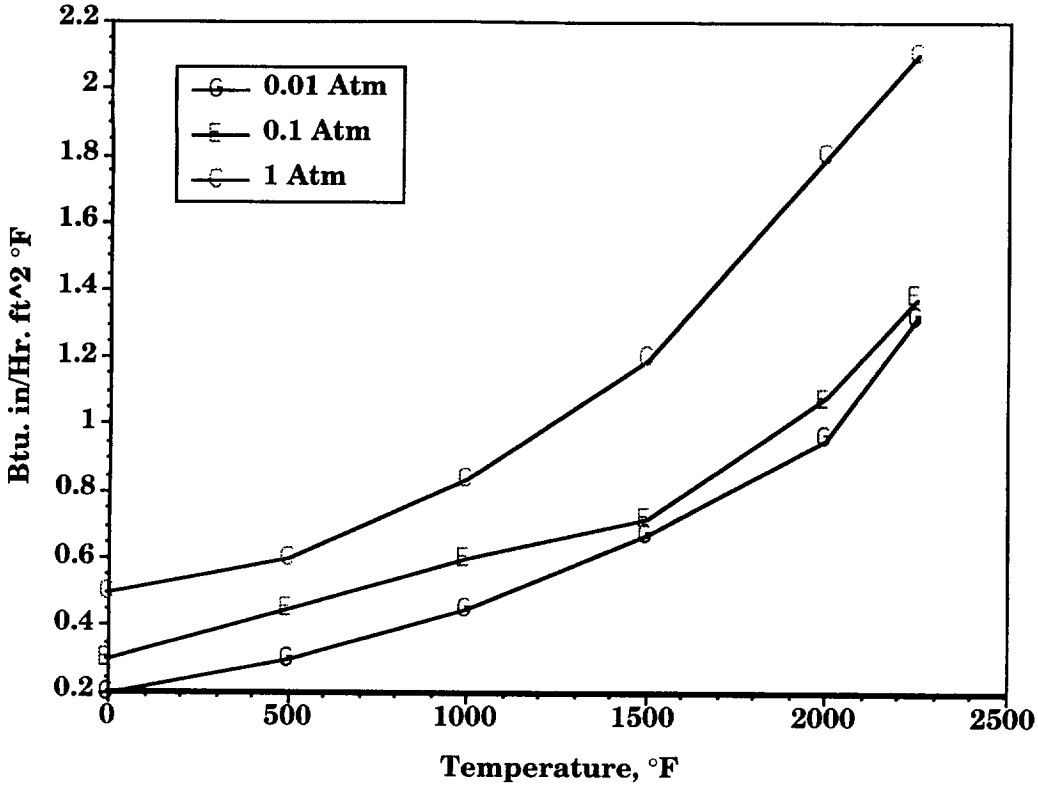

Figure 42. Thermal conductivity of ASMI. (Source: A. E. Hong, NASA/JSC)

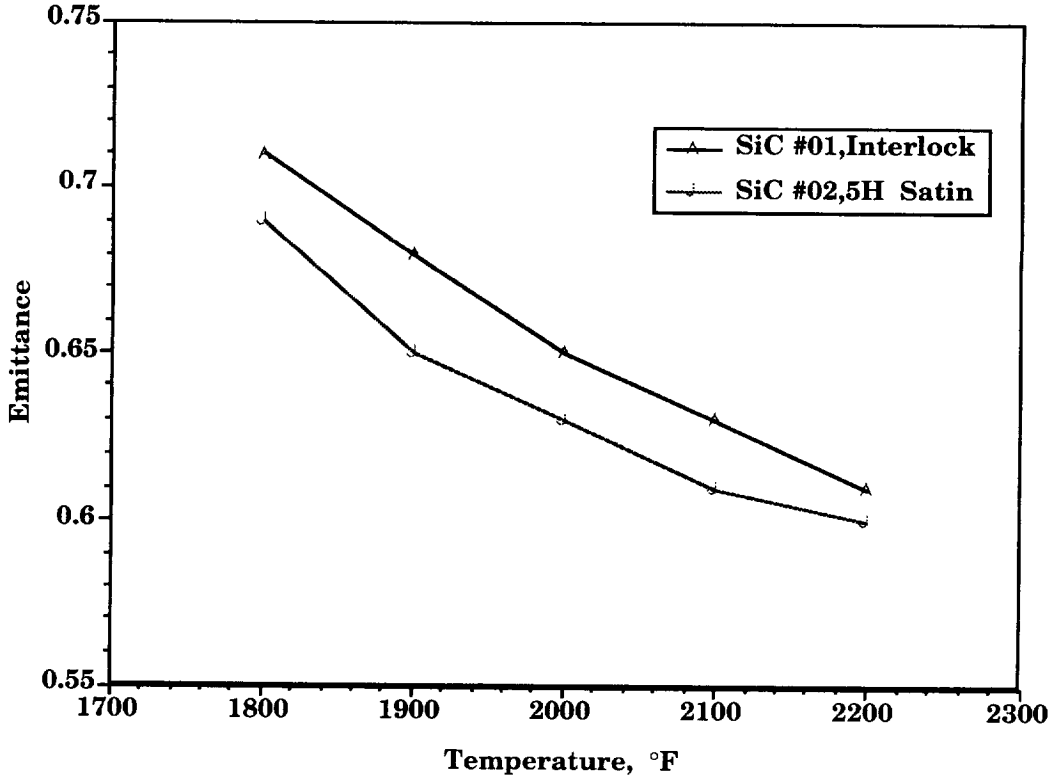

Figure 43. Emissivity of silicon carbide fabrics.

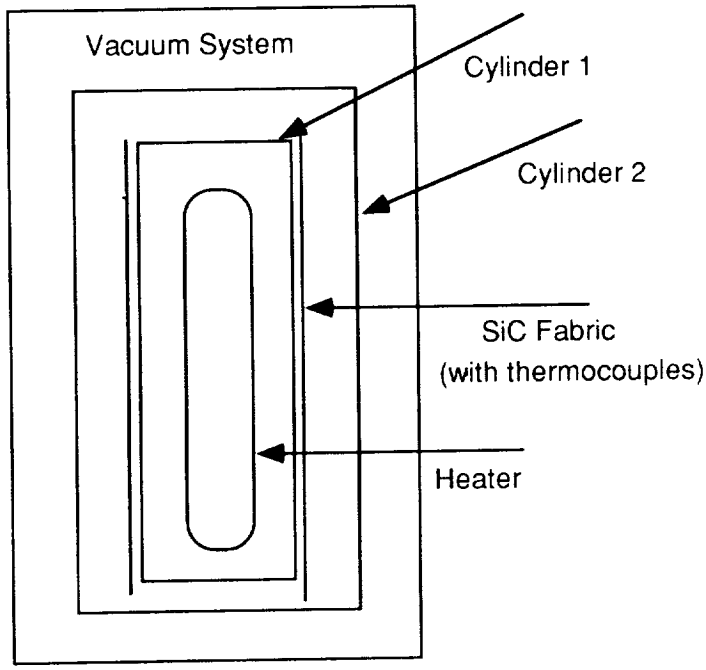

Concentric Cylinder Emissivity Apparatus

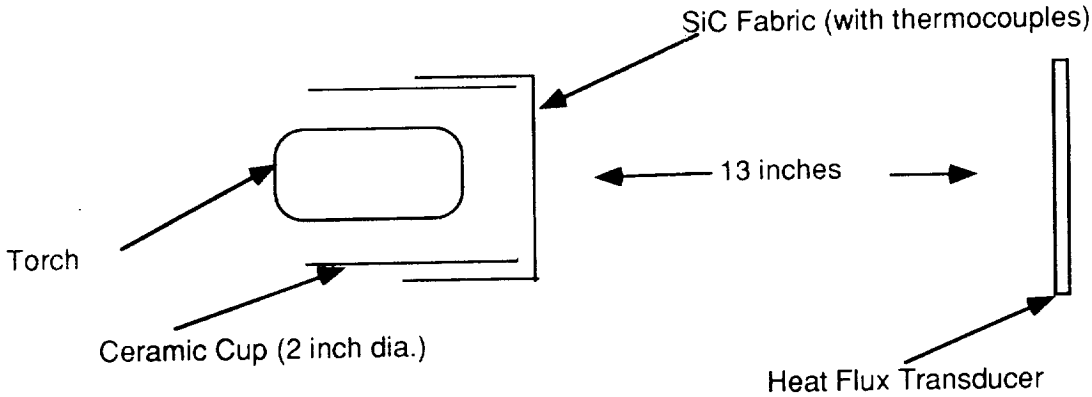

Ceramic Cup Emissivity Apparatus

Figure 44. Apparatuses for measuring emissivity of ceramic fabric.

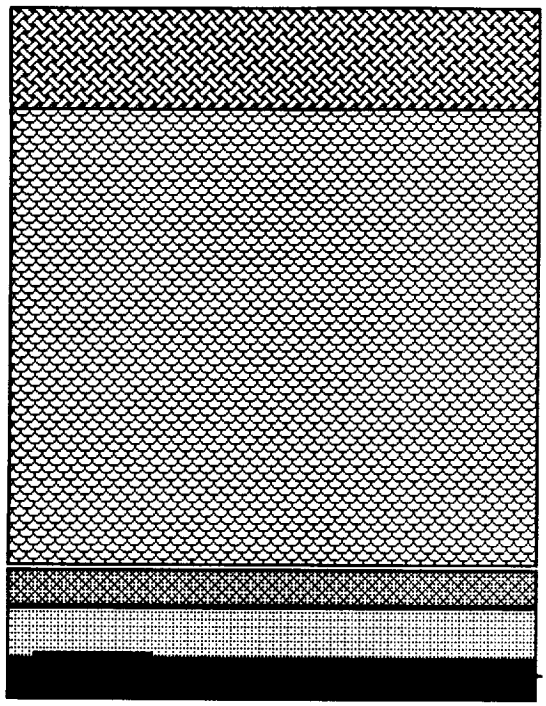

TOTAL NODES = 23

COMPONENTS

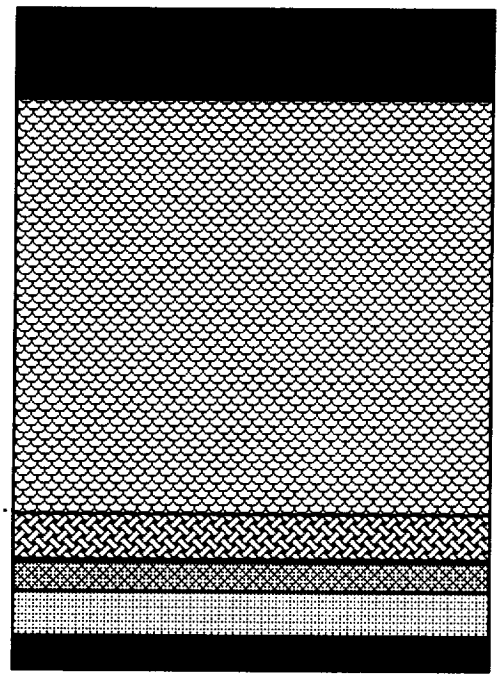

TOTAL NODES = 26

Figure 45. Thermal models of flexible (above) and rigid insulations (below).

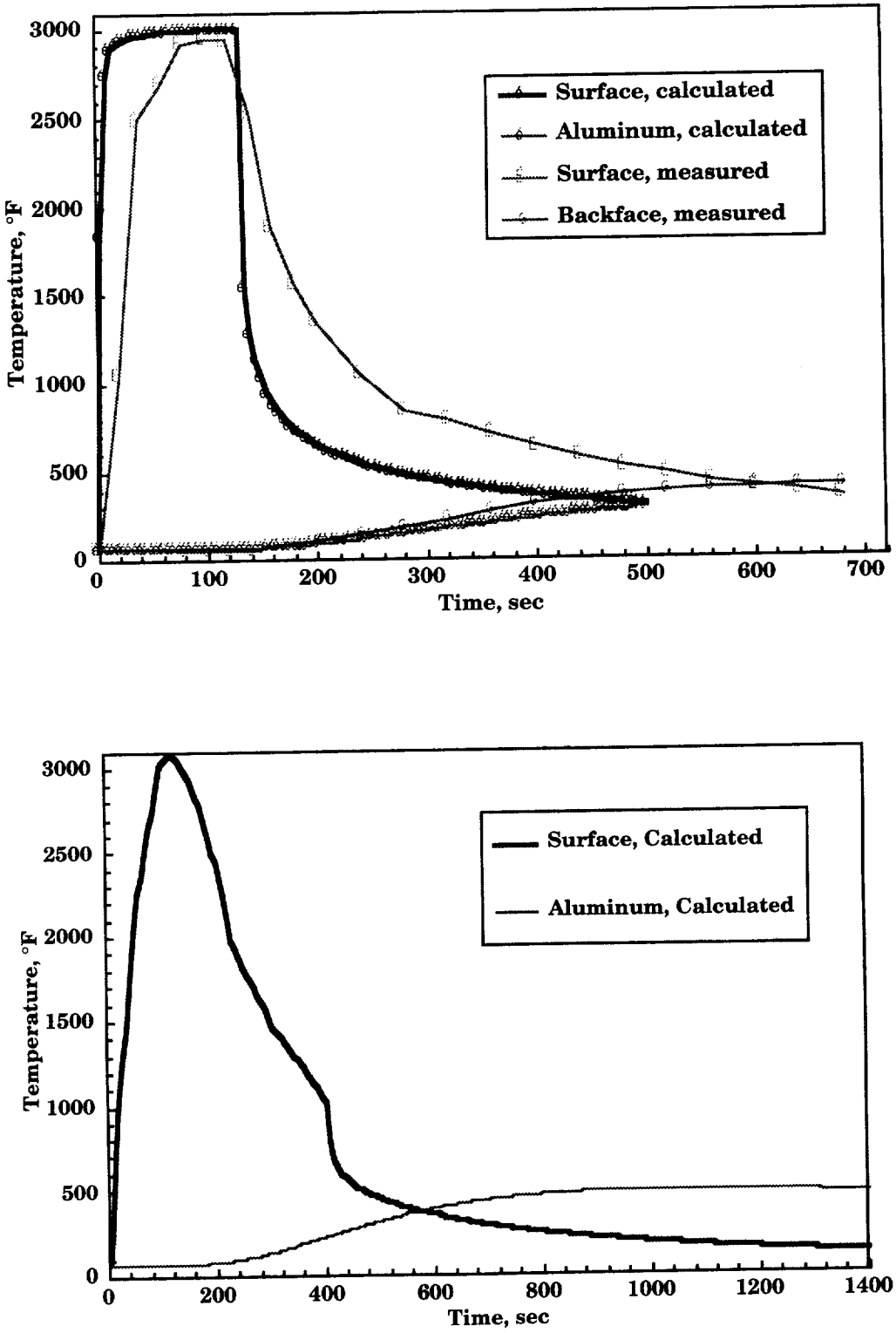

Figure 46. Calculated temperature profile of uncoated CFBI interlock at arc jet heating rate of 34.8 Btu/ft^2•s (above) and AFE heating rate of 36.8 Btu/ft^2•s (below).

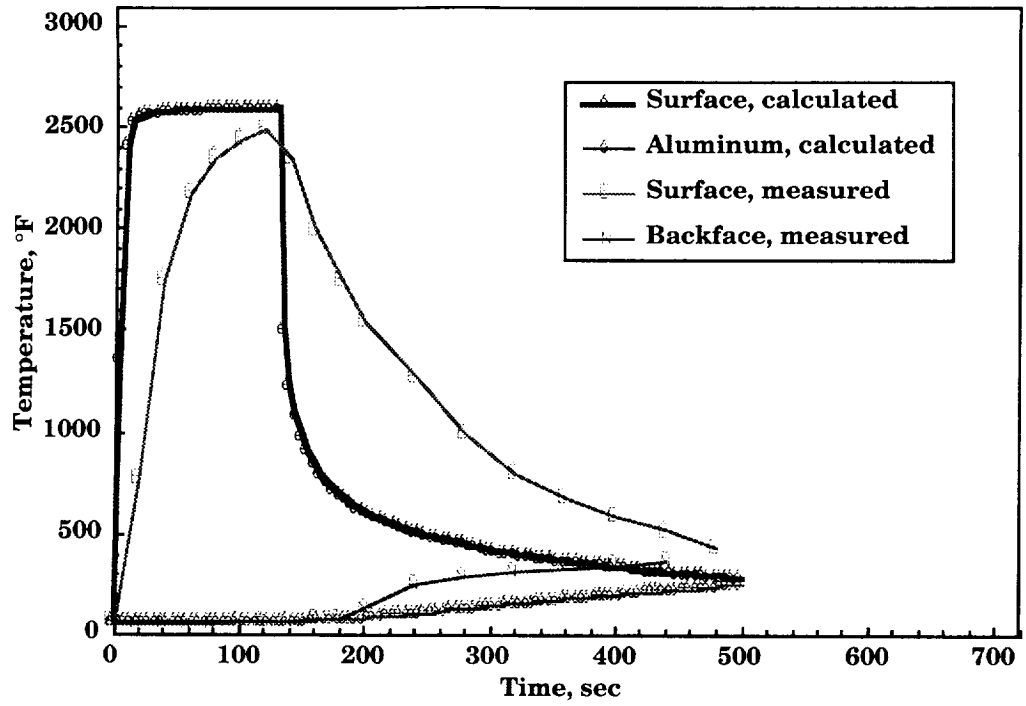

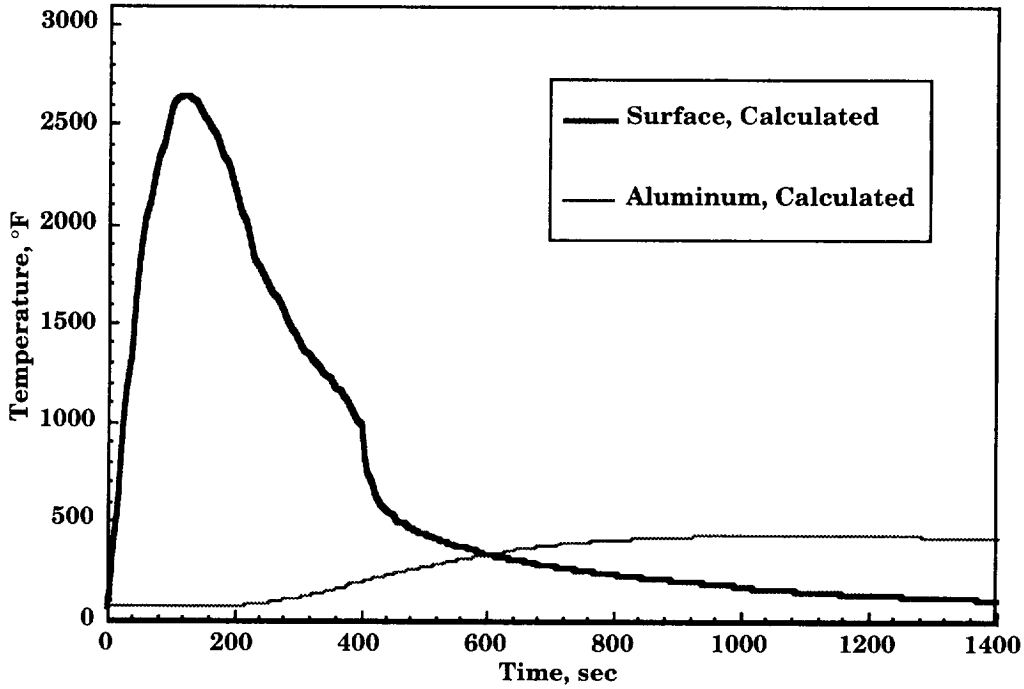

Figure 47. Calculated temperature profile of PCC coated CFBI interlock at arc jet heating rate of 34.8 Btu/ft^2•s (above) and AFE heating rate of 36.8 Btu/ft^2•s (below).

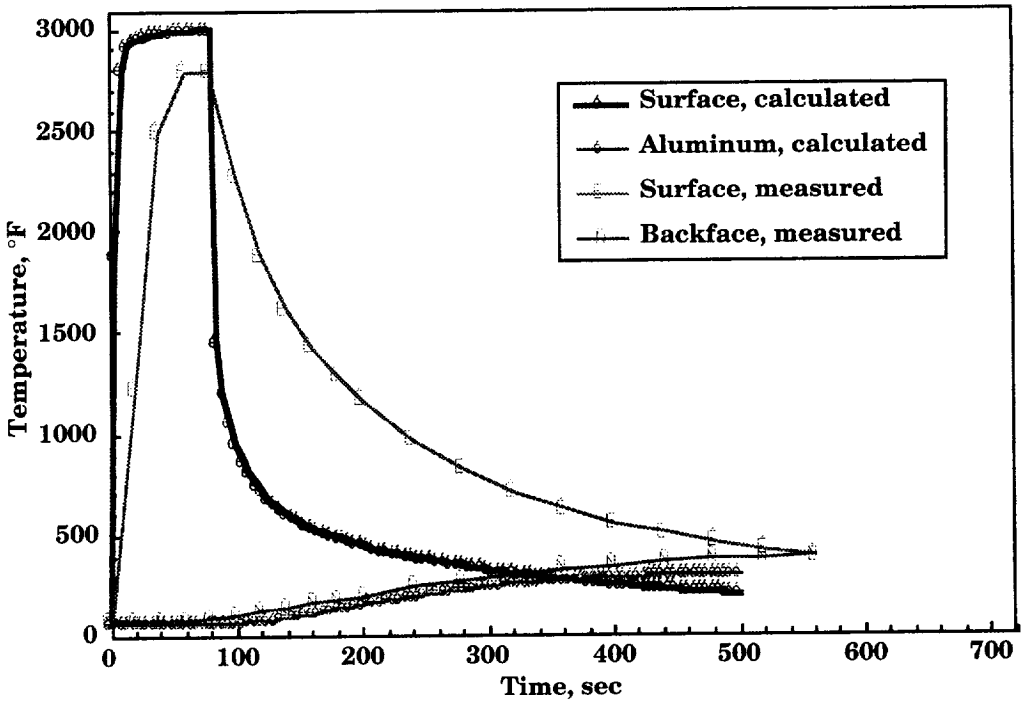

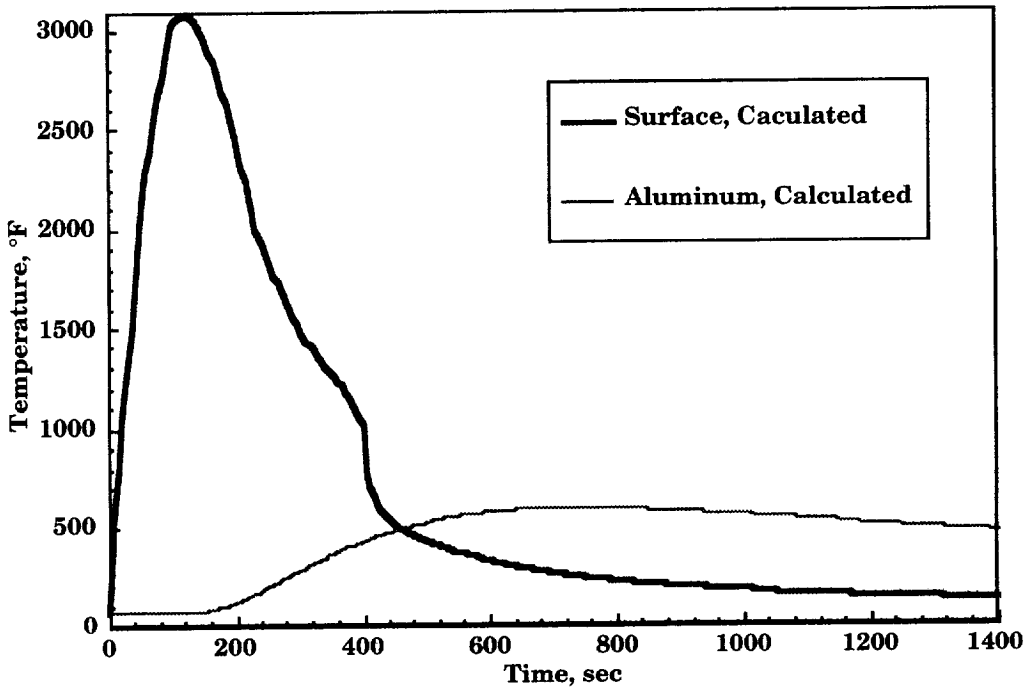

Figure 48. Calculated temperature profile of uncoated TABI layer/layer at arc jet heating rate of 34.8 Btu/ft^2•s (above) and AFE heating rate of 36.8 Btu/ft^2•s (below).

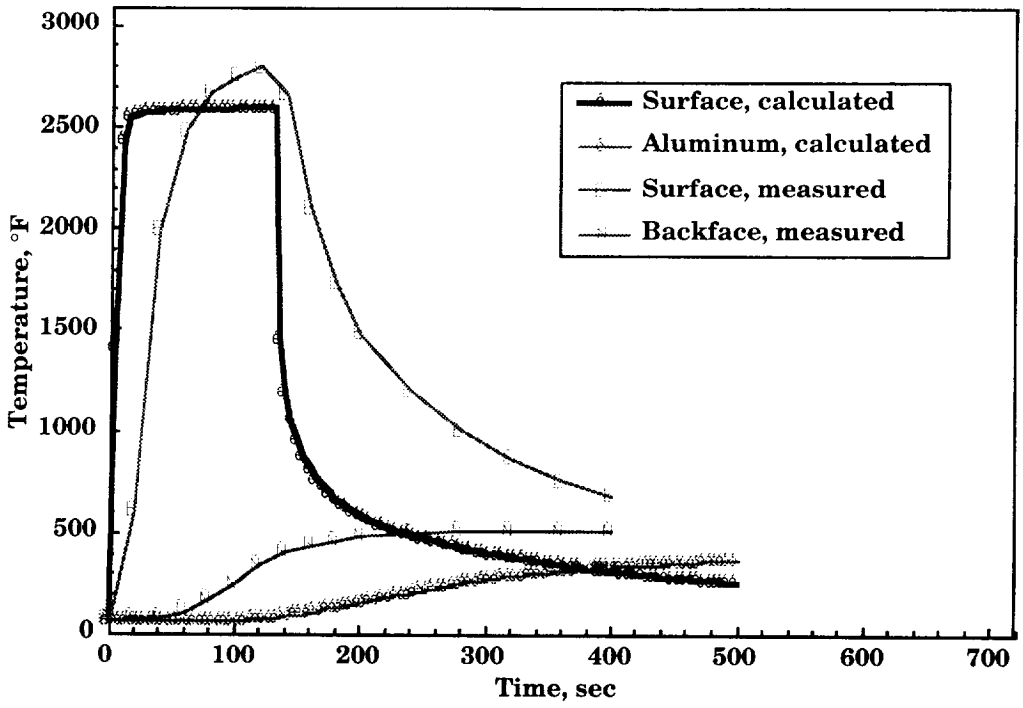

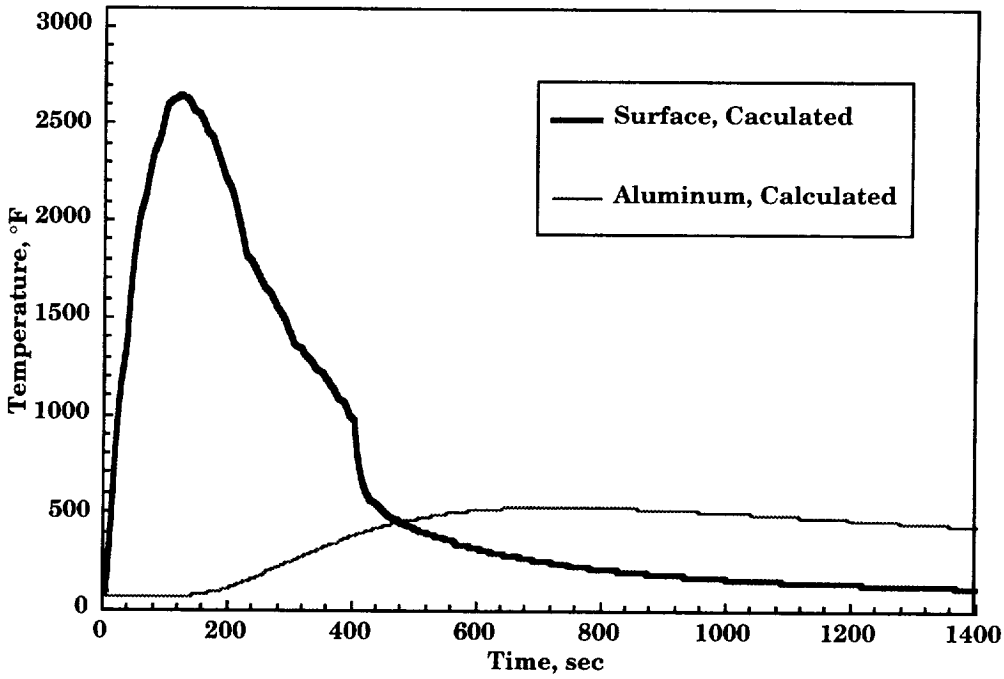

Figure 49. Calculated temperature profile of PCC coated TABI layer/layer at arc jet heating rate of 34.8 Btu/ft^2•s (above) and AFE heating rate of 36.8 Btu/ft^2•s (below).

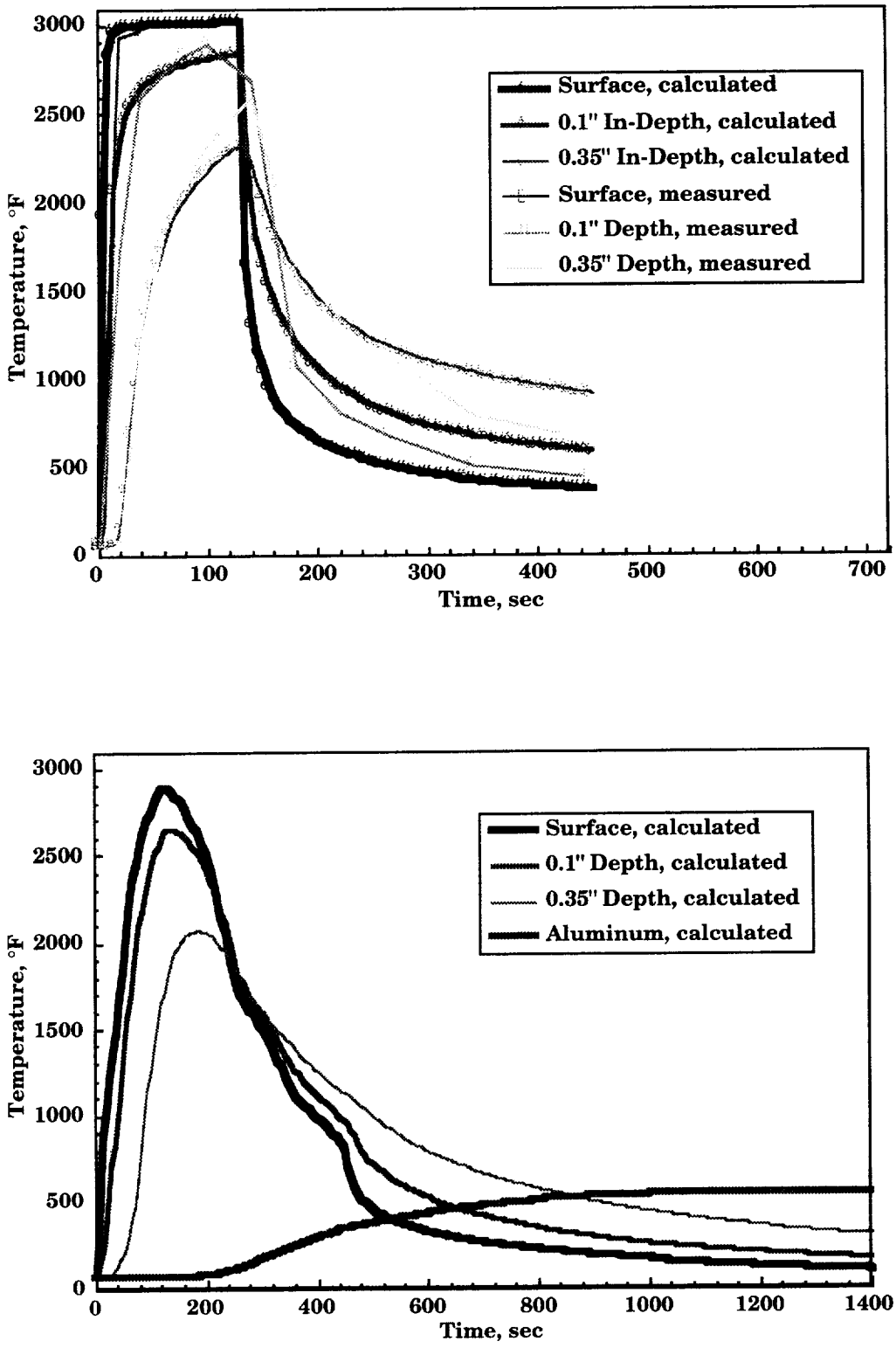

Figure 50. Calculated temperature profile of AETB-8 at arc jet heating rate of 58.7 Btu/ft^2•s (above) and AFE heating rate of 54.0 Btu/ft^2•s (below).

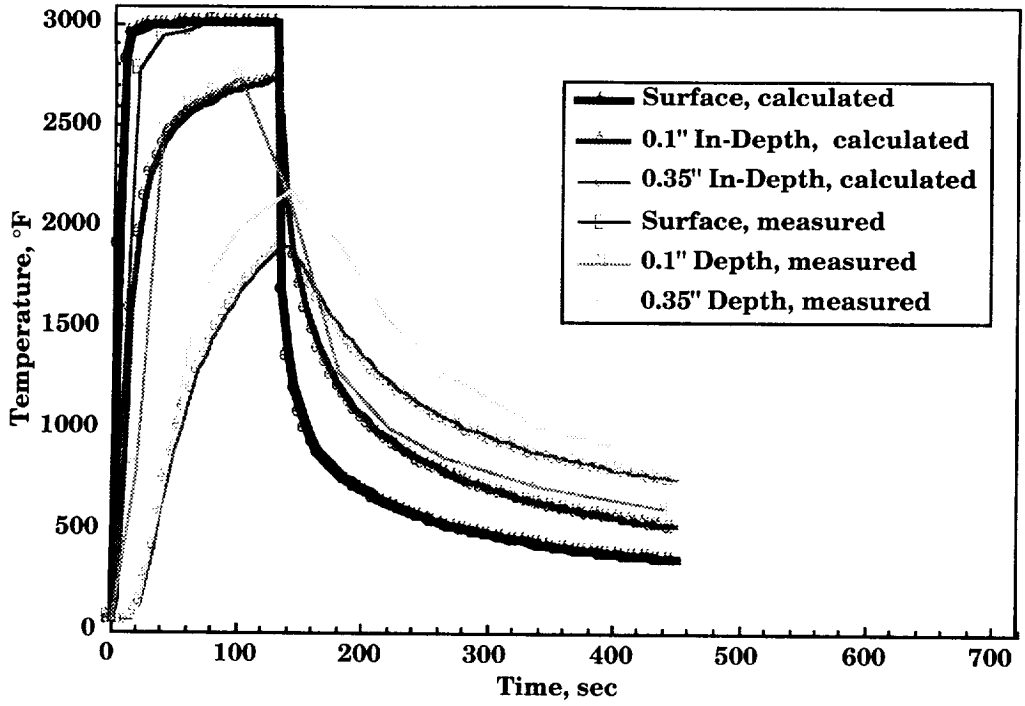

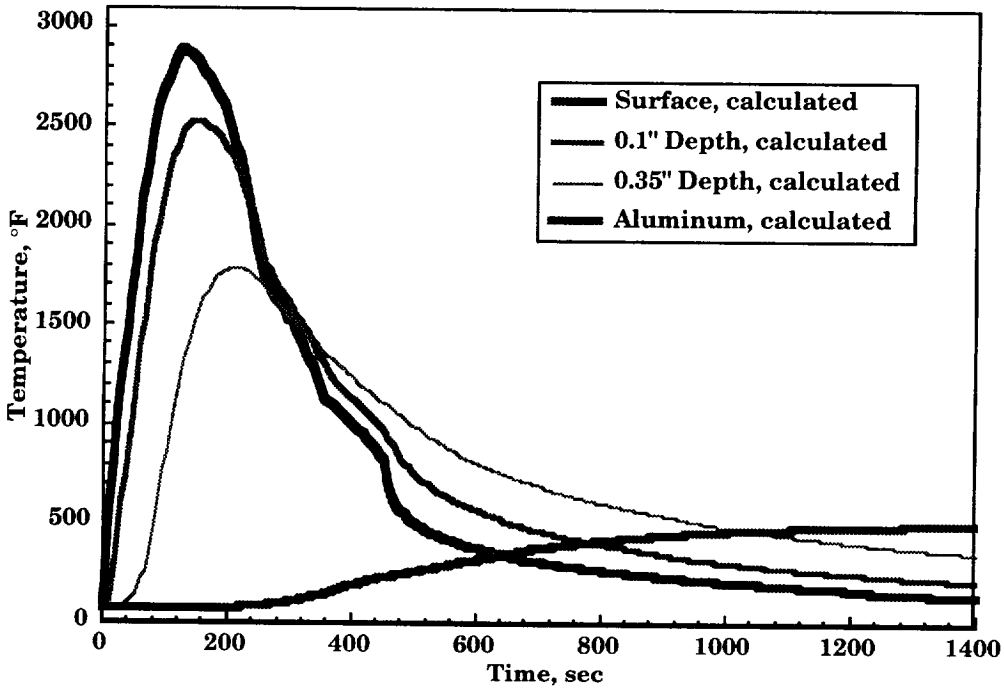

Figure 51. Calculated temperature profile of AETB-12 at arc jet heating rate of 58.7 Btu/ft^2•s (above) and AFE heating rate of 54.0 Btu/ft^2•s (below).

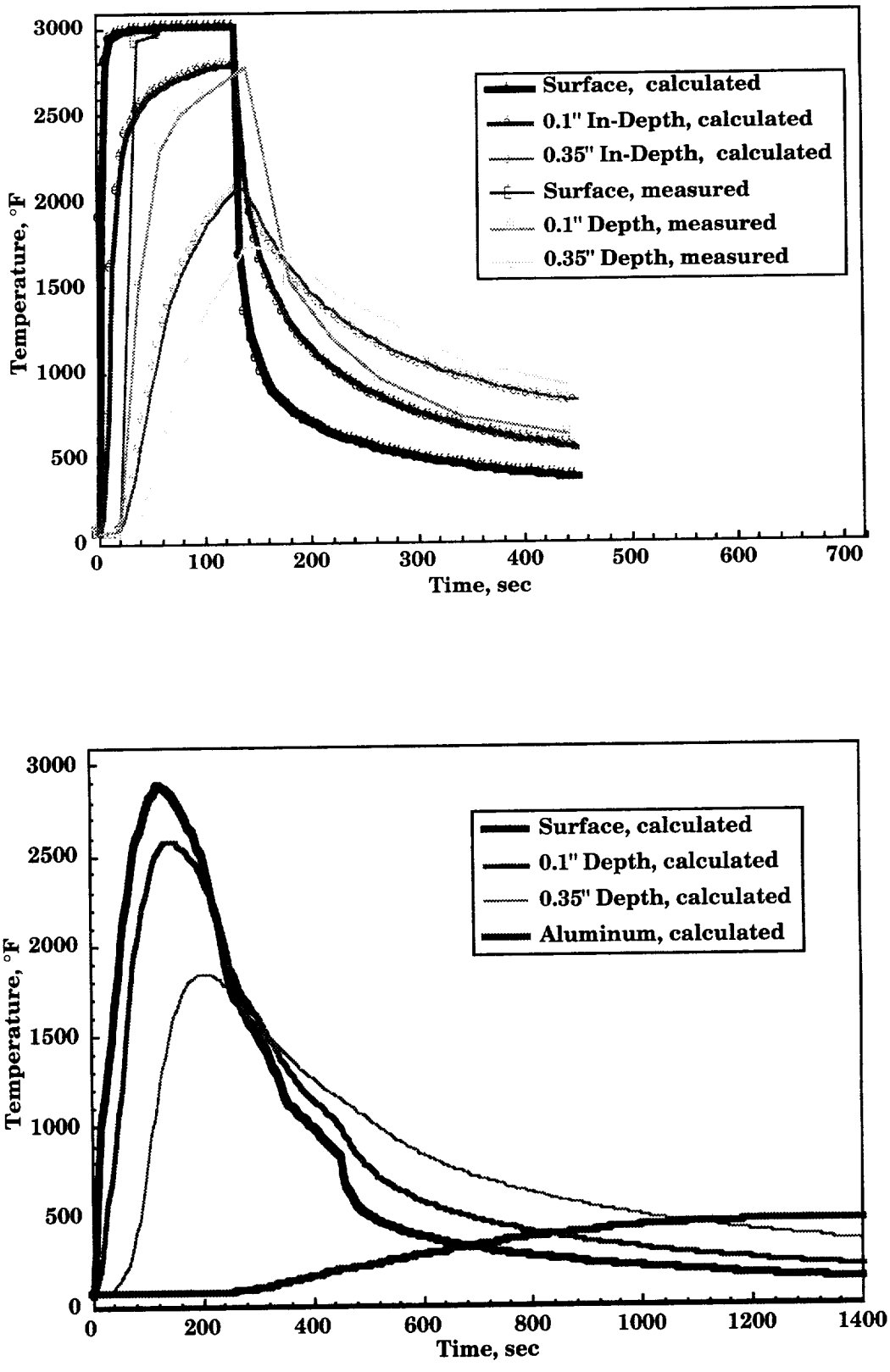

Figure 52. Calculated temperature profile of ASMI at arc jet heating rate of 58.7 Btu/ft^2•s (above) and AFE heating rate of 54.0 Btu/ft^2•s (below).

APPENDIX

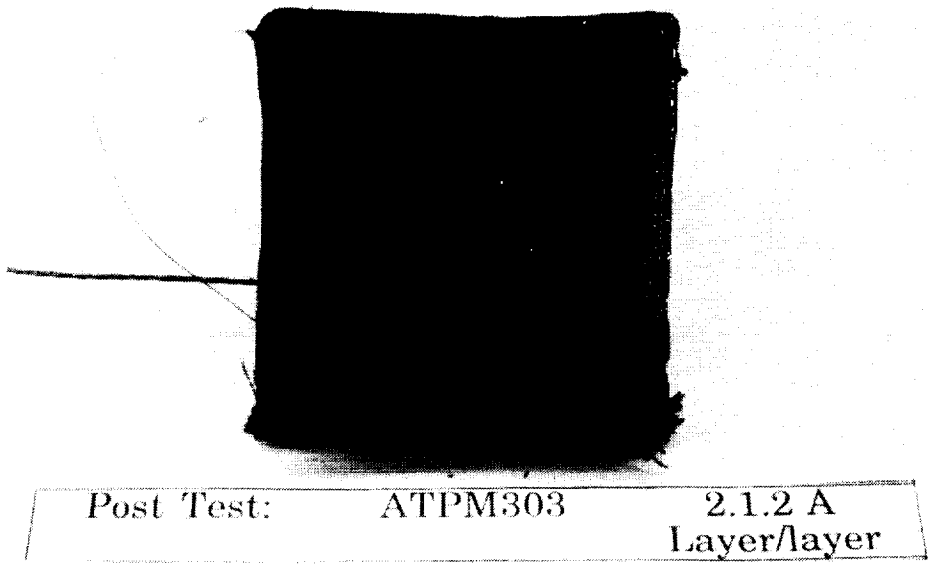

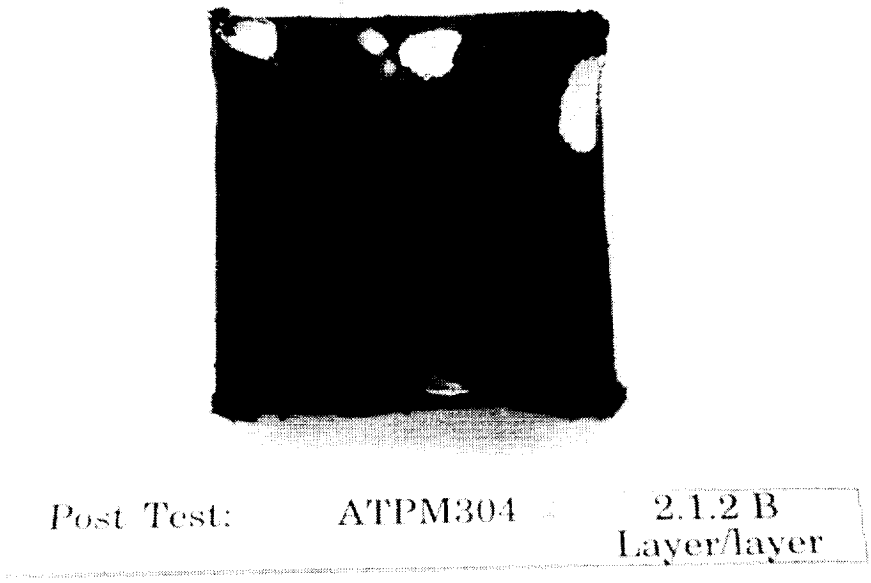

Figure A-1. TABI layer/layer after exposure to 30.7 Btu/ft^2•s (above) and 34.3 Btu/ft^2•s (below).

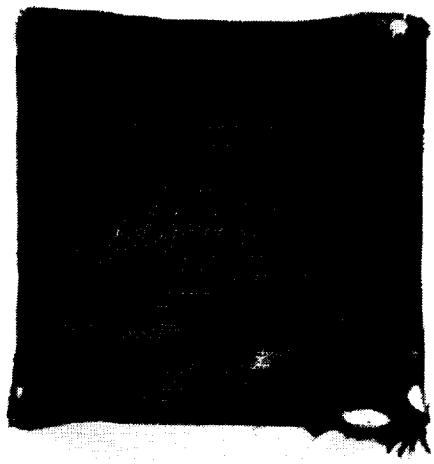

Post Test: ATPM306 2.1.x Interlock

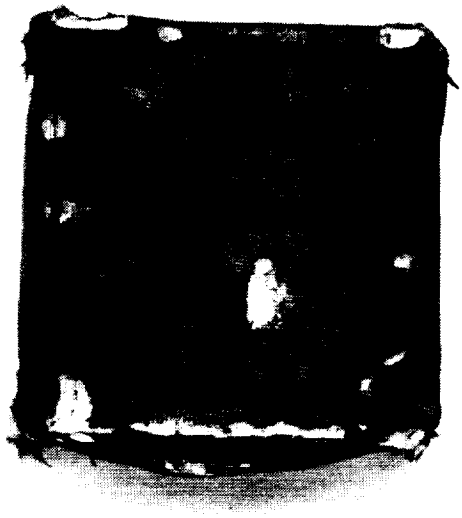

Post Test: ATPM306 2.1.x Interlock

Figure A-2. TABI interlock after exposure to 30.7 Btu/ft^2•s (above) and 34.3 Btu/ft^2•s (below).

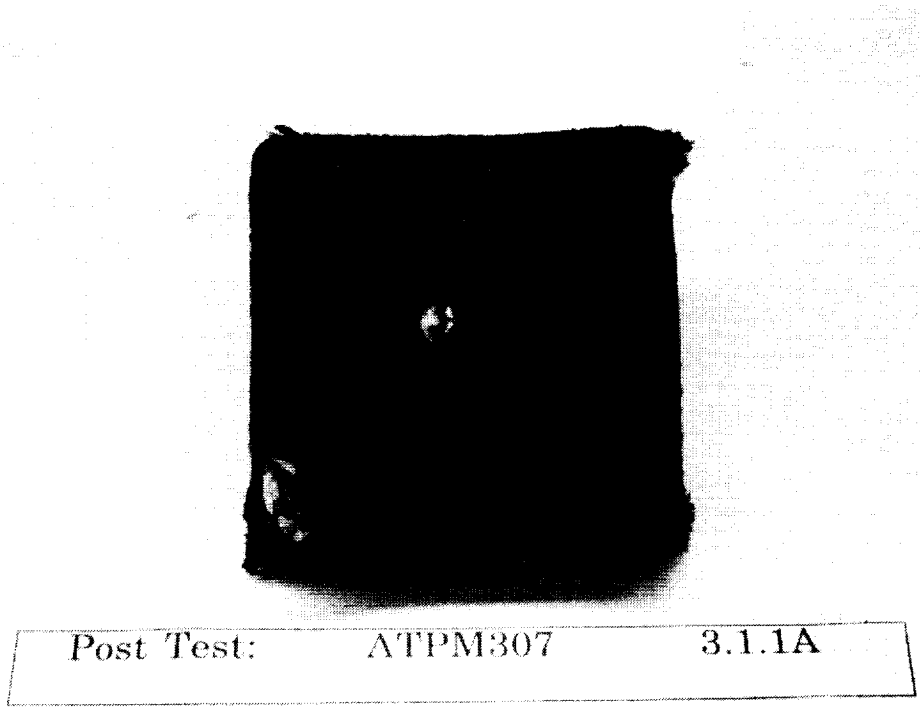

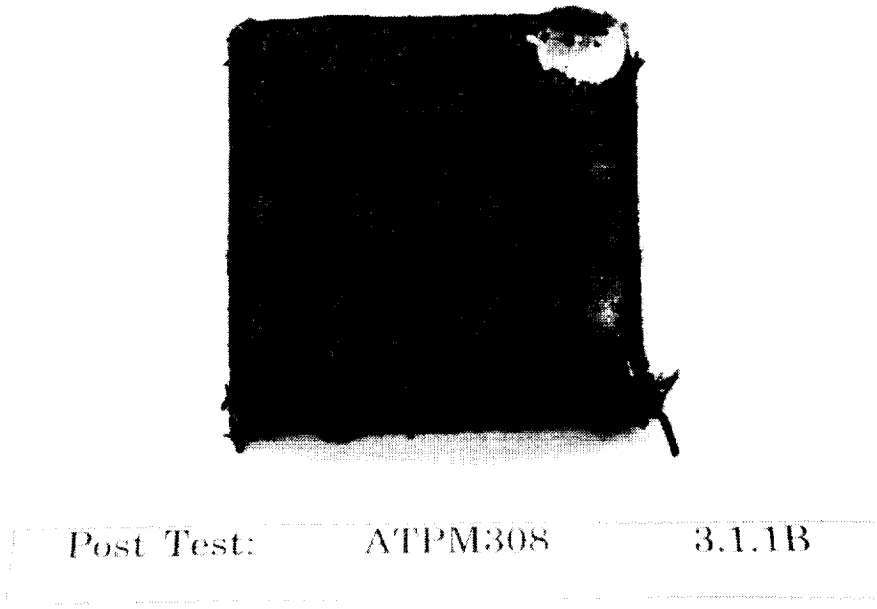

Figure A-3. CFBI 5HSW after exposure to 30.7 Btu/ft^2•s (above) and 34.3 Btu/ft^2•s (below).

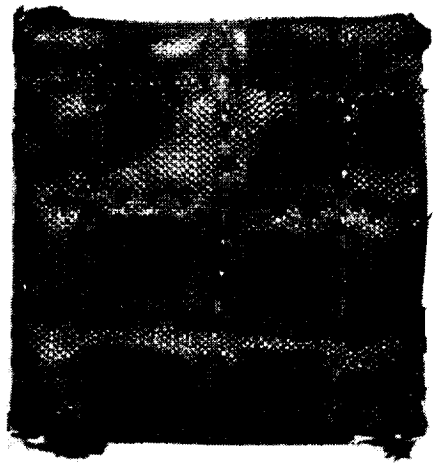

Post Test: ATPM327 3.6.1A

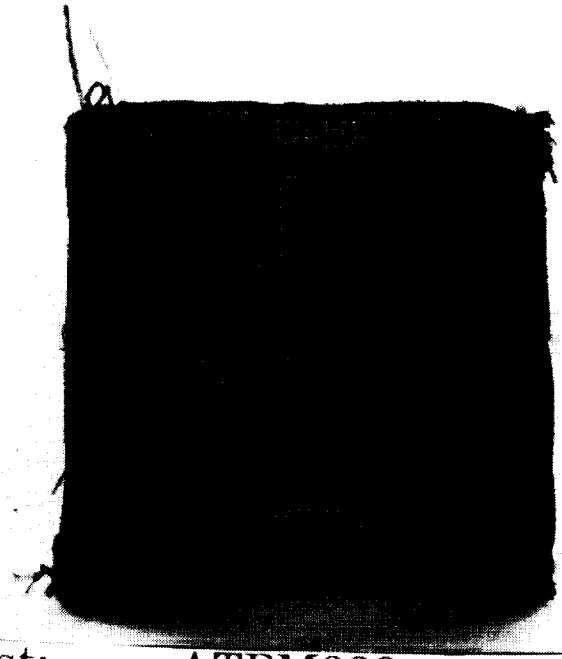

Post Test: ATPM328 3.6.1B

Figure A-4. CFBI-interlock after exposure to 30.7 Btu/ft^2•s (above) and 34.3 Btu/ft^2•s (below).

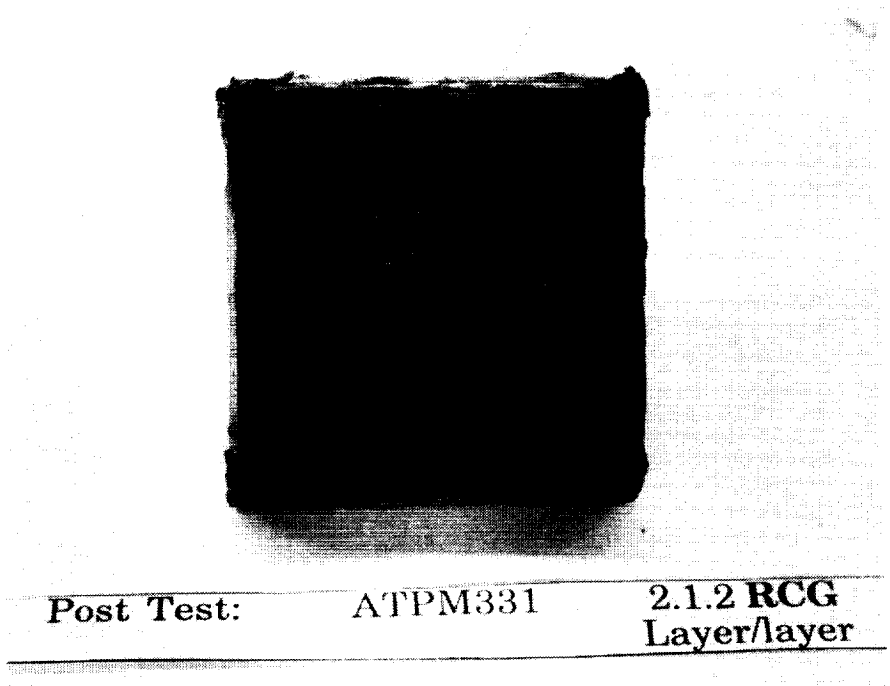

Figure A-5. TABI layer/layer RCG coated (above) and TABI layer/layer PCC coated (below) after exposure to 34.3 Btu/ft^2•s.

Post Test: ATPM329 3.6.1
RCG

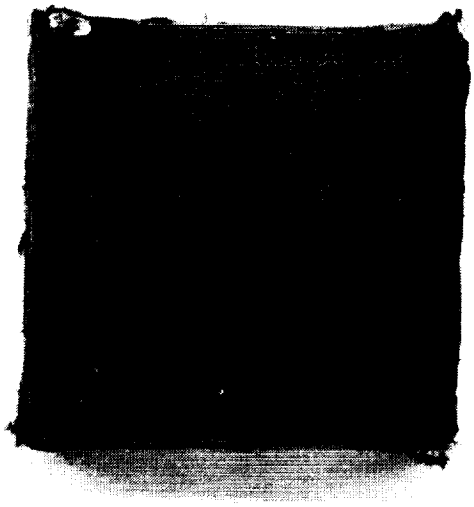

Post Test: ATPM330 3.6.1
A2

Figure A-6. CFBI-interlock RCG coated (above) and CFBI-interlock PCC coated (below) after exposure to 34.3 Btu/ft^2•s (below).

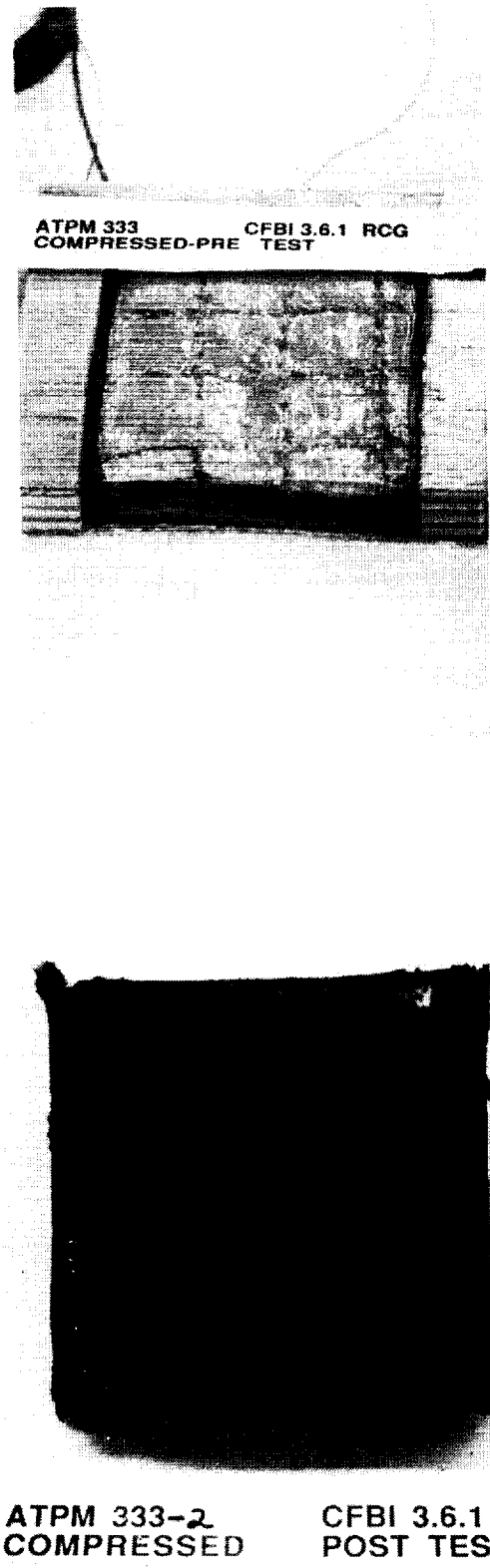

Figure A-7. CFBI-interlock RCG coated, vacuum bagged, before (above) and after exposure (below) to 34.3 Btu/ft^2•s.

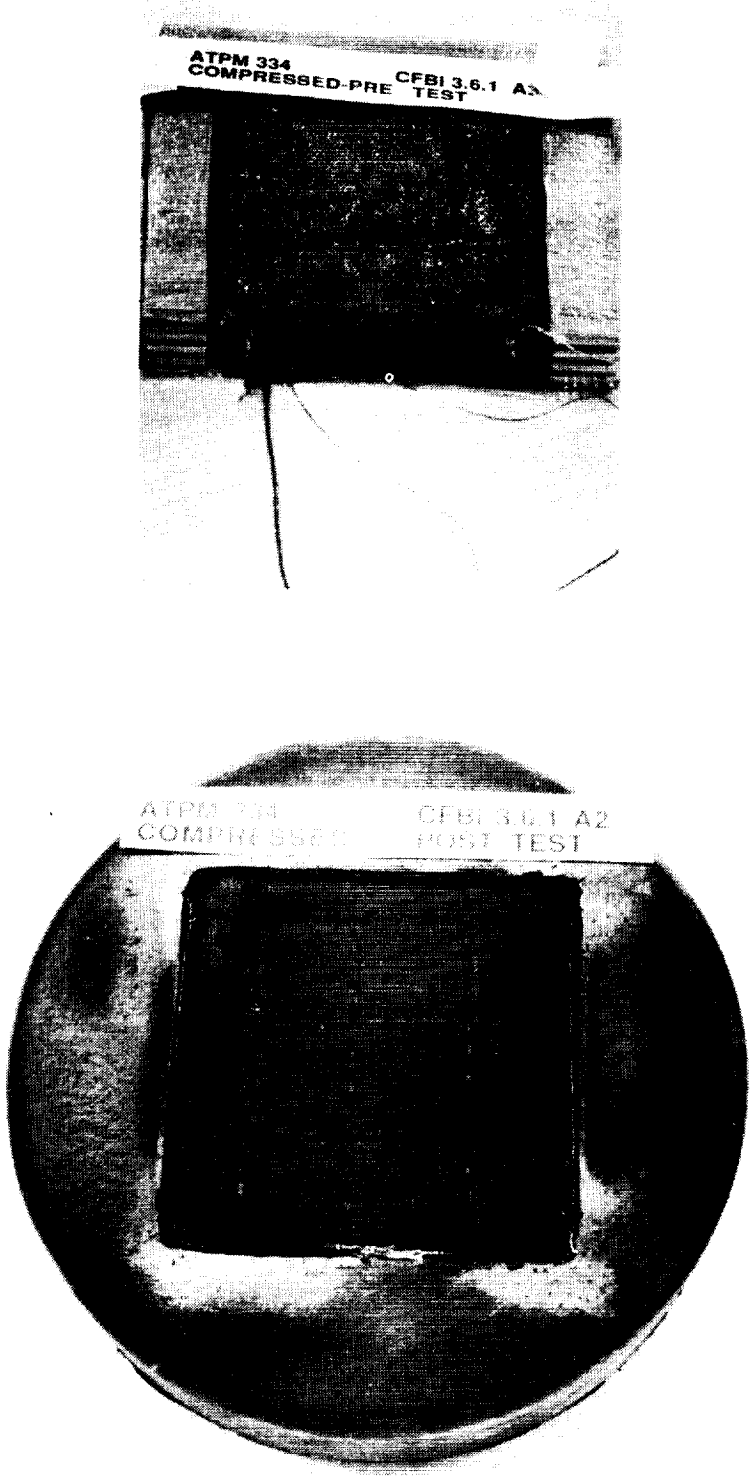

Figure A-8. CFBI-interlock PCC coated, vacuum bagged, before (above) and after exposure (below) to 34.3 Btu/ft^2•s.

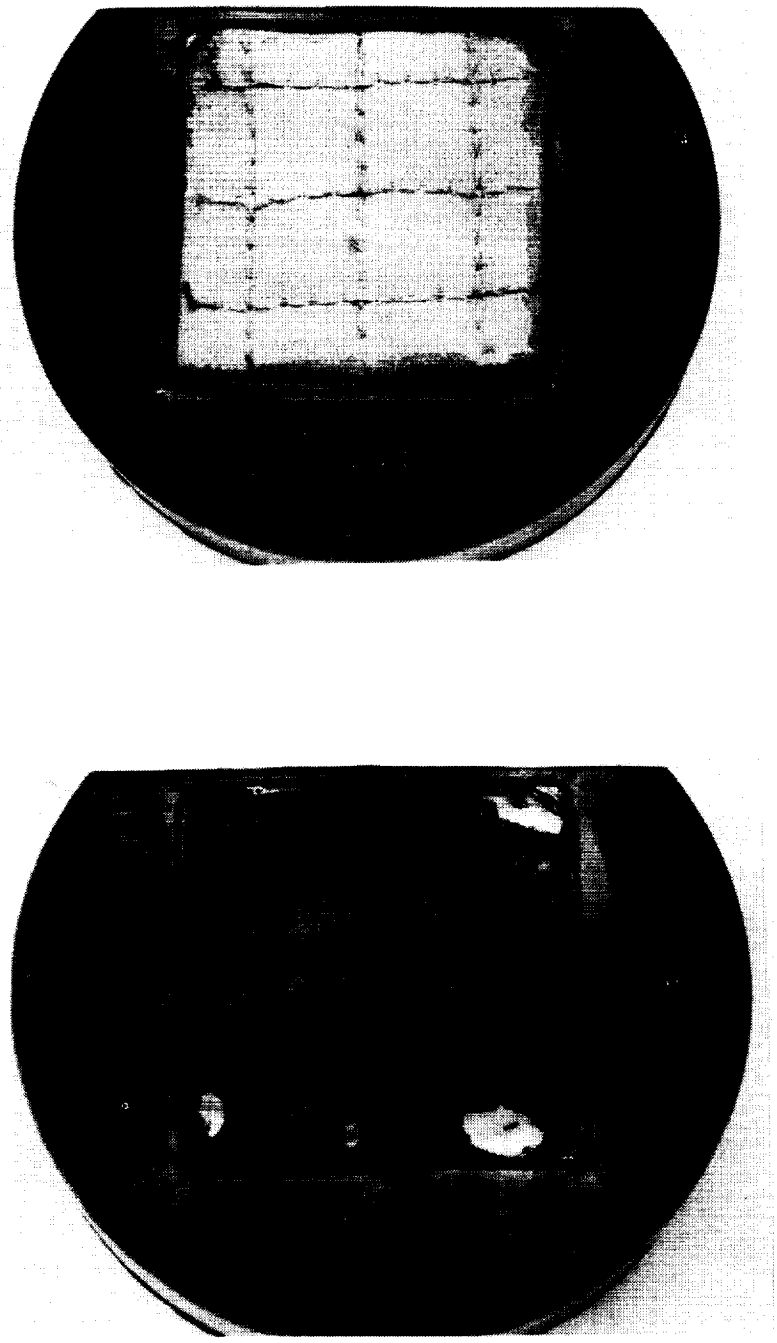

Figure A-9. CFBI-interlock RCG spray, before (above) and after exposure (below) to 34.3 Btu/ft^2•s.

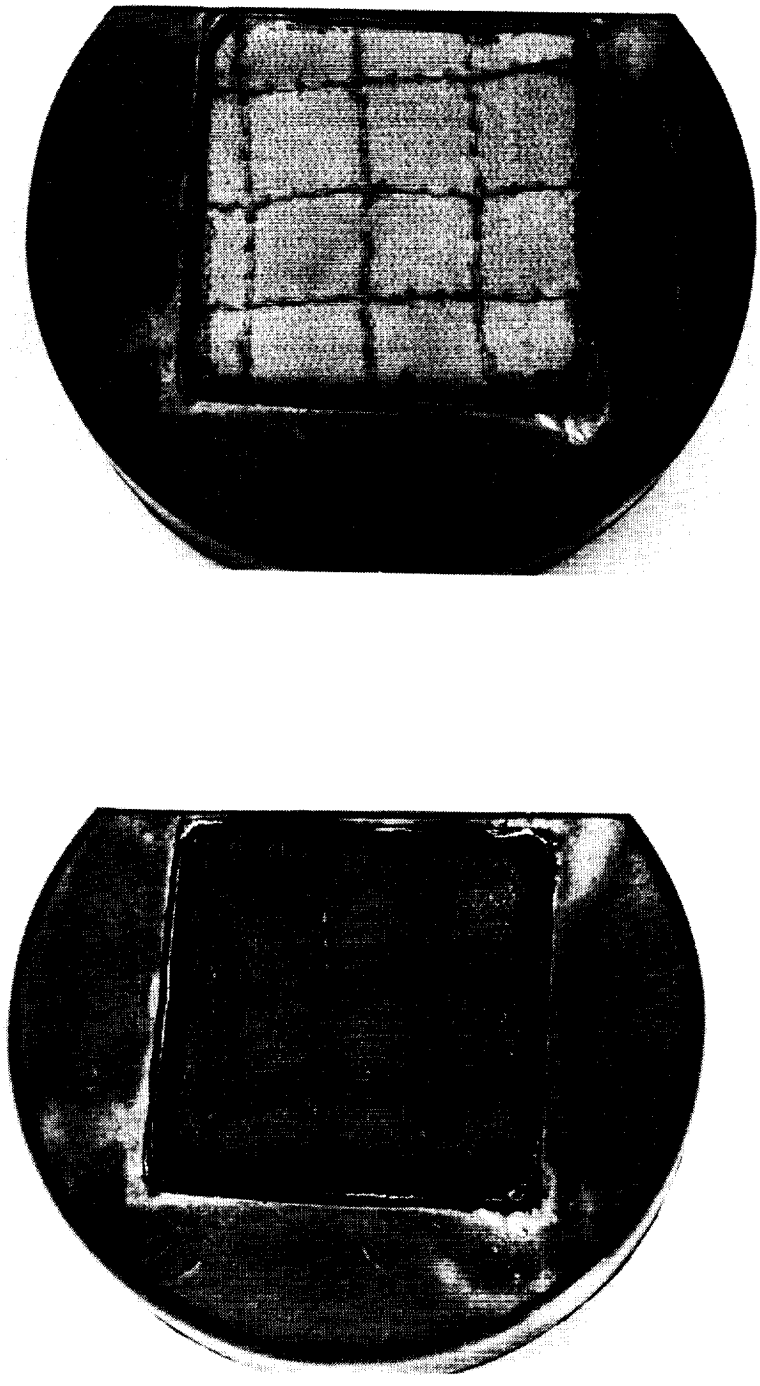

Figure A-10. CFBI-interlock PCC spray, before (above) and after exposure (below) to 34.3 Btu/ft^2•s.

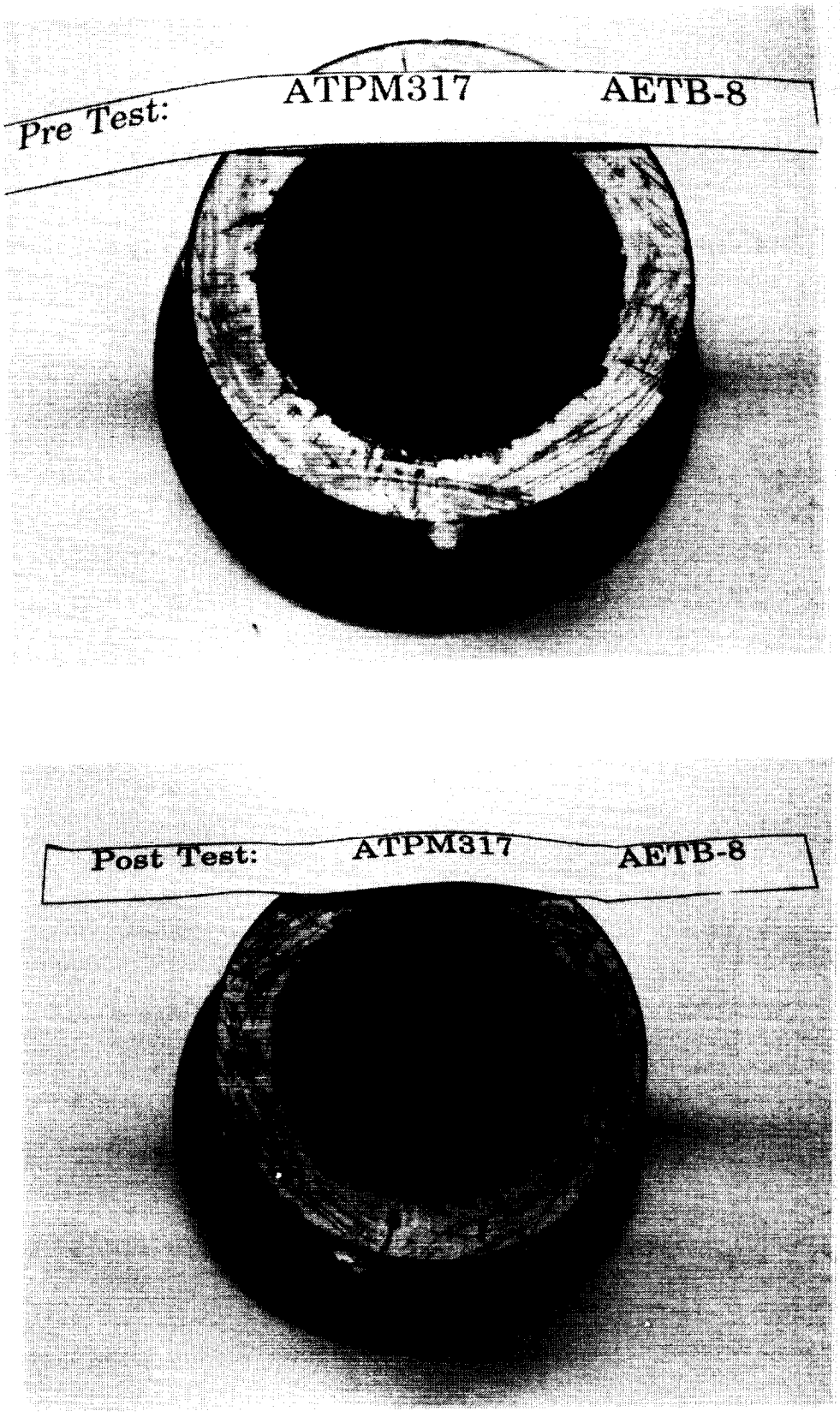

Figure A-11. AETB-8 before (above) and after exposure (below) to 47.0 Btu/ft^2•s.

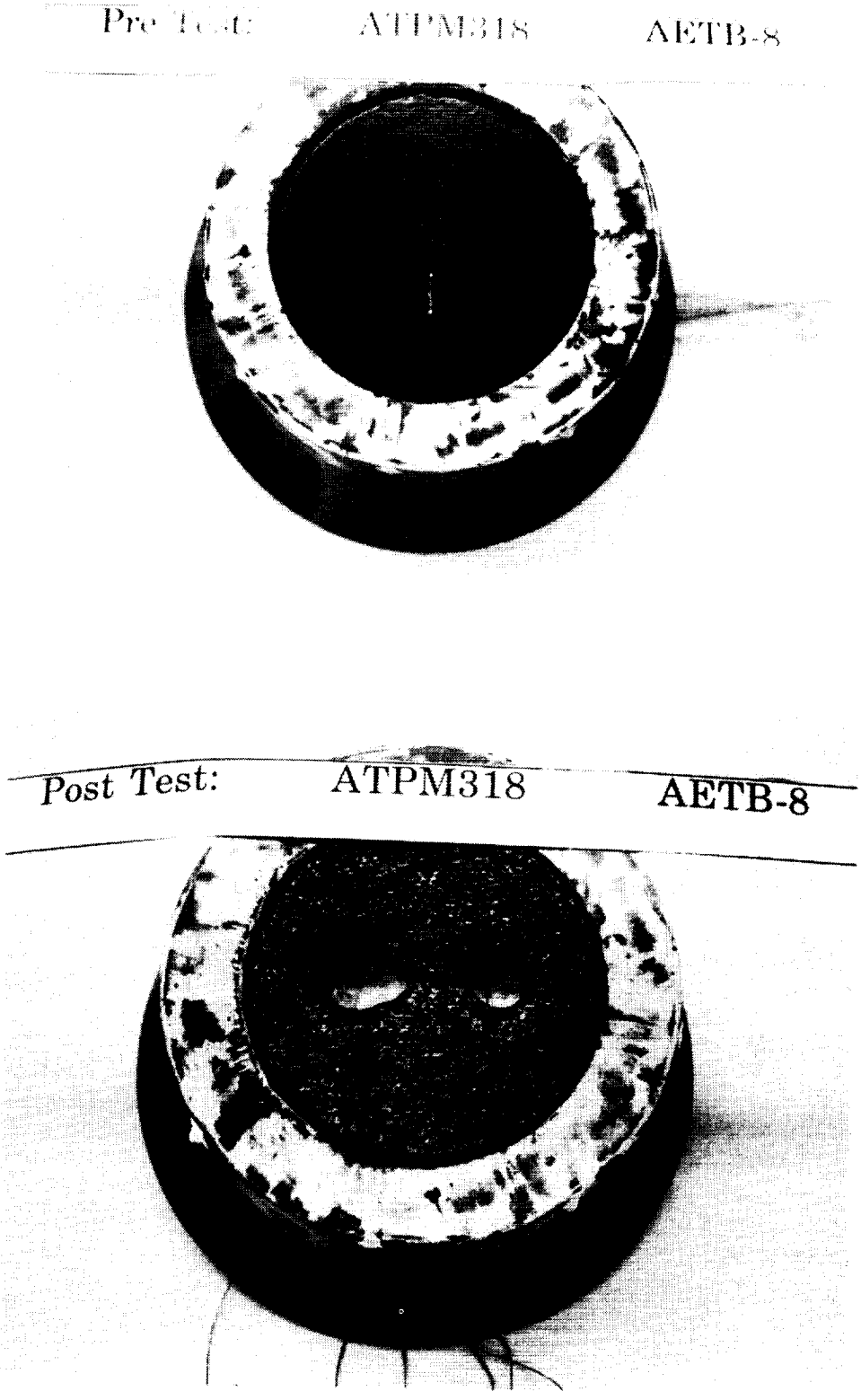

Figure A-12. AETB-8 before (above) and after exposure (below) to 58.7 Btu/ft^2•s.

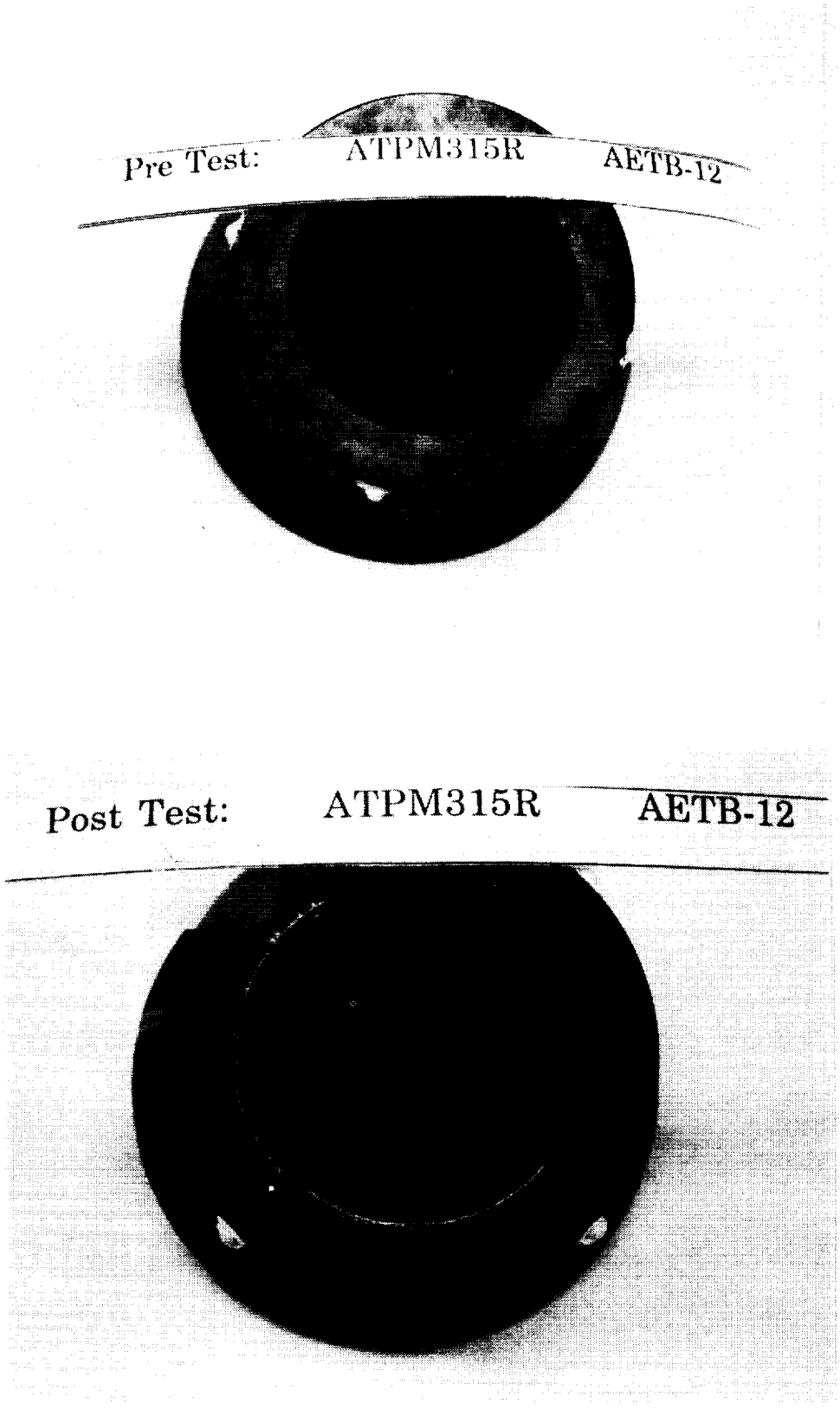

Figure A-13. AETB-12 before (above) and after exposure (below) to 47.0 Btu/ft^2•s.

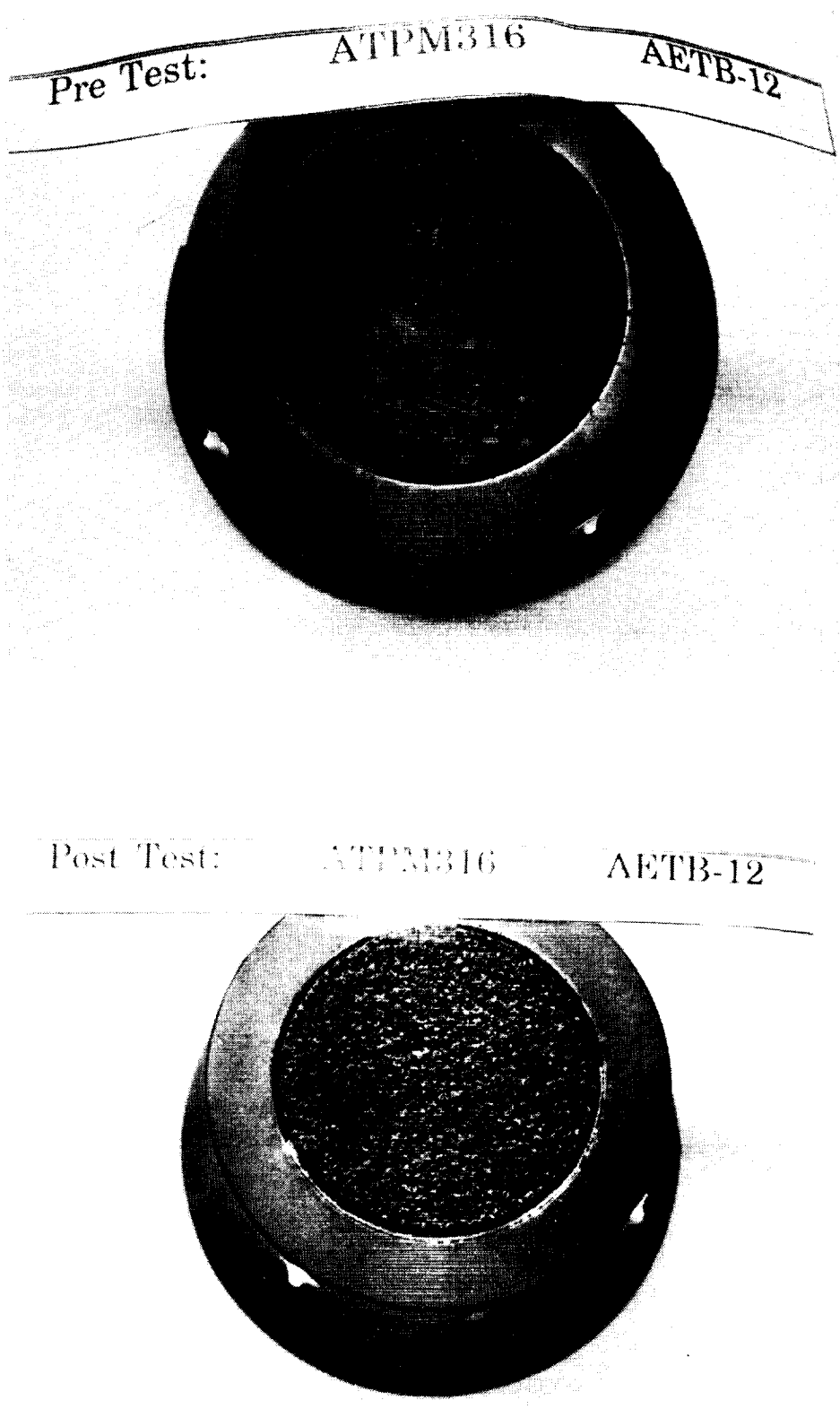

Figure A-14. AETB-12 before (above) and after exposure (below) to 58.7 Btu/ft^2•s.

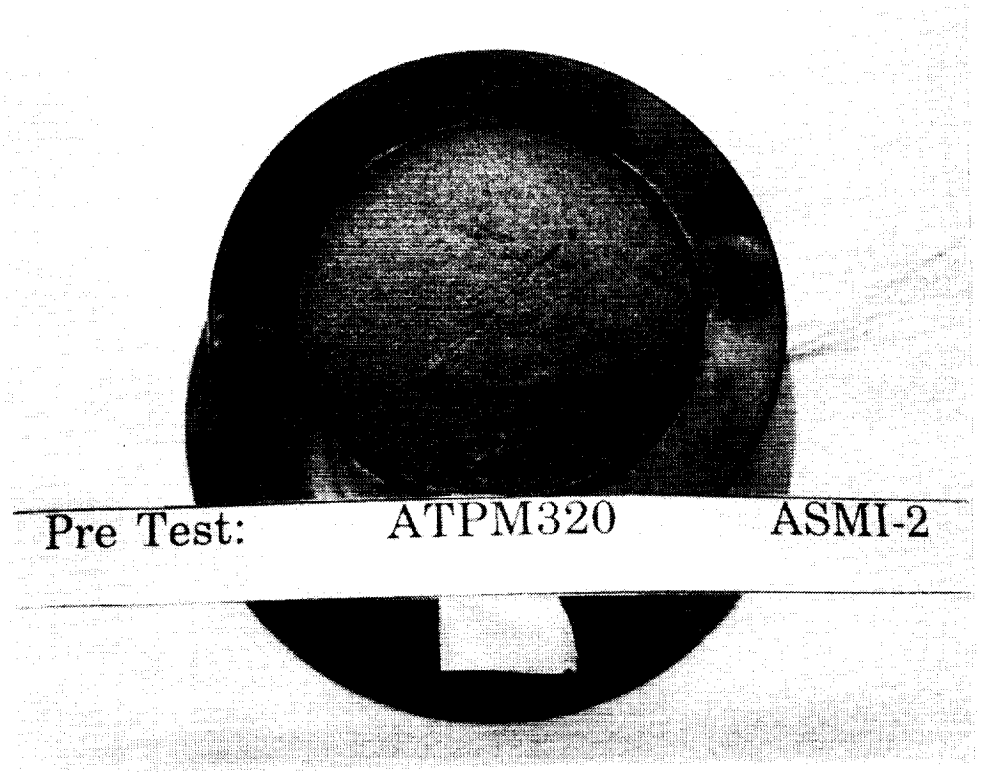

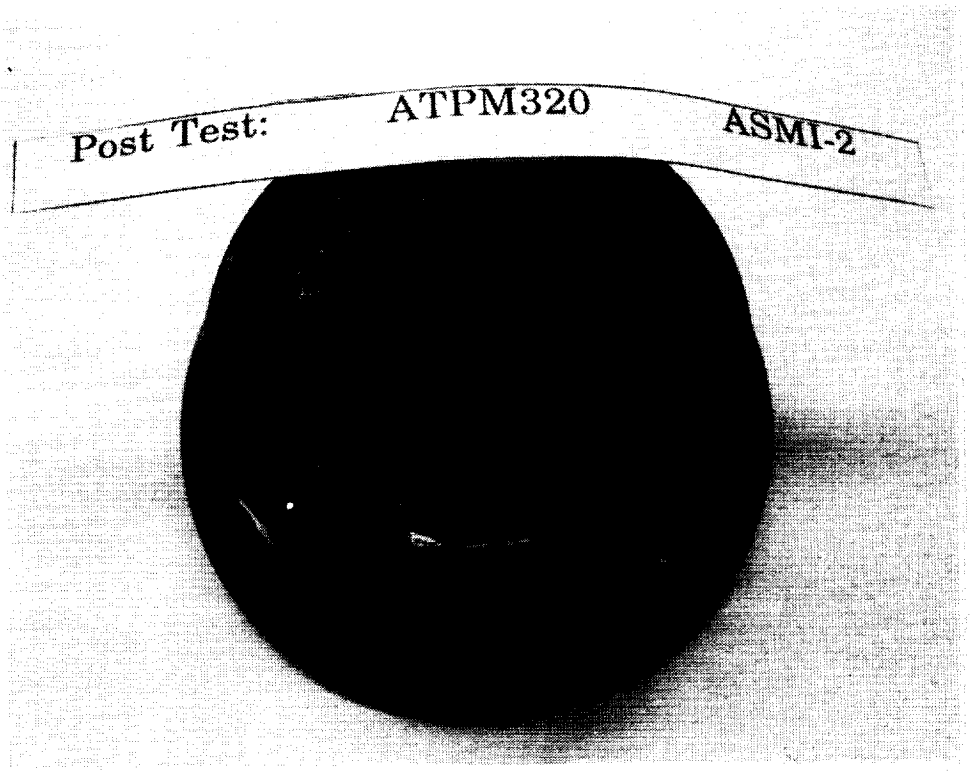

Figure A-15. ASMI before (above) and after exposure (below) to 47.0 Btu/ft^2•s.

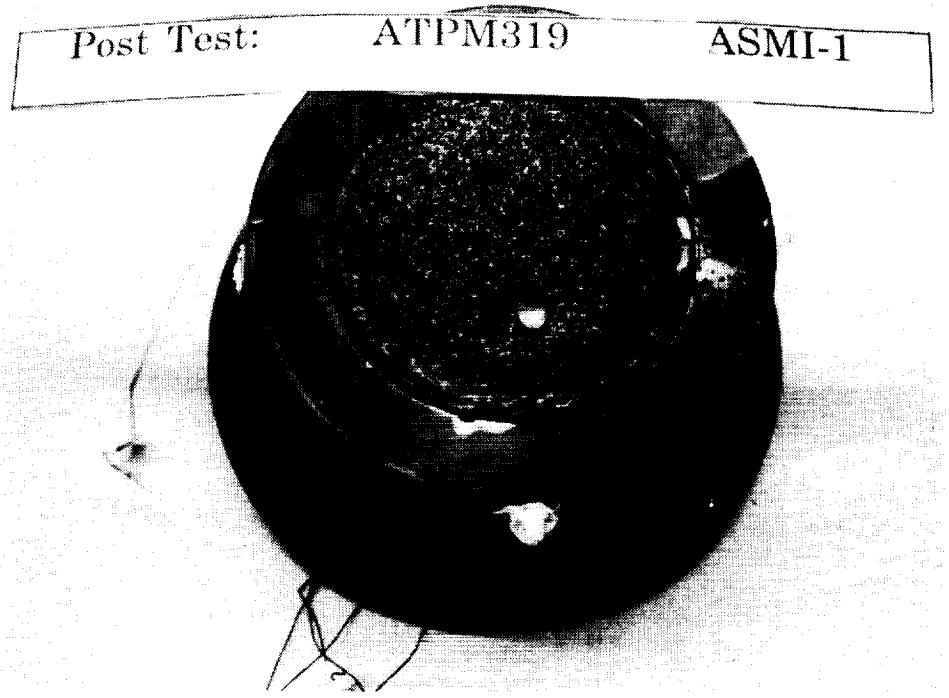

Figure A-16. ASMI before (above) and after exposure (below) to 58.7 Btu/ft^2•s.

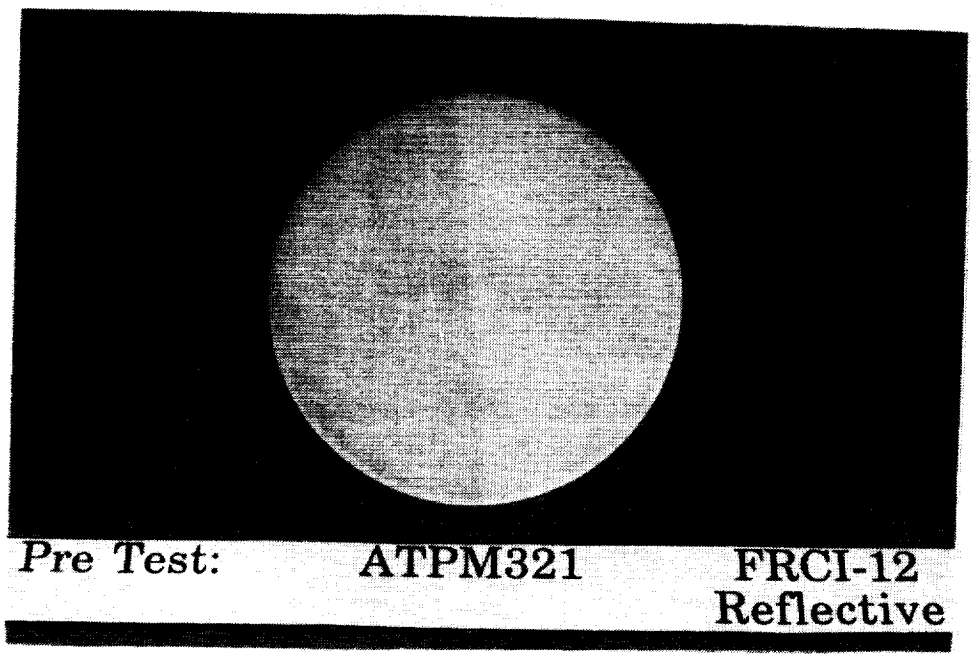

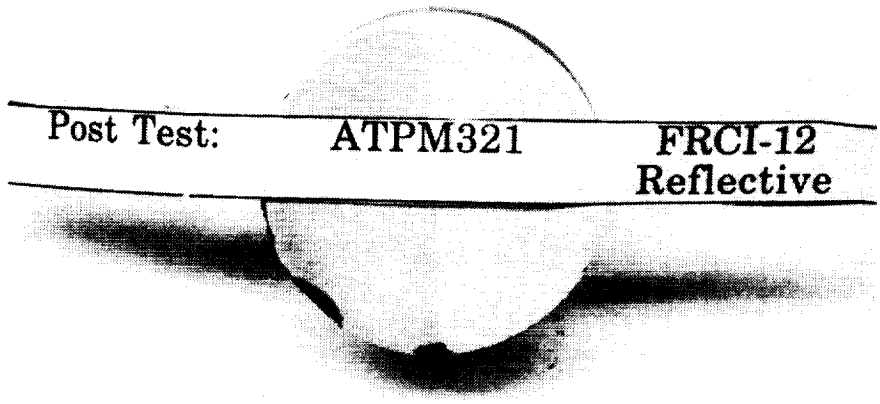

Figure A-17. FRCI-12 reflective before (above) and after exposure (below) to 33.4 Btu/ft^2•s.

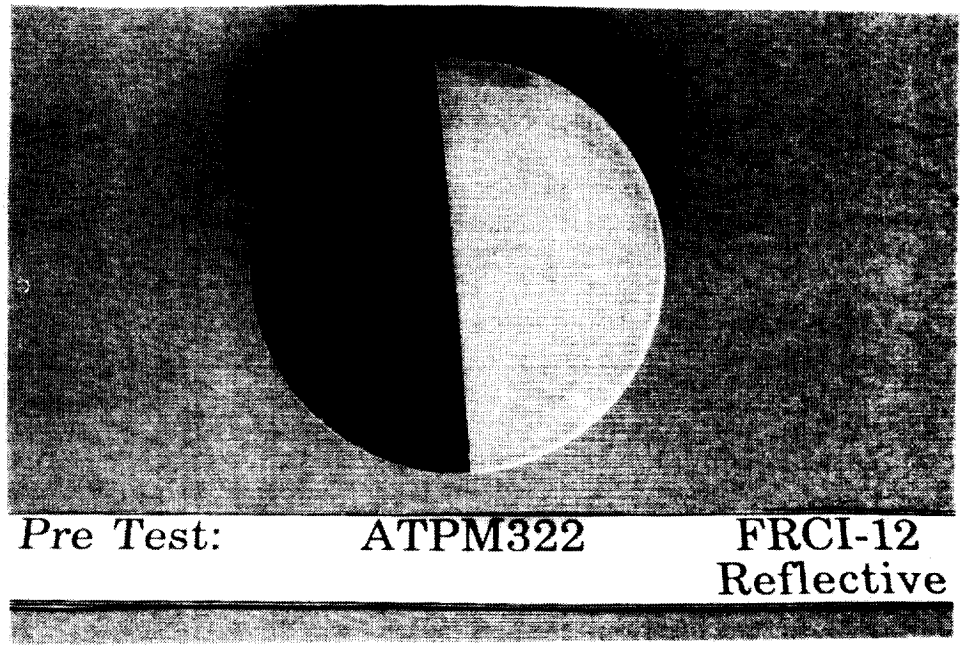

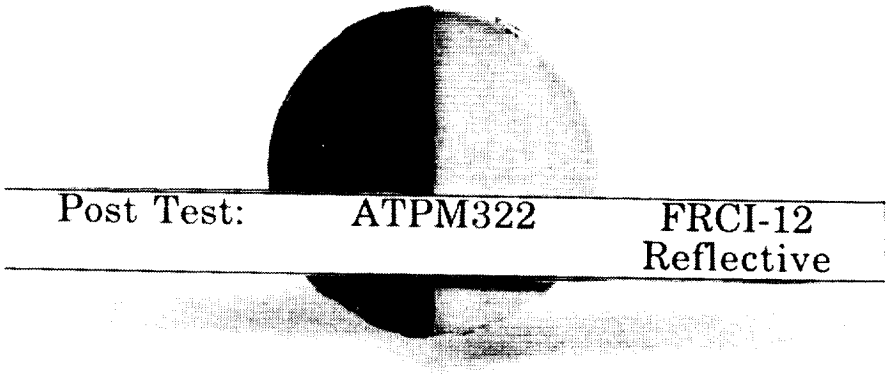

Figure A-18. FRCI-12 reflective before (above) and after exposure to 34.8 Btu/ft^2•s.

REPORT DOCUMENTATION PAGE

Form Approved
OMB No. 0704-0188

1. AGENCY USE ONLY *(Leave blank)*	2. REPORT DATE	3. REPORT TYPE AND DATES COVERED
	March 1992	Technical Memorandum

4. TITLE AND SUBTITLE

Thermal Response of Rigid and Flexible Insulations and Reflective Coating in an Aeroconvective Heating Environment

5. FUNDING NUMBERS

506-43-31

6. AUTHOR(S)

D. A. Kourtides, S. A. Chiu, D. J. Iverson, and D. M. Lowe

7. PERFORMING ORGANIZATION NAME(S) AND ADDRESS(ES)

Ames Research Center
Moffett Field, CA 94035-1000

8. PERFORMING ORGANIZATION REPORT NUMBER

A-92064

9. SPONSORING/MONITORING AGENCY NAME(S) AND ADDRESS(ES)

National Aeronautics and Space Administration
Washington, DC 20546-0001

10. SPONSORING/MONITORING AGENCY REPORT NUMBER

NASA TM-103925

11. SUPPLEMENTARY NOTES

Point of Contact: D. A. Kourtides, Ames Research Center, MS 234-1, Moffett Field, CA 94035-1000; (415) 604-4784 or FTS 464-4784

12a. DISTRIBUTION/AVAILABILITY STATEMENT

Unclassified — Unlimited
Subject Category 05

12b. DISTRIBUTION CODE

13. ABSTRACT ***(Maximum 200 words)***

This report describes the thermal performance of rigid and flexible thermal protection systems considered for potential use in future Aeroassist Space Transfer Vehicles. The thermal response of these materials subjected to aeroconvective heating from a plasma arc is described. Properties that were measured included the thermal conductivity of both rigid and flexible insulations at various temperatures and pressures and the emissivity of the fabrics used in the flexible insulations. The results are included from computerized thermal analysis models describing thermal response of these materials subjected to flight conditions.

The thermal performance of these thermal protection systems in the plasma arc is described in three sections: flexible insulations, rigid insulations, and reflective coating. The thermal conductivity measurements are described in two sections: flexible and rigid insulations. The thermal analysis section includes analyses for both the flexible and rigid insulations.

14. SUBJECT TERMS

Insulation, Composites, Thermal protection, Coating

15. NUMBER OF PAGES

93

16. PRICE CODE

A04

17. SECURITY CLASSIFICATION OF REPORT	18. SECURITY CLASSIFICATION OF THIS PAGE	19. SECURITY CLASSIFICATION OF ABSTRACT	20. LIMITATION OF ABSTRACT
Unclassified	Unclassified		